UILU-ENG 88-3605

Report No. 144

STRUCTURE AND PROPERTIES OF ION PLATED ALUMINUM COATINGS

by

Howard S. Savage and J. M. Rigsbee
Department of Materials Science and Engineering

A Report of the

MATERIALS ENGINEERING - MECHANICAL BEHAVIOR

College of Engineering, University of Illinois at Urbana-Champaign

October 1988

ABSTRACT

This research investigates the mechanical, microstructural, and chemical properties and their interrelationships with deposition parameters for evaporated and ion plated aluminum coatings on a variety of substrate materials. Ion plating is a plasma assisted physical vapor deposition technique. Substrate materials include: aluminum, copper, Formvar, NaCl, silicon, and titanium. Characterization techniques include: adhesion testing, scanning electron microscopy (SEM), transmission electron microscopy (TEM), energy dispersive analysis of X-rays (EDX), X-ray diffraction (XRD), Auger electron spectroscopy (AES), secondary ion mass spectroscopy (SIMS), and surface profilometry. Variations in ion plating process parameters include: applied substrate bias, argon pressure, in-situ sputter cleaning, and discharge current enhancement. In general, it was found that variations in parameters which produced increased ion bombardment of the substrate and growing film and hence, increased energy of deposition promoted increased coating adhesion and a coating structural transition from a zone 1 structure typical of evaporated coatings grown at high pressure and low T/T_{mp} to a zone 3 structure typical of coatings grown at high T/T_{mp}. The formation of an extended interfacial region was observed for coatings deposited at high energies.

ACKNOWLEDGEMENT

The author wishes to thank Professor J. M. Rigsbee for his encouragement,guidance and assistance throughout this study. The Army Research Office is acknowledged for financial support under DAAG-29-83-K-0151. The U. S. Army Construction Engineering Research Laboratory is acknowledged for the use of the ion plating facility under the charge of Mr. V. F. Hock and the SEM under the charge of Mr. R. Weber. The Center for Microanalysis of Materials at the University of Illinois is acknoledged for access to their facilities and personnel with thanks to J. Baker, N. Finnegan, and M. Mochel for assistance with equipment and data interpretation. R. Olson of the Center for Electron Microscopy at the University of Illinois is acknowledged for SEM instruction and access. The assistance of the Materials Science departmental faculty, students, and support staff is acknowledged. The assistance of JMR Group is acknowledged. Special thanks to D. M. Leet for hands on instruction on dissassembly/reassembly of the ion plater as well as valuable discussions on vacuum processing. R. Cathey, M. Shah, and J. Suarez are acknowledged for assistance with computers. P. Scott is acknowleged for valuable discussions. My wife Angela and my parents and family are acknowledged for their encouragement and patience.

TABLE OF CONTENTS

LIST OF TABLES

LIST OF FIGURES

I. INTRODUCTION

Vapor deposited aluminum coatings have found wide use in industry in applications such as conductive paths for microelectronics, corrosion protection, reflective coatings, and ornamental or decorative coatings. In all of these applications, long term coating performance is affected by the coating adherence, coating structure, and the nature of the coating/substrate interface.

The purpose and goals of this research are to investigate and develop an understanding of the mechanical, microstructural, and chemical properties of evaporated and ion plated coatings on a variety of substrate materials. Substrate materials include: aluminum, copper, Formvar, NaCl, silicon, and titanium. Characterization techniques include: adhesion testing, scanning electron microscopy (SEM), transmission electron microscopy (TEM), X-ray diffraction (XRD), energy dispersive analysis of X- rays (EDX), Auger electron spectroscopy (AES), secondary ion mass spectroscopy (SIMS), and surface profilometry. Some of the questions addressed by this thesis are:

1) What is the effect of increasing substrate cleanliness by chemical etching, chemical polishing, or in-situ sputter cleaning prior to deposition on the adhesion strength of evaporated and ion plated coatings?

2) What is the effect of the sputter cleaning process on substrate surface chemistry?

3) What is the effect of increasing deposition energy through the use of increased applied substrate bias and a discharge current enhancement system on coating adhesion strength?

4) What is the effect of deposition energy on coating texture?

5) What is the effect of deposition energy on coating microstructures?

6) What is the effect of increasing deposition energy on the microstructure, width, and chemistry of the coating/substrate interface?

7) What is the effect of substrate bias during deposition on coating thickness uniformity?

8) What is the effect of increasing applied substrate bias and argon working gas pressure on argon incorporation in the coatings?

II. BACKGROUND

II.A. ALUMINUM COATINGS

Vapor deposited aluminum coatings have found a wide variety of applications in industry. These applications include conductive paths for microelectronics, corrosion protection, reflective coatings and decorative coatings.

Al is currently the preferred metal for metallization of Si-based microelectronic devices due to its chemical stability, low electrical resistivity, and good overall processibility (1). Al has a melting point of 660 Celsius (933 K), allowing deposition via conventional evaporation sources, and a resistivity of 2.7 microohmcentimeters. Aluminum's strong affinity for oxygen allows it to adhere well to silica (1).

Problems with Al metallization in microelectronics include: Al's significant solubility for Si resulting in Al/Si interdiffusion at contacts; current-induced migration of Al along grain boundaries (electromigration); stress relaxation artifacts arising from thermal cycling due to an order of magnitude difference in thermal expansion coefficients ($\alpha(Al) = 23.5 \times 10^{-6}/K$, $\alpha(Si) = 2.5 \times 10^{-6}/K$); and corrosion (1). Appropriate alloying can usually reduce the extent of the first 3 problems at the expense of increased resistivity and reduced corrosion resistance (1).

Pure aluminum is a very reactive material; but, the formation of an adherent, stable oxide film protects it from corrosion in many environments (2). The oxide film is inert and stable in most neutral and acid solutions; but, it is rapidly attacked by alkalies (2). Al

coatings can protect the materials they are deposited on by: 1) providing a continuous physical barrier and 2) providing cathodic protection when the coating becomes discontinuous as in being scratched. The first mechanism will work to protect almost any substrate. The second mechanism may backfire if the material being protected is more anodic than the aluminum coating. As an example, Al on a Mg alloy will produce a galvanic reaction should a break in the coating occur, and the result will be enhanced corrosion of the substrate.

Aluminum's reflectivity and adherence to glass and plastics make it useful in the manufacture of many durable reflective products. Applications of reflective aluminum coatings include: mirrors for lasers, telescope mirrors, "one way" windows, cosmetic mirrors, architectural glass, sequins, glitter, fire/heat resistant clothing, Christmas ornaments, tinsel, car trim, jewelry, and "space blankets".

II.B. ALUMINUM/SUBSTRATE INTERFACES

One of the most important considerations in the adherence of Al films to their substrates is the "nature" of the Al/substrate interface. The "nature" of the interface includes all the particulars of the interface which affect its properties and behavior such as microstructure, composition, width, residual stress, and coherency. An interface can generally be considered as a microstructural and or compositional discontinuity between the coating and substrate and the nature of the interface will depend on the type and extent of interactions between the coating and the substrate. Such

interactions include: mutual solubilities, intermetallic compound formation, diffusion, relative reactivities, lattice mismatch/coherency and residual stresses. The interface interactions may be modified by the presence of oxides and contamination at the substrate surface and by variations in process parameters during coating deposition. For physical vapor deposited coatings, critical process parameters include: sputter cleaning, substrate temperature, residual gas composition and pressure, and ion bombardment during film growth. Based on the research objectives of this thesis it is relevant to briefly discuss interface considerations in the following film/substrate couples: 1) Al/Al, 2) Al/Cu, 3) Al/Ti, 4) Al/Si, 5) Al/oxide, and 6) Al/polymer.

II.B.1. ALUMINUM/ALUMINUM

The Al/Al interface is created by deposition of Al films onto Al and Al alloy substrates. Such interfaces are also created by interruptions of the Al film deposition process, as in multipass deposition to minimize substrate heating. The structure and chemistry of the Al/Al interface can be degraded by oxidation, contamination, and incorporation of residual gases during coating growth. In the case of film deposition on age hardenable Al alloy substrates, heating of the substrate during deposition may significantly degrade the properties of the substrate region adjacent to the interface. An extreme example of Al/Al interface degradation by oxidation can be seen in work by Safai and Herman (3) on Al coatings made by plasma spraying in air. Safai and Herman (3) described oxidation of the particles as: 1) hindering particle-

particle interactions, 2) promoting the formation of interparticle pores, and 3) providing an easy path for crack propagation thereby promoting failure by delamination. An example of the effects of interfacial oxidative contamination can be found in the works of Ferraglio and D'Antonio (4) and Mcleod and Hughes (5). Ferraglio and D'Antonio (4) found that Al films formed distinct multilayers when the evaporation process is interrupted and that the scatter in resistivity values for these multilayer structures is greater than that for single layer structures. Annealing work on these films indicated that there was no interaction between the layers at temperatures up to 200 Celsius (473 K) and that the scatter in resistivity data was not significantly reduced by annealing at temperatures above 200 Celsius (473 K) (4). Mcleod and Hughes (5) deposited multilayer Al structures in a sputter deposition system by making multiple passes in front of the source. They found that the smaller the number of passes used to make the coating, the lower the resistivity of the coating (5). The effects of residual water vapor were also noted in this work; increasing water vapor pressure was found to decrease coating reflectivity and increase resistivity (5). Work by Kubovy and Janda (6) indicated that residual gas incorporation, especially oxygen, increases coating resistivity and residual stress, with residual stress being more sensitive to oxygen incorporation than resistivity.

II.B.2. ALUMINUM/COPPER

The properties of the Al/Cu interface may be degraded by the presence of contamination on the substrate surface prior to

deposition and the influence of residual gases during deposition, similar to the Al/Al interface. The Al/Cu interface may also be subjected to residual stress due to differences in thermal expansion coefficients of Al and Cu ($\alpha(Al) = 23.5 \times 10^{-6}/K$ and $\alpha(Cu) = 16.6 \times 10^{-6}/K$). Aluminum's strong interaction with copper may also allow intermetallics such as $CuAl_2$ (theta) to form along the interface (7). Thermal stresses may cause cracking of a hard, brittle continuous interfacial film of $CuAl_2$ leading to delamination of the coating at the interface. Processing parameters such as substrate temperature during deposition may give some control over the formation of interfacial intermetallics. With proper process control it may be possible to deposit an adherent, hard, wear resistant $CuAl_2$ coating on the copper surface. One of the more serious considerations for the Al/Cu interface is corrosion failure due to galvanic coupling between Al and Cu in the presence of a suitable electrolyte such as Cl contamination and residual water vapor from the environment (1). This corrosion is enhanced by the inability of Cu and $CuAl_2$ to form a protective oxide film (1). Solutions to minimize this corrosion problem in the case of computer chips include rinsing with deionized water to remove aggressive (halogen) species and hermetically sealing the chip from the environment (1). Ultimately, the Al coating will be sacrificed by corrosion and the Cu substrate protected as long as unoxidized Al remains: This may or may not be desirable depending on the application.

II.B.3. ALUMINUM/TITANIUM

The Al/Ti interface is also subject to contamination and intermetallic formation effects similar to the Al/Cu interface. Work by Teer and Salem (8) indicates that $TiAl_3$ has better wear and friction properties than Al and Ti. Additionally, Teer and Salem (8) found that an interfacial layer of $TiAl_3$ created during ion plating of Al on Ti inhibited galvanic corrosion between Ti and Al. Similar to the Al/Cu galvanic interaction, the less noble Al will be sacrificed to protect the Ti. The Al/Ti interface is also subject to thermal stresses ($\alpha(Al) = 23.5 \times 10^{-6}/K$ and $\alpha(Ti) = 8.5 \times 10^{-6}/K$). The magnitude of the thermal stress that can be generated in the Al/Ti system is greater than that for the Al/Cu system due to the greater difference in expansion coefficients in the Al/Ti system.

II.B.4. ALUMINUM/SILICON

The Al/Si interface is also subject to degradation due to contamination and residual gas incorporation as discussed above. The Al/Si system forms a eutectic mixture at almost all ranges of composition and no intermetallics. The potential for thermal stress in the Al/Si interface is greater than in the Al/Ti system ($\alpha(Al) = 23.5 \times 10^{-6}/K$ and $\alpha(Si) = 2.5 \times 10^{-6}/K$). Al/Si interface failures in Si device related applications are related to the increased solubility of Si in Al at elevated temperatures causing dissolution of Si at the Al/Si interface leading to degradation of the Si semiconductor region and short circuiting as Al enters the semiconductor junction (1). In this case, an extended interfacial region would not be desirable.

II.B.5. ALUMINUM/OXIDE

The Al/oxide interface is representative of the interfaces generated when depositing Al coatings on a metallic substrate's native oxide film or depositing on an oxide ceramic substrate. Interfacial stress in these systems due to thermal expansion mismatches will depend on the relative expansion coefficients for the Al, the oxide , and the underlying metal substrate such that greater mismatches will promote increased stress and poorer adhesion. Bonding of the aluminum to the oxide will depend to some extent on the relative affinities of the Al and the oxide base metal for oxygen and the degree of mechanical and/or thermal mixing forming a reaction zone at the interface. From the Ellingham diagram in figure (1) (Gaskell (9)) we can see that aluminum has a stronger affinity for oxygen than Si, Ti, and Cu so we can expect aluminum to react with oxides of these elements in the interfacial region. Another consideration in the Al/surface oxide interfacial region is bonding of the oxide to the substrate; if the native oxide will not adhere to the substrate, then even if the Al adheres to the oxide, the coating will fail when the substrate oxide delaminates. In general, it is necessary to consider both the substrate/substrate oxide and substrate oxide/Al interfaces in this type of system.

II.B.6. ALUMINUM/POLYMER

Al/polymer interfaces can be degraded by contamination, similar to the previously discussed interfaces. Work by Hurley and Williams (10) has shown that the Al/polymer interface is sensitive to ion and photon bombardment which may cause damage to the

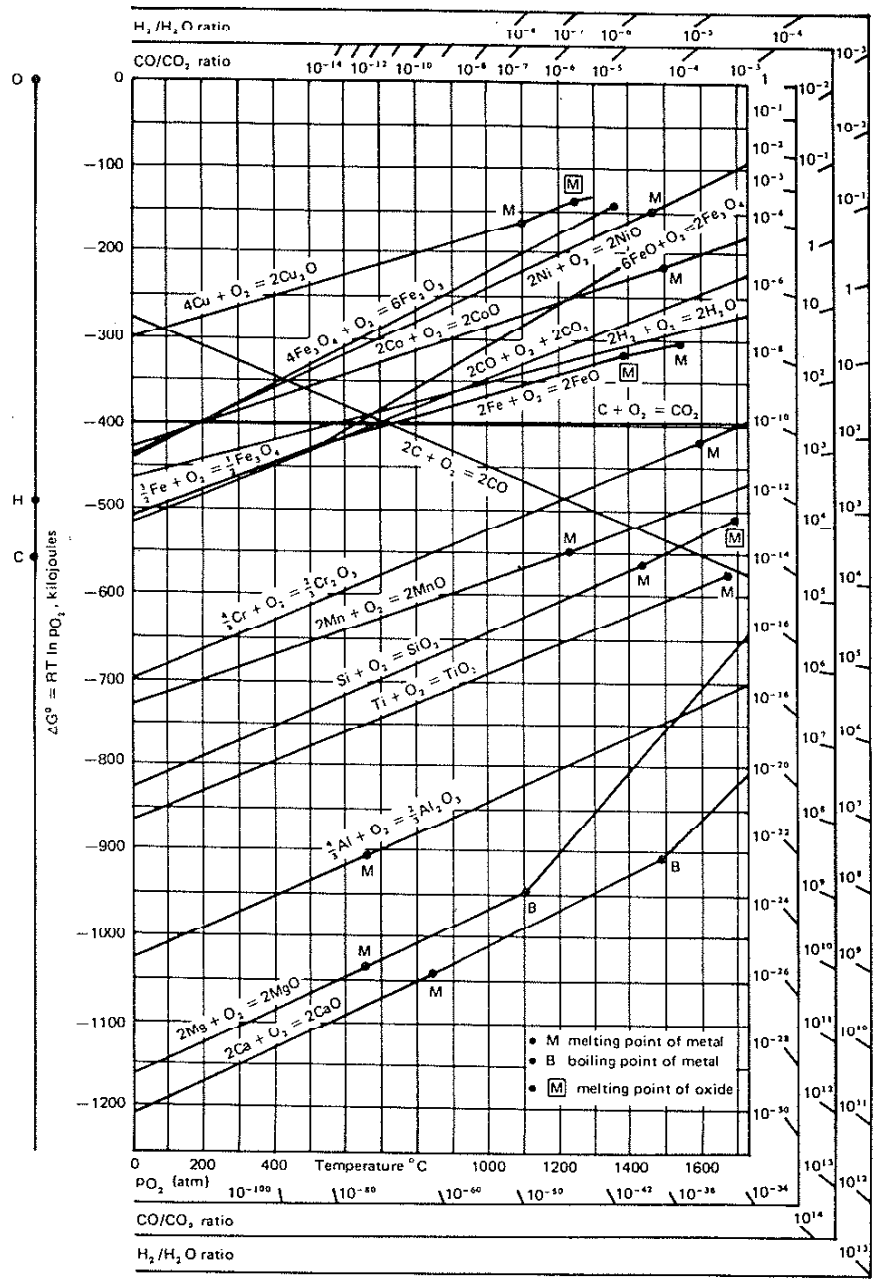

Figure 1. The Ellingham diagram for metallurgically important oxides. From Gaskell (9).

polymer substrate. Work by Goldstein and Bertone (11) has shown that surface reactivity is also a consideration in metal/polymer interfaces. Goldstein and Bertone (11) deposited Al and Ag coatings on Teflon and found that the aluminum (which is more reactive than the Ag) adhered more strongly to the Teflon under flexing and scratching tests. Coating thickness and hardness should also be considered since most polymers have lower elastic moduli than metals; the interface should not fail when the substrate undergoes a reasonable amount of distortion. A "reasonable amount" of distortion will be defined by the application of the Al/polymer composite. For example, an aluminized "space blanket" would be expected to undergo a lot more deformation without delamination than an aluminized car grill or stereo cabinet.

II.C. ADHESION FUNDAMENTALS

Coating adhesion is one of the least understood phenomena in thin film technology. Adhesion in its most general sense can be considered as a macroscopic measurement of the performance of the film/substrate composite under an applied stress. Extended reviews of tests of adhesion have been discussed by Campbell (12) and Chapman (13) and are briefly reviewed here. The more popular methods of adhesion testing include scratch tests, peel tests, and pull tests. Table (1) is a listing of other methods of adhesion testing taken from Campbell (12).

The scratch test is performed by drawing a pointed probe across the coated surface while applying a vertical load (12, 13). The measure of adhesion is taken as the critical value of the

Table 1. Table of engineering techniques for measuring adhesion. From Campbell (12)

Method	Principle
Bending	Substrate bent or twisted until film removed
Squashing	Substrate squashed until film removed
Abrasion	Burnishing or abrasion of surface to remove film
Heating and quenching	Heating and sudden quenching will cause film to be removed because of stresses developed by thermal expansion and contraction
Scratching	Film scratches through by probe. Alternatively parallel grooves cut into the film with decreasing separation until intervening material lifts from substrate
Hammering	Hammering breaks up and removes film
Indentation	Substrate indented from side opposite to film. Coating examined for cracking or flaking off at various stages of indent formation
Pulling	Film pulled off directly if it is thick enough. If not, backing attached using: Solder Adhesives Electroforming
Peeling	Film peeled off using a backing of: adhesive tape Electroplated coating
Deceleration	The film and substrate are subject to violent deceleration, which removes the film. Various experimental arrangements are possible: Coated bullet stopped by steel plate Ultracentrifuge Ultrasonic vibration
Blistering	Film Deposited so that no adhesion exists over a particular area. Air is then introduced into this area and the pressure at which the film starts to lift from the area of no adhesion is measured

vertical load which causes the coating to be completely penetrated or removed from the substrate at the bottom of the scratch (12, 13). The deformation process in the coating and the substrate that occurs during scratching is a complex function of coating surface conditions such as density, porosity, grain size, film thickness, the presence of intermetallics, and surface roughness (13). This indicates that the scratch test may really only be comparatively valid when used on the same film/substrate combination where the film morphologies are nearly the same (13).

The peel test involves applying an adhesive tape to the coating surface and then pulling the tape off (12, 13). If the coating is removed by the tape, then it has poor adhesion; if the coating remains on the substrate, then it has good adhesion (12, 13). Attempts have been made to quantify this test in the case where the film is removed by controlling the stripping speed, the stripping angle, and the sample and measuring the force to pull the tape (12, 13).

The pull test consists of bonding (via adhesive, soldering, or brazing) a pin to the coating surface and then measuring the force normal to the substrate surface required to remove the coating (12, 13). Problems associated with this test include difficulty in applying the force exactly normal to the surface to avoid a peeling (shear) force and bonding the pin to the coating without grossly affecting the properties of the film or film/substrate interface (13). The topple test, a variation of the pull test, is designed to overcome the problem of applying a force normal to the coating surface. The topple test consists of bonding a notched bar to the

coating and then applying a horizontal force to the bar at a specified height such that one leg of the bar is in tension and the other is in compression (13). Adhesion is measured as the force that causes the bar to "topple" when the coating fails (13). This test is also subject to problems associated with modifying coating properties when bonding the bar to the coating surface (13).

Problems associated with evaluation of adhesion data can be as complex as the problems associated with the various testing methods. The failure mechanisms involved in each test are different, so it is not reasonable to quantitatively compare values between the different tests. Problems may arise due to the particular coating/substrate combination and the parameters used during the coating deposition as seen below.

Adhesion of evaporated Al coatings on some materials may increase with time. Work by Weaver (14) indicates that the adhesion of Al on some plastics increases with time. Although the mechanism for this is not completely understood, it is believed to arise from charge transfer interactions at the interface (14). Work by Laugier (15) and Mattox (16) indicates that adhesion of evaporated aluminum on glass increases with time. The mechanism for this increase has been described as migration of oxygen to the interface leading to the formation of an oxide bonding layer in a more extended reaction zone (15, 16). The effect of increased adhesion caused by an extended reaction zone was also observed by Collins, Perkins, and Stroud (17) when they bombarded Al on glass with ions in the energy range 80-120 keV to increase interfacial width. In these cases, adhesion

variation with time may not be easily distinguishable from a variation in processing parameters.

Interfacial intermetallic compounds may also make interpretation of adhesion data difficult. Teer and Salem (8) deposited Al on Ti with suitable parameters to develop a 5 micron wide interfacial region composed of $TiAl_3$ and solid solution Al in Ti. The interfacial region was very adherent to both the Al and the underlying Ti (8). The wear and friction properties of the interfacial material were found to be superior to both Al and Ti and the material was found to inhibit galvanic corrosion when the Al coating was removed and the Ti (coated with interfacial material) was coupled to Al alloys (8). Microhardness tests on these specimens indicated the Al film had a hardness of 80 kg/sq mm, the interface had a hardness of 500 kg/sq mm, and the Ti substrate hardness was 350 kg/sq mm (8). Scratch adhesion testing of this sample would indicate coating failure when the Al coating is penetrated; yet the interfacial material with its superior properties would not have failed.

It is clear that no single adhesion test is applicable for every situation. Adhesion tests should be designed to mimic the conditions the coating will be subjected to in service. In service, coatings may be subjected to abrasion, pull forces, peeling forces, corrosive atmospheres, and thermal cycling (13). Adhesion under these conditions is only one parameter reflecting the durability of the film (13). From a practical point of view, it is probably better to develop tests of coating durability in service like conditions rather than generic adhesion tests (13).

Adhesion forces at interfaces ultimately arise from the summation of interatomic bonding forces that exist when atoms are brought near each other. A diagram of interatomic force and energy as a function of distance for a pair of atoms is shown in figure (2). The magnitude of the attractive interaction between the atoms will determine the bond energy between the atoms. Physical interactions (as in physisorption) have energies of several tenths of an eV and chemical interactions (as in chemisorption) have energies up to about 10 eV (13).

Macroscopic effects such as increased contact area due to surface roughness will result in more interfacial bonds over the same apparent area and will give better bonding if the roughness is not accompanied by detrimental effects such as severe film stress (13). Surface roughness may also decrease adhesion by allowing self-shadowing mechanisms to operate during deposition thereby leaving some regions of the substrate uncoated (13).

Adhesion mechanisms may be divided into 4 basic types depending on the substrate surface finish and the various substrate/coating interactions which can arise from specific coating/substrate chemical interactions and/or deposition parameters. The four basic mechanisms according to Chapman (13) are: 1) two distinct film and substrate materials meet at a well-defined, chemically and structurally abrupt interface; 2) interdiffusion between the two materials or solubility of one or both materials in the other causes the interface to be chemically or structurally graded; 3) the coating and substrate are separated by one or more intermediate layers of either intermetallic compounds

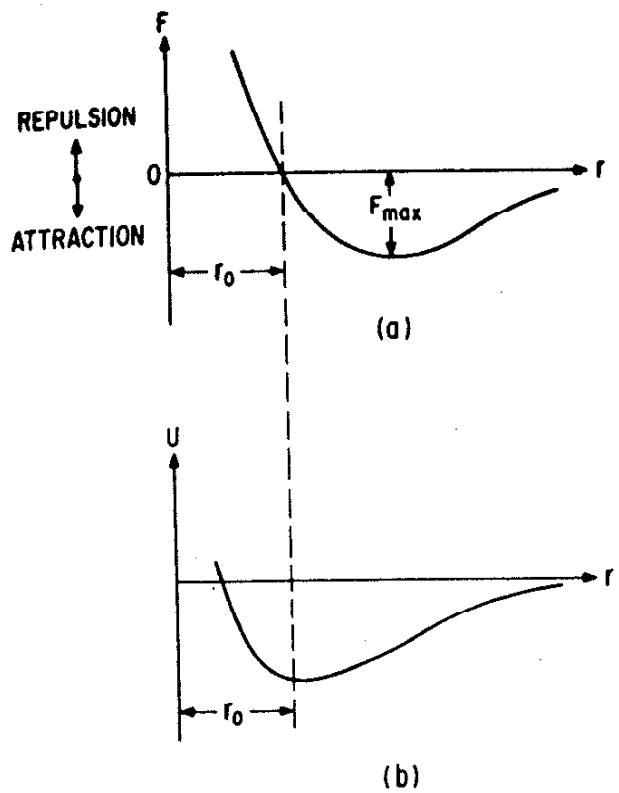

Figure 2. Variation of (a) interaction force and (b) interaction energy for 2 atoms. From Chapman (13).

or compounds such as oxides; and 4) adhesion occurs by mechanical interlocking of the coating into the substrate because the surface is never completely flat.

II.D. DEPOSITION TECHNOLOGIES

Aluminum coatings have been deposited both by chemical vapor deposition (CVD) and physical vapor deposition (PVD). PVD, the emphasis of this thesis, is generally divided into sputtering, evaporation, and ion plating. The coating microstructure will depend on deposition parameters such as residual gas pressure and effective substrate temperature. A schematic representation of the effect of residual argon pressure and substrate temperature on coating structural zones is shown in figure (3) from Thornton (18). In general, it can be seen from figure (3) that decreasing residual gas pressure and increasing substrate temperature promotes the formation of a denser coating microstructure. Dense coating microstructures are generally desirable; however, elevated substrate temperatures to achieve this may cause damage to the substrate properties. A counter example to this would be catalytic applications where the increased surface area associated with a porous coating may be desirable.

II.D.1. CHEMICAL VAPOR DEPOSITION

CVD generally involves the thermal decomposition of metal bearing organic compounds such as tri-isobutyl aluminum resulting in deposition of the metal on the substrate (1). Thermal energy for this process may be provided by heating the substrate, laser

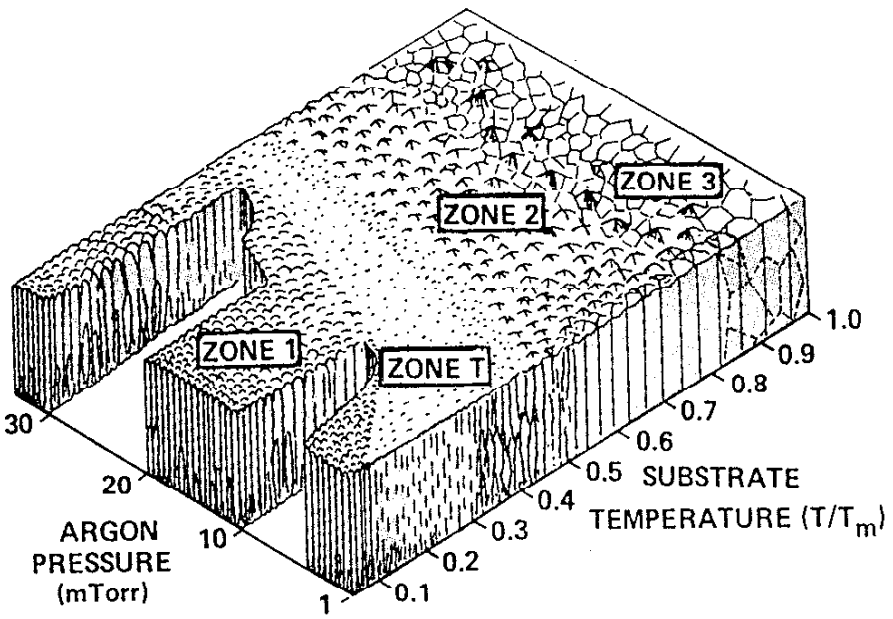

Figure 3. Schematic representation of the influence of substrate temperature and argon working pressure on the structure of metal coatings deposited by sputtering using cylindrical magnetron sources. From Thornton (18).

photons, a glow discharge (Plasma-Assisted CVD), or other imaginative methods. CVD offers an advantage in metallization deposition due to its ability to deposit materials on complex-shaped surfaces uniformly, thereby providing good step coverage (1). Problems with CVD include incorporation of reaction products as impurities and poor adhesion due to interfacial contamination if adequate steps are not taken to ensure substrate cleanliness prior to deposition. Work by Coad, Dugdale and Martindale (19) indicates that adhesion may be promoted by heating the substrate to 300 Celsius or more to remove organic contaminants prior to deposition; this may or may not have a desirable effect on the substrate microstructure. Substrate cleaning may be effected by ion bombardment (19,20) prior to CVD; this variant is plasma-assisted CVD (PACVD). CVD of W is presently used in production applications; but, CVD of Al has had only limited use in microcircuit fabrication (1).

II.D.2. SPUTTER DEPOSITION

The sputter deposition process uses energetic ions from a glow discharge to volatilize target atoms to be deposited onto the substrate (1, 21). A schematic of a DC sputter deposition system is shown in figure (4). The power supply is not restricted to DC; radio frequency (RF) power supplies may also be employed to allow sputtering of insulators (1,21). DC magnetron sputter sources employ magnetic fields to trap secondary electrons emitted from the target to increase ionization in the glow discharge, increase target erosion rates, and correspondingly increase deposition rates at the substrate (1, 21, 22). The physics of the process are

discussed by Chapman (21) and Thornton (22). Advantages of the magnetron source include high deposition rates and magnetic shielding of the substrates from energetic electron bombardment (21, 22). Biased sputtering is a modification of the sputtering process whereby a bias up to several hundred volts is imposed on the substrate to subject it to ion bombardment during deposition (21, 23). Work by Park, Zold, and Smith (23) indicates that bias sputtering improves step coverage of Al films. Problems with sputter deposition include arcing, difficulties in target cooling (especially in magnetrons), and target contamination (by oxides and fixture materials) (21). Argon pressures during sputtering are typically on the order of 10^{-3} Torr (0.13 Pa) (1).

II.D.3. EVAPORATION

Evaporation methods for Al involve heating the metal until vaporization occurs and condensing the vapor onto the substrate. Evaporation is generally carried out in vacuum of 10^{-6} Torr (1.33×10^{-4} Pa) or better to reduce contamination and to reduce gas scattering of coating atoms thus providing higher deposition rates (1). Sources of heat may include inductive heating, resistance heating, laser beams, and electron beams (1). Evaporated Al coatings typically have a columnar structure with submicron grain sizes and a strong (111) fiber texture (1). Work by Hartman (24) indicates that the resistivity of evaporated Al coatings is higher than that of bulk Al and approaches the bulk value as coating thickness increases. The deviation from the bulk value was found to be due to effects of contamination and porosity (24). The fibrous,

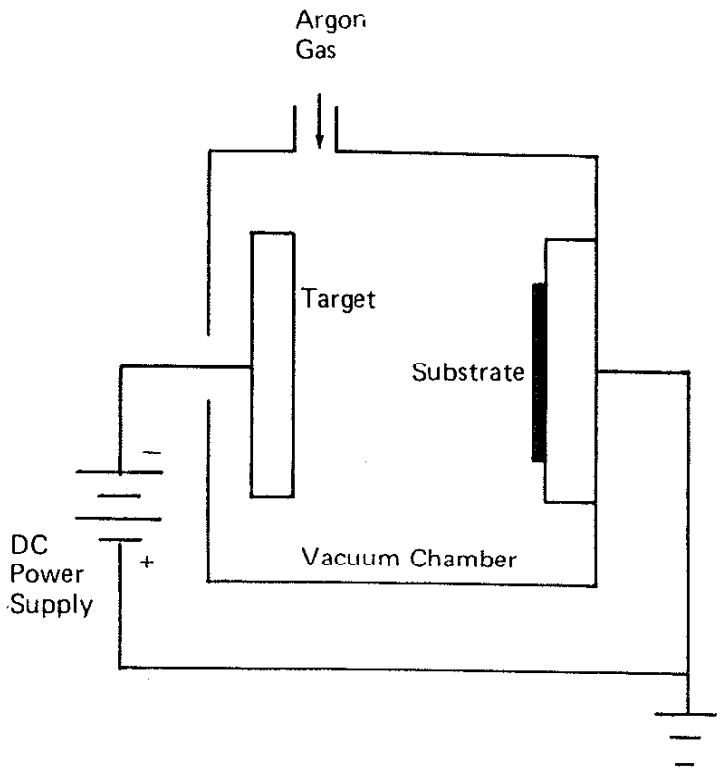

Figure 4. Schematic of a DC sputtering system. From Chapman (21).

columnar structure of evaporated Al coatings deposited at low substrate temperatures arises from active self-shadowing mechanisms during deposition (25). Dirks and Leamy (25) successfully used atomistic computer simulations of evaporation to show the formation of a columnar, fibrous structure with intercolumnar porosity due to a self-shadowing mechanism. Crack formation at substrate surface steps due to shadowing effects has been computer modelled by Blech (26). Work by Learn (27) indicates that increasing substrate temperature during evaporative deposition promotes better step coverage; this effect may also be inferred from the zone model in figure (3). Deposition rate and geometry can affect the grain size and thus the properties of evaporated Al films. Work by Barna and co-workers (28) indicates that a directed evaporant source (as opposed to a point source) gives a finer coating grain size. Work by Dhere and co-workers (29, 30) indicates that evaporated Al grain size increases with deposition rate up to rates of about 10^5 angstroms per minute (10^4 nm per minute) and then shows a decrease.

II.D.4. ION PLATING

Ion plating is a plasma-assisted physical vapor deposition process that combines elements of evaporation and sputtering. The ion plating process was first described by Mattox (20) in 1963. The ion plating process involves making the substrate the cathode of a glow discharge to subject it to sputter erosion and then exposing it to a coating vapor flux while maintaining the discharge. For coating growth to occur, it is necessary that the condensation rate of the

coating vapor be greater than its sputter removal rate. Ion plating provides improved coating adhesion due to sputter removal of surface contaminants prior to deposition and physical mixing of coating and substrate atoms at the interface by ion bombardment. Coating vapor sources for the ion plating process may include metal bearing gases, magnetron sputter sources, and evaporation sources. Ion plating is typically carried out in a vacuum of several millitorr, which is achieved by evacuating to a pressure of 10^{-6} Torr (1.33×10^{-4} Pa) or better and then backfilling with an inert gas such as argon to the working pressure. Ion plating is discussed in detail in appendix A (references 8, 9, 18, 20, 21, 25, 26, and 34 - 46), and a chronological review of some of the literature relevant to ion plating of aluminum coatings is presented in appendix B (references 1 - 135).

II.D.5. IMPURITY INCORPORATION

Incorporation of impurity atoms into a growing film is an important consideration in all deposition technologies. Maissel (31) gives the general expression for the fraction f_i of impurity species i trapped in a film as

$$f_i = \alpha_i{}^* N_i/(\alpha_i{}^* N_i + R) \qquad (1)$$

where N_i is the number of atoms of species i bombarding unit area of the growing film in unit time, α_i is the effective sticking coefficient of species i and R is the film deposition rate. From this expression we can see that impurity concentration can be minimized

by either increasing the deposition rate R, reducing either α_i or N_i, or both (31).

Sources of gaseous impurities in vacuum deposition systems include residual gasses, vacuum leaks, outgassing, and backstreaming pump oil (32). Impurity gases typically include oxygen, nitrogen, hydrogen, and hydrocarbons (32). In deposition processes such as sputtering and ion plating where the process chamber is backfilled to a "soft" vacuum with an inert gas, contamination of the growing coating may be caused by incorporation of the inert gas and/or impurities in the gas (32). Other sources of impurities may include impurities present in the source metal to be vaporized and deposited and materials sputtered off the substrate holder and/or other biased parts within the vacuum chamber. Work by Love and Bower (33) on electron beam evaporated Al showed the following sources of contamination: Fe from the saw used to cut the source material; F from the acid used to clean the source material; Si from backstreamed diffusion pump oil; Cu from the high voltage leads to the e- beam gun and the water cooled Cu hearth; Ag from the soldered connectors on the leads; Na, Cl, and Mg from handling the source material.

Incorporation of impurities in the coating material is not always undesirable. In the case of Al coatings for conductive paths on Si computer chips, small additions of Si are sometimes made to reduce the rate of interdiffusion at the junctions and small additions of Cu and Mg are made to reduce electromigration. Reactive evaporation utilizes relatively high pressures of reactive gasses such as oxygen and nitrogen to produce fully oxidized or

nitrided metal films (34). Impurity additions to Al often reduce its natural corrosion resistance so it is important to weigh improvements in other coating properties (electromigration and interdiffusion resistance) against problems associated with reduced corrosion resistance.

III. EXPERIMENTAL PROCEDURE

III.A. MATERIALS DESCRIPTION

The source material used to grow the films in this work was 99.8% pure aluminum obtained in granular form from Aesar, Inc. The granule size ranged from about 2 - 10 mm in diameter. The granules were consolidated to a single charge by electron beam melting in a "dry run" prior to coating the substrates. Al was chosen for its properties and applicability as discussed in earlier sections and for the ability to minimize interfacial contamination by lining the inside of the deposition chamber with commercial Al foil which is essentially pure Al.

The substrate materials varied in size shape, composition, and surface condition. Substrate materials included Al, Cu, Formvar, NaCl, Si, and Ti.

Aluminum substrates were fabricated from a 99.9% pure Al ingot cold rolled to less than 0.89 mm thickness. Surface conditions included as cold rolled (tarnished), chemically washed (clean), and heavily oxidized (annealed in air).

Copper substrates were fabricated from commercial OFHC copper sheet. Thicknesses used were 0.89 mm and ~ 130 μm (5 mils). Surface conditions included as received (tarnished), chemically etched, and chemically polished.

Formvar substrates were fabricated by dipping chemically polished copper substrates into a Formvar - Chloroform solution and then allowing the Chloroform to evaporate. Coatings were then deposited onto the copper backed Formvar.

NaCl substrates were fabricated by cleaving from single crystal laser windows.

Si substrates were fabricated by cleaving from polished Si single crystal wafers.

Ti substrates were fabricated from 99.7% pure Ti foil 0.89mm thick. Surface conditions included as received (tarnished) and chemically polished (clean).

III.B. DESCRIPTION OF COATING FACILITIES

The films used for this study were grown in the ion plating facility at USA-CERL (United States Army Construction Engineering Research Laboratory) located in Champaign Illinois. The ion plating system itself was built by Torr Vacuum, Inc.. A schematic of the USA-CERL ion plating system is shown in figure (5). The system itself is a split chamber design which allows easy access for both mounting substrates on the substrate holder and loading of source material into the electron beam evaporators. Access to the chamber is attained by lifting the upper chamber with an electric hoist and then pivoting the upper chamber on the hoist axis.

The upper chamber is a water cooled 0.66 m diameter stainless cylinder topped with a circular stainless steel plate. The top plate is bolted to the cylinder and sealing is accomplished with rubber o-rings. The water cooled substrate holder is held by an insulating Teflon feedthrough; the combination of which is designed to allow the source to substrate distance to be varied by raising and lowering the substrate holder. Water and electrical connections to the substrate holder are made outside the vacuum at the top of the pipe

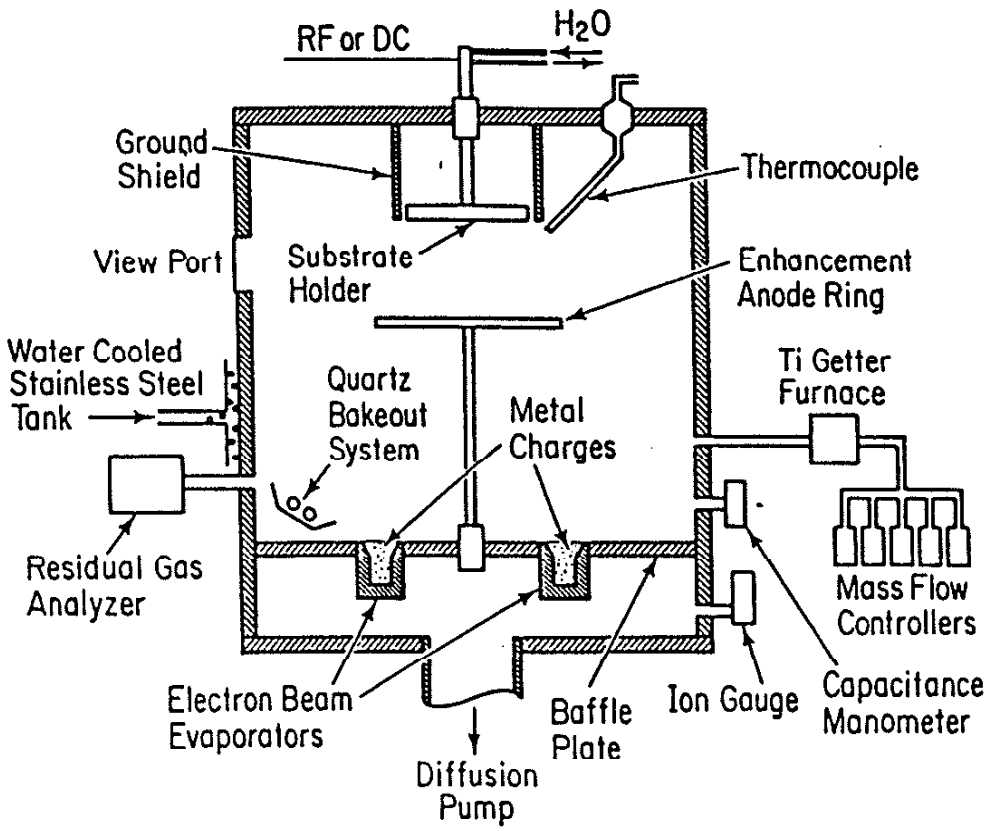

Figure 5. Schematic of the USA-CERL ion plating system.

that feeds through to the substrate holder. Inside the chamber, the substrate holder is surrounded by a ground shield which is attached to the lid. The ground shield extinguishes the glow discharge on the back surfaces of the substrate holder. Observation of the source and substrates during deposition is accommodated by two 0.115 m diameter viewports in the upper chamber. Disposable glass inserts are mounted inside the viewports to collect coating material that would otherwise cover the port windows making them opaque after 1 or 2 deposition runs. There are various other ports in the upper chamber and top to accommodate accessories to the system such as the capacitive manometer for monitoring upper chamber pressure.

The lower chamber is also a water cooled 0.66 m diameter stainless steel cylinder. A 6 inch (15.2 cm) oil diffusion pump opens into the side of the lower chamber and a 10 inch (25.4 cm) oil diffusion pump opens into the bottom of the lower chamber. Both the oil diffusion pumps are backed by a single mechanical rotary pump. Electrical and water feedthroughs for the electron beam evaporation sources mounted in the lower chamber also come through the bottom of the lower chamber. A baffle plate at the level of the evaporation sources provides a limited conductance between the upper and lower chambers. This limited conductance allows processing in the upper chamber at pressures above 10^{-3} Torr (0.13 Pa) while maintaining the lower chamber at pressures below 10^{-3} Torr (0.13 Pa) for extended life of the electron beam source filaments. Pressure in the lower chamber (below the baffle plate) is monitored by an ionization guage. There are various other ports in the lower chamber to accommodate accessories to the system such

as a residual gas analyzer (RGA), a gas inlet from the mass flow controllers, and a chamber vent valve.

The electron beam evaporation sources are powered by a 14 kilowatt Airco Temescal CV14 power supply. A system of interlocks shut down the power supply under conditions such as inadequate vacuum and inadequate cooling water flow rates. Evaporation for this study was generally done from a single source at 9 kilowatts (10 kV beam potential and 0.9 A beam current). The sources are composed of a thermionic emission filament, a magnetic beam deflection system and a water cooled copper crucible to contain the coating source material. The beam is bent through 270 degrees to allow the electron source to be remotely located (below the baffle plate) from the crucible to minimize coating of the filament assembly and maximize the filament life.

Power to the substrate holder (cathode) to sustain the glow discharge for sputter cleaning and ion plating is supplied by a Sloan model 7 power supply. The Sloan allows a maximum voltage of 7.5 kV and a maximum current of 0.75 A d.c. Interlocks prevent access to the cathode from inside or outside the chamber while the power supply is on.

An anode ring for discharge enhancement is powered by four Hewlett - Packard power supplies. Each power supply is rated at 60 V and 5 A and can be run in parallel or series with the others.

Gases used during deposition are controlled by a battery of mass flow controllers which allow 0.1 sccm control over the flow rate in the range of 0 to 50 sccm. Inert gases such as argon can be further purified by a Ti getter furnace in line between the flow

controllers and the vacuum chamber. Gas composition is monitored with a Inficon model 1000 residual gas analyzer (RGA) which samples gas composition from just above the baffle plate. The RGA is equipped with a leak detect mode which allows leaks to be detected by spraying helium around the seal in question and then monitoring the helium signal on the RGA.

III.C. DEPOSITON PROCEDURE

Prior to making a set of coatings, it is generally necessary to first clean out the chamber. Clean aluminum foil is used to cover the chamber walls and fixtures to collect stray coating flux and minimize system down time when the next user needs a clean chamber for a different coating composition as is the case in a multiuser situation. The aluminum foil can be easily installed and removed and it is cheap enough that it can be thrown away unless someone is making coatings with precious metals. Clean gloves and the use of tweezers is encouraged when handling anything inside the clean chamber to minimize substrate contamination and out gassing from fingerprints. When depositing coatings other than aluminum, a "dry run" is usually conducted to coat the substrate holder and the mounting bolts with the material to be deposited and to consolidate the coating source material. Coating the substrate holder and fixtures with the source material prior to deposition on substrates minimizes the possibility of unwanted cross-contamination due to sputtering of the substrate holder; in the case of depositing Al coatings, contamination is minimized by covering everything with aluminum foil which is essentially pure aluminum. Consolidation of

the source material prior to deposition on substrates minimizes the "spitting" which sometimes accompanies the initial melting and causes nodules of the ejected material to be deposited on the substrate surfaces.

After refoiling the system and changing the view port inserts, the substrates are mounted onto the substrate holder. In cases where it is desirable to compare evaporated and ion plated coatings made under nearly identical conditions, substrates can also be mounted onto the chamber walls. Overlapping pieces of silicon wafers may be mounted in various locations to determine coating thickness from step height after deposition. Substrates are attached to the substrate holder by bolting into the pretapped pattern of holes.

When the substrates are mounted, the chamber is closed and evacuated first by the mechanical pump to a pressure of about 150 mTorr (20 Pa) and then by the diffusion pumps to a base pressure of about 10^{-6} Torr (1.33×10^{-4} Pa) or better; the pumpdown sequence is automated and initiated by a single button. Pump down is improved by using the liquid nitrogen cold traps above the diffusion pumps and a thermal bake out system. When sufficient vacuum is acquired, a flow of argon is introduced to the upper chamber to attain the desired working pressure. Sputter cleaning of substrates mounted on the cathode is accomplished by applying a bias of several kV to the cathode which ignites a glow discharge and causes ion bombardment of the cathode surfaces. During the sputter cleaning, the evaporation source(s) is turned on to allow the filament assemblies to warm up. After a suitable sputter cleaning time

(several minutes) the substrate bias is adjusted to the desired value and the evaporation source is powered up to the operating level (generally 0.9 A at 10kV for this work). After a period of time to allow coating formation, the substrate power and the evaporation power is shut down. The chamber is allowed to cool for a few minutes and then vented to atmospheric pressure with nitrogen. When the chamber is opened, the substrates are removed and the set of substrates mounted in their place.

III.D. ANALYTICAL PROCEDURE

III.D.1. ADHESION

A semiquantitative test of adhesion was used to evaluate the film substrate bonding for most of the coatings made in this study. In most cases, this took the form of an epoxy bonded pull stub test. For the Sebastian adherence tester employed in this study, an epoxy coated Aluminum stub is mounted on the coating surface with a spring fixture to apply pressure during the 1 hour 150° C (423 K) epoxy cure cycle. The spring clip is then removed and the sample is loaded into the tester and a tensile force is applied to the stub. If the stub pulls the coating off the substrate or the epoxy fails or some other failure mode occurs at a stress below about 10.5 ksi (72.14 MPa) then the adherence tester gives a value for failure. If no failure occurs, then the sample is assumed to have good adhesion. If failure occurs, then optical and SEM observations can be made to further investigate the failure mode. Numbers generated by the adherence tester give a comparative measure of the variation of

coating adhesion with processing parameters during coating deposition.

A more qualitative test of adhesion employed in this study involves sharply bending the coating/substrate composite and observing the failure surfaces using SEM.

III.D.2. ELECTRON MICROSCOPY

Both scanning electron microscopy (SEM) and transmission electron microscopy (TEM) were used in this study to observe coating and substrate structures. TEM was the major focus for observing details of the coating/substrate interface. The majority of the SEM micrographs were taken using the JEOL U-3 (with EDX) and the ISI DS-130 (with EDX) located in the University of Illinois Center for Electron Microscopy. SEM work was also done on the Jeol JSM-25S in Talbot Laboratory at the University of Illinois and the AMRAY 1610 Turbo (with EDX) at USA-CERL in Champaign Illinois. The TEM micrographs were taken using the Philips EM400 and Philips EM430 analytical electron microscopes located in the Center for Microanalysis of Materials at the University of Illinois.

SEM was used to observe both the thickness and morphology of the coated surfaces at original magnifications up to about 40 kx. EDX data collected during SEM observations were used to determine coating argon content. Specimens observed with SEM included fractured samples, sharply bent samples, adhesion tested samples, and undisturbed samples. A qualitative test of adhesion employed in this study involved sharply bending the coating/substrate composite and observing the failure surface using SEM.

TEM was used to observe the details of coating and substrate structure such as grain size, texturing, dislocations, and intermetallics. Bright field imaging, dark field imaging, selected area diffraction, and EDX techniques were utilized. Original magnifications of micrographs ranged from 60 x to 410 kx. TEM samples included: broadface specimens prepared by thinning from the substrate side and using the thin areas adjacent perforations; broadface specimens prepared by depositing onto a Formvar coated copper substrate and dissolving away the copper or depositing onto NaCl and then dissolving away the salt; and interface specimens prepared by the techniques described in appendix C. The principle of the techniques described in appendix C is that coated substrates are bonded together in a 3 mm diameter tube and stabilized with epoxy so that slices may be cut and thinned to generate electron transparent regions in a plane containing the substrate surface normal so that direct observations of the coating/substrate interface may be made.

III.D.3. X-RAY DIFFRACTION

X-ray diffraction (XRD) was done on diffractometers located in the Center for Microanalysis of Materials and in the Metallurgy and Mining building at the University of Illinois. The diffractometers used were of the single tilt axis type so data interpretation is pretty much limited to answering the following questions: 1) What are the major phases present? 2) Is there a significant (greater than 10%) shift in the lattice parameter? 3) Is there a significant deviation of the coating texture from a random orientation? The

radiation used for all the x-ray diffraction work in this study was copper $K\alpha$ which is a mixture of $K\alpha_1$ and $K\alpha_2$ which have wavelengths of 1.540562 and 1.544390 angstroms (10 angstroms = 1 nm) respectively with the intensity of the Cu $K\alpha_1$ being stronger than that of the Cu $K\alpha_2$.

III.D.4. SURFACE CHEMISTRY

Surface chemistry was evaluated using Auger electron spectroscopy (AES) and secondary ion mass spectroscopy (SIMS) performed on instruments located in the Center for Microanalysis of Materials at the University of Illinois. Both instruments provided information on film cleanliness, and both have the ability to do depth profiling to determine variations in coating chemistry with distance into the sample. The SIMS has intrinsic depth profiling with the probing beam, and the AES has a separate ion beam to do the depth profiling.

III.D.5. SURFACE TOPOGRAPHY

Surface topography was evaluated by the three following methods in this study: 1) using a Tencor Instruments alpha - step profilometer, 2) using SEM, and 3) using TEM. The alpha - step works by moving a diamond stylus along a 3 mm distance on the substrate and monitoring the up and down motion of the stylus; this technique is especially useful for determining coating thickness when a step from the coating to the substrate is produced by masking a portion of the substrate during coating deposition. The alpha step works

best when the coating thickness is greater than the substrate surface roughness.

IV. RESULTS

IV.A. INTRODUCTION

The results of how the ion plating processing variables affect the microstructure, microchemistry, and properties of the coating and the coating/substrate interface are presented in the following subsections. Ion plating and specimen parameters used as variables in this study included; 1) coating/substrate material combinations, 2) substrate surface pretreatment, 3) in-situ sputter cleaning prior to deposition, 4) applied substrate bias during deposition, 5) use of ion plasma density enhancement during deposition, and 6) argon pressure during deposition. Choice of substrate materials and their surface conditions were discussed in an earlier section and summarized in table (2); rationale for the choice of surface conditions will be further discussed in the Discussion section.

Sputter cleaning was normally carried out at 5 kV in 5 mTorr (0.67 Pa) argon pressure for 5 minutes prior to coating deposition. Some specimens were not sputter cleaned. Applied biases to the substrates during deposition included 0, 2.5, and 5kV. 90 volts and 1.2 amps on the enhancement electrode roughly doubled the current to the cathode (substrate holder) from approximately 20 mA at 5 kV to approximately 40 mA at 5 kV with enhancement. Upper chamber pressure was maintained as near as possible to 5 mTorr (0.67 Pa) by varying the argon flow rate during all depositions except those in which the effects of pressure were being studied and a pressure of 20 mTorr (2.67 Pa) was used.

Table 2. Table of substrate surface conditions.

ID/Substrate	Condition	
1 Al	Tarnished	- as-cold-rolled (CR), EtOH rinse
2 Al	Chem etch	- as-CR, 50% KOH wash, 2%$HN0_3$ rinse, EtOH rinse
3 Al	Oxidized	- as CR, 50% KOH wash, dil. acid rinse, EtOH rinse, air anneal at 600 C, EtOH rinse
4 Cu	Tarnished	- as received, EtOH rinse
5 Cu	Chem etch	- as received, 40% HNO_3 wash, EtOH rinse
6 Cu	Chem polish	- as received, 40% HNO_3wash, 6%HNO_3 + 65% acetic acid + 27% H_3PO_4 polish, EtOH rinse
7 Ti	Tarnished	- as received, EtOH rinse
8 Ti	Chem polish	- as received, 20% HNO3 + 20% HF + 50% H3PO4 + 20% acetic acid polish, EtOH rinse

IV.B. EFFECT OF SUBSTRATE BIAS ON ADHERENCE

Coating adherence and coherence were both observed to increase with increasing applied substrate bias. This is shown qualitatively in figures (6) (evaporated aluminum on aluminum) and (7) (5kv ion plated aluminum on aluminum) which are typical of the structures observed with the SEM for evaporated and ion plated aluminum films. Note that for the evaporated structure there is little evidence of plastic deformation at the fracture surfaces between the column boundaries and that there are significant regions where the coating has delaminated from the substrate, indicating that the evaporated coating exhibits higher cohesive than adhesive strength. Also, note that for the ion plated structure, there is extensive evidence of ductile tearing at the column boundary fracture surface and that the coating is well bonded to the substrate.

A numerical demonstration of the effects of substrate bias on coating adherence is given by the adhesion data presented in tables (3) and (4). The average adhesion value for each deposition condition on each substrate is given in table (3); these values are the average of at least 5 tests on each substrate/deposition condition combination presented. Raw data values are tabulated in appendix D. The maximum adhesion value for each deposition condition on each substrate is given in table (5). The mean plus standard deviation adhesion value for each deposition condition on each substrate is given in table (6). The mean plus standard deviation values are calculated by adding one sigma (standard deviation) to the average (mean) value of each set to generate a number that more closely

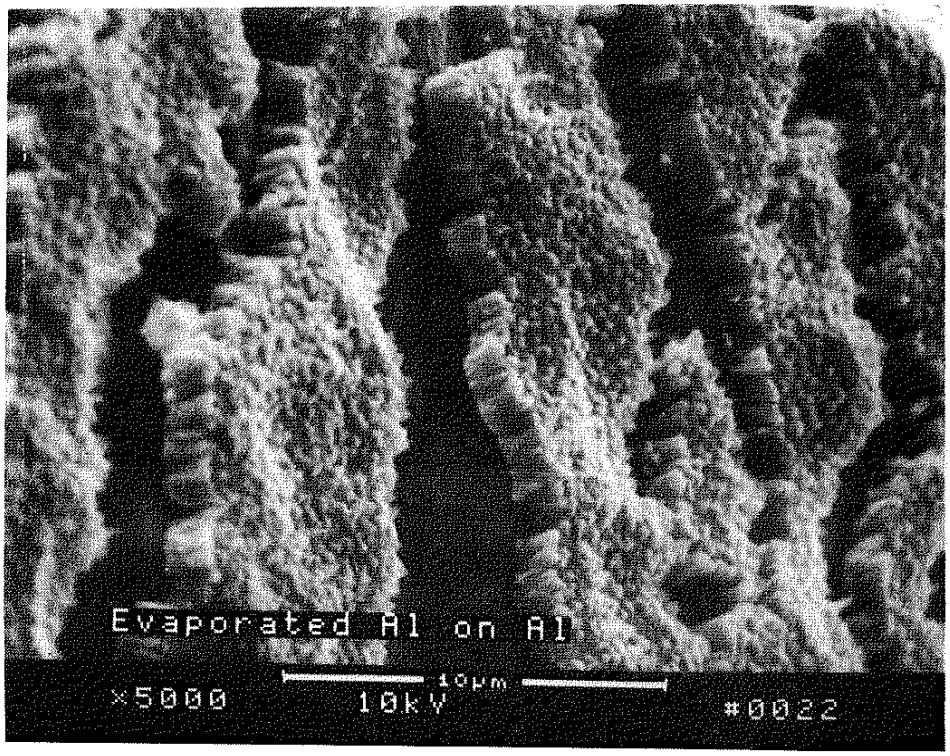

Figure 6. SEM micrograph of evaporated aluminum on chemically etched aluminum bent after coating deposition.

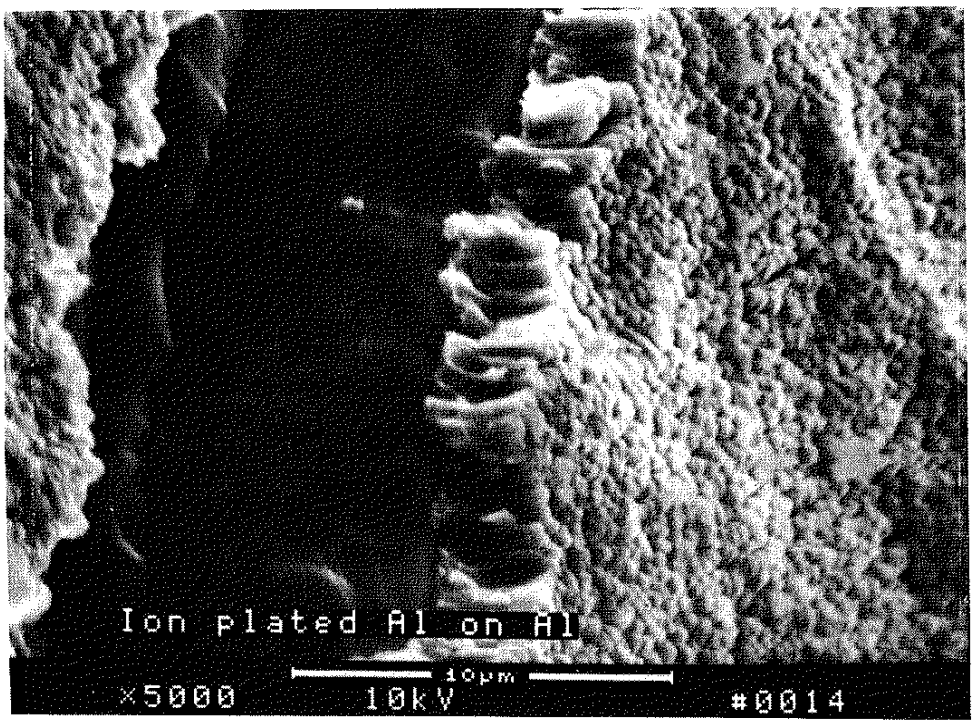

Figure 7. SEM micrograph of aluminum ion plated onto chemically etched aluminum with a 5 kV substrate bias and bent after coating deposition.

Table 3. Table of average values of adhesion in ksi (MPa) for all substrates.

Substrate	Bias only 0kV	Bias only 2.5kV	Bias only 5kV	Enhancement + bias 2.5kV	Enhancement + bias 5kV	Bias + Sputter cleaning 0kV	Bias + Sputter cleaning 5kV
1 (Al)	0.04 (0.27)	0.56 (3.85)	5.05 (34.7)	0.83 (5.70)	1.23 (8.45)	---	---
2 (Al)	1.43 (9.83)	1.59 (10.9)	5.57 (38.3)	8.93 (61.4)	5.91 (40.6)	1.80 (12.4)	4.59 (31.5)
3 (Al)	0.16 (1.10)	2.09 (14.4)	2.37 (16.3)	3.09 (21.2)	2.64 (18.1)	---	---
4 (Cu)	0.00 (0.00)	0.58 (3.99)	0.40 (2.75)	0.27 (1.86)	0.44 (3.02)	---	---
5 (Cu)	0.02 (0.14)	7.54 (51.8)	6.60 (45.4)	6.33 (43.5)	5.33 (36.6)	---	---
6 (Cu)	0.10 (0.69)	6.33 (43.5)	6.48 (44.5)	0.85 (5.84)	5.65 (38.8)	---	---
7 (Ti)	0.00 (0.00)	1.30 (8.93)	3.01 (20.7)	1.80 (12.4)	3.72 (25.6)	---	---
8 (Ti)	0.28 (1.92)	7.08 (48.6)	7.72 (53.0)	5.55 (38.1)	5.69 (39.1)	7.17 (49.3)	10.37 (71.3)

Note. See table (2) for substrate surface conditions.

Table 4. Table of effect of deposition parameters on average adhesion in ksi (MPa) to all substrates.

	Substrate bias		
Parameter	0kV	2.5kV	5kV
Bias only	0.25 (1.72)	3.38 (23.2)	4.65 (32.0)
Enhancement	---	3.46 (23.8)	3.83 (26.3)
Sputter clean	4.49 (30.9)	---	7.48 (51.4)

Table 5. Table of maximum values of adhesion in ksi (MPa) for all substrates.

Substrate	Bias only 0kV	Bias only 2.5kV	Bias only 5kV	Enhancement + bias 2.5kV	Enhancement + bias 5kV	Bias + Sputter cleaning 0kV	Bias + Sputter cleaning 5kV
1 (Al)	0.08 (0.55)	0.78 (5.36)	6.73 (43.8)	1.41 (9.69)	1.49 (10.2)	---	---
2 (Al)	2.45 (16.8)	3.27 (22.5)	8.18 (56.2)	10.40 (71.5)	9.81 (67.4)	3.18 (21.5)	5.10 (35.0)
3 (Al)	0.45 (3.09)	3.10 (21.3)	3.27 (22.5)	5.00 (34.4)	4.34 (29.8)	---	---
4 (Cu)	0.01 (0.07)	1.66 (11.4)	0.74 (5.08)	0.67 (4.60)	1.51 (10.4)	---	---
5 (Cu)	0.09 (0.62)	9.62 (66.1)	9.89 (68.0)	10.08 (69.3)	10.42+ (71.6+)	---	---
6 (Cu)	0.37 (2.54)	9.45 (64.9)	9.47 (65.1)	1.19 (8.18)	10.44+ (71.7+)	---	---
7 (Ti)	0.00 (0.00)	2.39 (16.4)	3.87 (26.6)	3.02 (20.6)	5.68 (39.0)	---	---
8 (Ti)	1.39 (9.55)	10.37+ (71.3+)	9.53 (65.5)	10.52+ (72.3+)	10.49+ (72.1+)	10.38+ (71.3+)	10.39+ (71.4+)

+ denotes adhesion in excess of limit of test device.

Table 6. Table of mean plus standard deviation values of adhesion in ksi (MPa) for all substrates.

Substrate	Bias only 0kV	Bias only 2.5kV	Bias only 5kV	Enhancement + bias 2.5kV	Enhancement + bias 5kV	Bias + Sputter cleaning 0kV	Bias + Sputter cleaning 5kV
1 (Al)	0.08 (0.55)	0.79 (5.43)	6.39 (43.9)	1.35 (9.28)	1.52 (10.4)	---	---
2 (Al)	2.28 (15.7)	2.89 (19.9)	7.68 (52.8)	10.20 (70.1)	10.65 (73.2)	2.96 (20.3)	5.20 (35.7)
3 (Al)	0.34 (2.34)	2.84 (19.5)	3.26 (22.4)	4.96 (34.1)	4.19 (28.8)	---	---
4 (Cu)	0.01 (0.07)	1.27 (8.73)	0.60 (4.12)	0.50 (3.44)	1.04 (7.15)	---	---
5 (Cu)	0.06 (0.41)	9.96 (68.4)	9.80 (67.3)	9.22 (63.4)	9.49 (68.3)	---	---
6 (Cu)	0.26 (1.79)	9.61 (66.0)	9.14 (62.8)	1.08 (7.42)	10.14 (69.7)	---	---
7 (Ti)	0.00 (0.00)	2.25 (15.5)	3.98 (27.4)	2.95 (20.3)	5.36 (36.8)	---	---
8 (Ti)	0.90 (6.18)	9.55 (65.6)	8.78 (60.3)	9.84 (67.6)	10.19 (70.0)	11.01 (75.7)	10.39 (71.4)

represents the real value of adhesion since errors in setting up and conducting the test always act to reduce the measured adhesion value rather than increasing it. The mean plus standard deviation values are close to the maximum values for each data set.

The effects of deposition parameters on the average adhesion for all substrates tested are tabulated in table (4); these values are the column averages of the values presented in table (3). The effect of deposition parameters on the maximum adhesion to all substrates tested is tabulated in table (7); these values are the column averages of the values presented in table (5). The effect of deposition parameters on the mean plus standard deviation adhesion to all substrates tested is tabulated in table (8); these values are the column averages of the values presented in table (6).

The general trend of the adhesion data is that there is an increase in adhesion with increasing applied substrate bias. The use of chemical cleaning and/or sputter cleaning prior to coating deposition gave a further increase in adhesion over that attained by using a substrate bias alone. The use of enhancement during deposition gave a further increase in adhesion over that attained by using bias alone. There is a large amount of scatter in the adhesion values such that the scatter increases with increasing failure stress. This scatter arises from problems in bonding the stub to the coating completely and applying the pull force perpendicular to the substrate surface. More scatter arises from fracture of the epoxy at higher adhesion values. Observed failure modes for the adhesion samples appeared to be dependent on the adhesive strength of the coating. For weakly adherent coatings (adhesion below 1 ksi (6.87

Table 7. Table of effect of deposition parameters on average maximum value of adhesion in ksi (MPa) to all substrates tested.

Parameter	0kV	2.5kV	5kV
Bias only	0.61 (4.19)	5.08 (34.9)	6.46 (44.4)
Enhancement	---	5.29 (36.4)	6.77 (46.5)
Sputter clean	6.78 (46.6)	---	7.75 (53.2)

Table 8. Table of effect of deposition parameters on average mean plus standard deviation value of adhesion in ksi (MPa) to all substrates tested.

Parameter	0kV	2.5kV	5kV
Bias only	0.49 (3.37)	4.90 (33.7)	6.20 (42.6)
Enhancement	---	5.01 (34.4)	6.57 (45.1)
Sputter clean	6.99 (48.0)	---	7.80 (53.6)

MPa)), failure occurred primarily by delamination of the coating from the substrate. For strongly adherent coatings (adhesion above 7 ksi (48.1 MPa)), failure occurred primarily by fracture of the epoxy bonding the pull stub to the coating; this indicates that the actual adhesion of the coating is in excess of what was measured. For intermediately adherent coatings (1 - 7 ksi (6.87 - 48.1 MPa)), failure occurred by mixed fracture of the epoxy, the coating, and the coating/substrate interface.

IV.C. ADHERENCE (SUBSTRATE CONDITION)

The average adhesion values for bias only and enhancement conditions for the various substrate conditions described in table (2) are tabulated in table (9); these are the row averages for the first 5 adhesion values presented in each row of table (3). The average maximum adhesion values for bias only and enhancement conditions for the various substrate conditions described in table (2) are tabulated in table (10); these are the row averages for the first 5 adhesion values presented in each row of table (5). The average mean plus standard deviation adhesion values for bias only and enhancemant conditions for the various substrate conditions described in table (2) are tabulated in table (11); these are the row averages for the first 5 adhesion values presented in each row of table (6). In general, cleaning the substrate surface and removing surface oxides will improve adhesion. Sputter cleaning can be considered a surface condition modifier which improves adhesion as shown in tables (4) and (7). Surface roughness is also a factor as shown by the improvement in adhesion on chemically etched copper

Table 9. Table of effect of substrate condition on average adhesion in ksi (MPa) for all deposition conditions on a given substrate material.

Condition	Substrate material Al	Cu	Ti
Tarnished	1.54 (10.6)	0.34 (2.34)	1.97 (13.5)
Chem polish	---	3.88 (26.7)	5.26 (36.1)
Chem etch	4.69 (32.2)	5.16 (35.5)	---
Oxidized	2.07 (14.2)	---	---

Table 10. Table of effect of substrate condition on average maximum adhesion in ksi (MPa) for deposition with bias only and enhancement on a given substrate material.

	Substrate material		
Condition	Al	Cu	Ti
Tarnished	2.10 (14.4)	0.92 (6.32)	2.99 (20.5)
Chem polish	---	6.18 (42.5)	8.46 (58.1)
Chem etch	6.82 (46.9)	8.02 (55.1)	---
Oxidized	3.23 (22.2)	---	---

Table 11. Table of effect of substrate condition on average mean plus standard deviation adhesion in ksi (MPa) for deposition with bias only and enhancement on a given substrate material.

Condition	Substrate material Al	Cu	Ti
Tarnished	2.03 (13.9)	0.68 (4.67)	2.91 (20.0)
Chem polish	---	6.05 (41.6)	7.85 (53.9)
Chem etch	6.74 (46.3)	7.71 (53.0)	---
Oxidized	3.12 (21.4)	---	---

over chemically polished copper in tables (9) and (10).

IV.D. COATING THICKNESS

Coating thicknesses for various coating runs were generally in the range of few thousand angstroms (few hundred nanometers) to about 2 μm. There was some variation in thickness from run to run due to variations in the deposition parameters (time, electron beam current, etc.) and a variation in thickness from substrate to substrate within a given run due to geometry effects (cosine distribution, shadowing, etc.). Sets of overlapping silicon substrates were mounted in each of four quadrants of the substrate holder to generate steps for profilometer thickness measurements after coating. At least 20 step heights were measured at random locations on each of the coated silicon substrates to determine a coating uniformity quality factor, Q. Q is defined as the average of the coating thicknesses for a given processing condition for the 4 Si test substrates divided by the standard deviation in the thickness measurements; this is simply the reciprocal of the "relative deviation" in statistical terms. A high value of Q would indicate a reasonably uniform coating thickness distribution. For this experiment, the Q for ion plating was found to be 2.839 and the Q for evaporation was found to be 2.677. The difference between the two is about 6%. The substrate holder area is less than 0.25 steradians of the source. Values for Q were also calculated using the data presented by Chevallier in reference (63) for Ir on a graphite crucible. The Q for Chevalliers evaporated coating was 1.2456 and

the Q for his ion plated coating was 1.6041, a difference of about 28%.

IV.E. ARGON INCORPORATION

Argon incorporation in the coatings was found to increase with increasing applied substrate bias and increasing argon background pressure during deposition as shown in table (12). Table (12) was obtained from semiquantitative analysis of EDX data collected from the coatings. It should be noted that these values are near the lower limit for EDX detection so the absolute values may not be accurate; but, the relative values and trends should still hold.

IV.F. ION PENETRATION (BIAS)

The average penetration of ions of a given energy in the substrate materials was calculated using the computer program PRAL written by J. Ziegler, et al. (reference (41)). The results for aluminum and argon ions are tabulated in tables (13) and (14). "m" is the mean penetration of the ions in angstroms and "m+s" is the mean penetration plus a straggle distance. The straggle distance is an indication of the statistical fluctuation in the ion penetration depth about the average value due to variations in the number of collisions encountered and the distance between collisions encountered for individual penetrating atoms. In general, the depth of penetration increases at a decreasing rate as the ion energy increases. The average ion penetration for substrate biases used in this work is on the order of 10 nm or less.

Table 12. Table of argon incorporation in atomic percents for aluminum coatings deposited at listed substrate biases and argon working gas pressures.

	Bias (kV)		
Pressure (μ)	0.0	1.0	2.5
5	---	---	0.244
20	---	0.170	0.275

Table 13. Table of aluminum ion ranges in various substrate materials.

	Substrate material			
z	13	14	22	29
keV	Al	Si	Ti	Cu
1 m	30	33	24	14
m+s	51	52	43	27
2 m	49	51	37	22
m+s	78	80	66	41
3 m	65	68	49	29
m+s	102	104	86	53
4 m	80	84	60	35
m+s	124	127	104	64
5 m	95	99	71	41
m+s	146	148	122	75

Ranges in angstroms as calculated by PRAL written by J. Ziegler, et al., The Stopping and Range of Ions in Solids, V1, Pergamon, New York, 1985.

Table 14. Table of argon ion ranges in various substrate materials.

	Substrate material			
z	13	14	22	29
keV	Al	Si	Ti	Cu
1 m	29	31	22	12
m+s	45	47	38	23
2 m	44	47	33	19
m+s	67	70	56	34
3 m	57	61	43	25
m+s	86	89	71	44
4 m	70	73	52	30
m+s	103	107	85	52
5 m	81	86	60	35
m+s	120	124	99	61

Ranges in angstroms as calculated by PRAL written by J. Ziegler, et al., The Stopping and Range of Ions in Solids, V1, Pergamon, New York, 1985.

IV.G. COATING STRUCTURE (BIAS)

The effect of increasing substrate bias during deposition is to promote surface smoothness and intercolumnar bonding as observed in figures (6) and (7) of evaporated and ion plated aluminum on aluminum. Increasing substrate bias also tends to round and smooth off the column tops as opposed to the faceted and pointed column tops that are observed in the evaporated coatings. Figure (8) is a TEM dark field micrograph of evaporated aluminum on Formvar. The star shaped regions were created by coating growth into the surface voids left by bubbles in the Formvar. The peaked surface structure of the evaporated coating can be seen where the columns project into the holes. It is interesting to observe that column growth is not directly into the source direction; but instead has some component of the local substrate surface normal as is evidenced by the columnar structures directed inward in the hole and crater structures in figure (8). Figure (9) is a TEM dark field micrograph of ion plated aluminum on Formvar. In this case, the grain size of the ion plated coating is finer than that of the evaporated coating. The ion plated aluminum on Formvar does not exhibit the peaked structures seen in the evaporated case; however, the structure is still roughly columnar and exhibits a tendency to grow with a component of the local substrate surface normal. Figures (10) and (11) are the corresponding TEM bright field micrographs of the regions shown in figures (9) and (8).

Figure (12) is a dark field TEM micrograph of aluminum ion plated onto a sputter cleaned aluminum substrate with a 5 kV substrate bias. Significant features of this figure are: 1) The

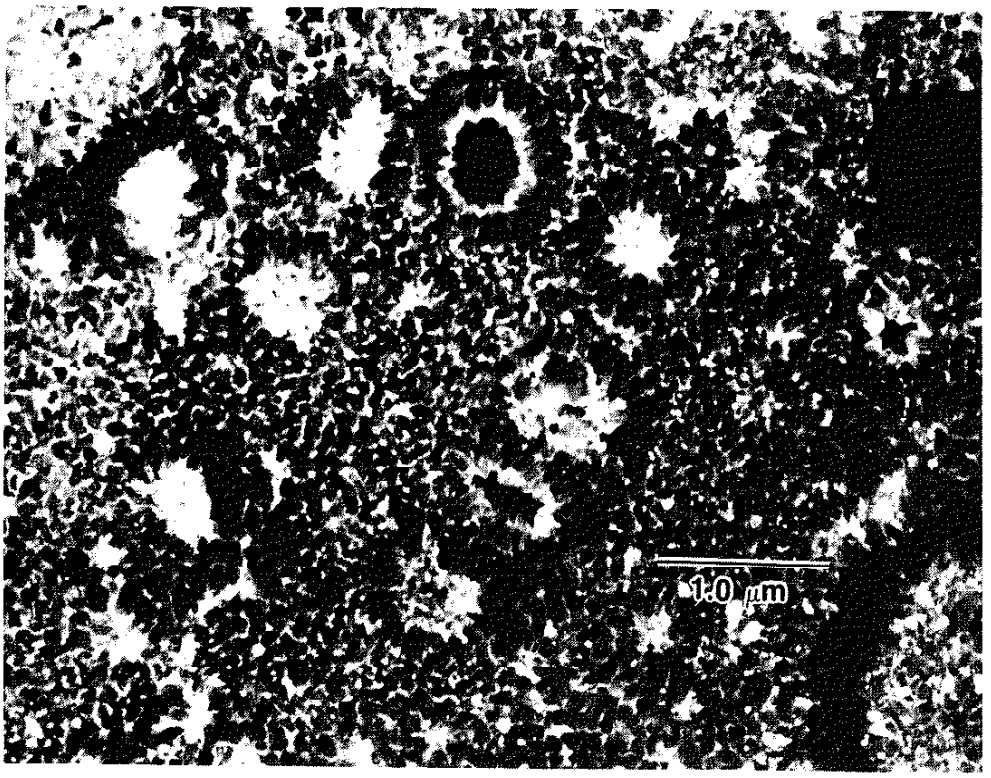

Figure 8. TEM dark field micrograph of evaporated aluminum on Formvar.

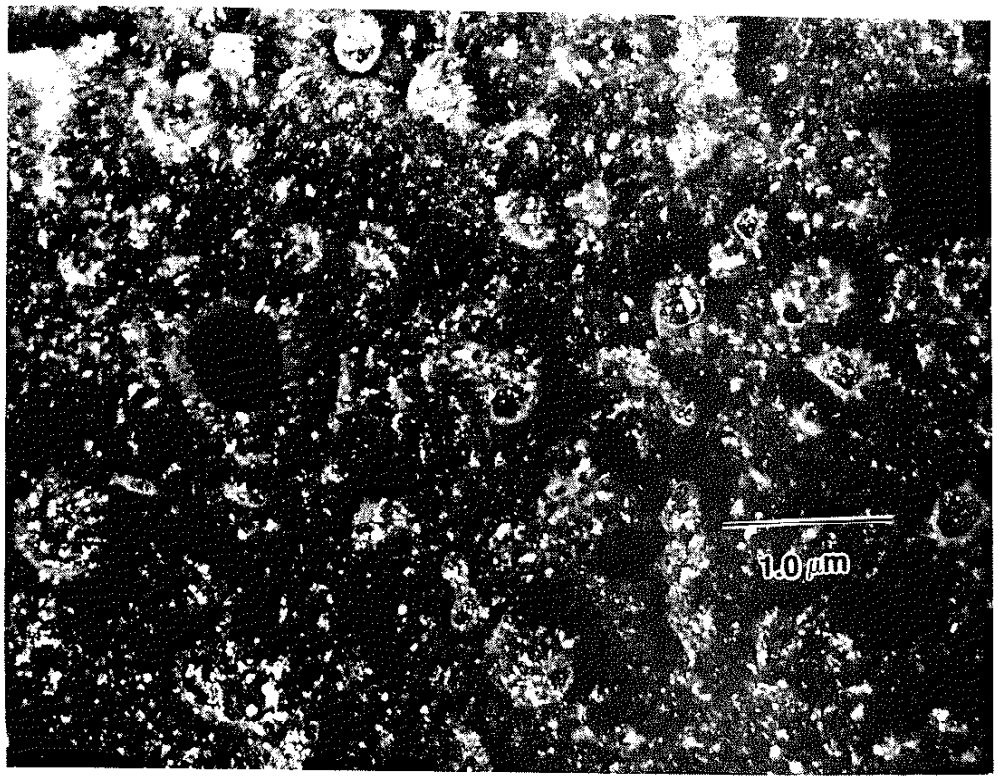

Figure 9. TEM dark field micrograph of aluminum ion plated onto Formvar with a 5 kV substrate bias.

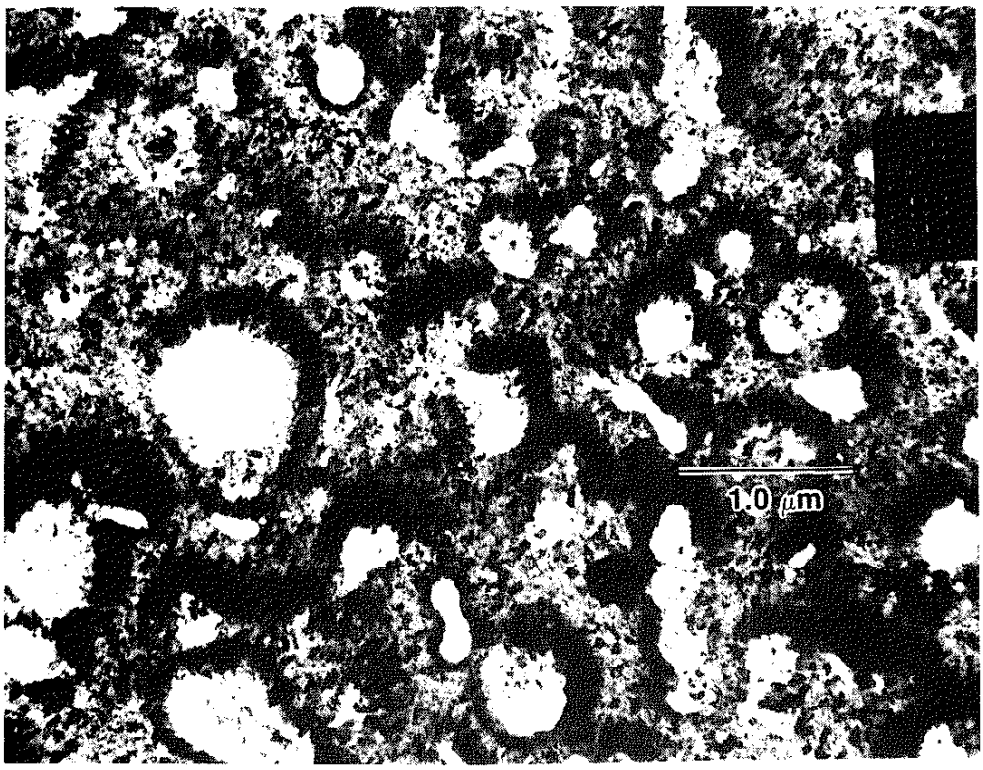

Figure 10. TEM bright field micrograph of aluminum ion plated onto Formvar with a 5 kV substrate bias.

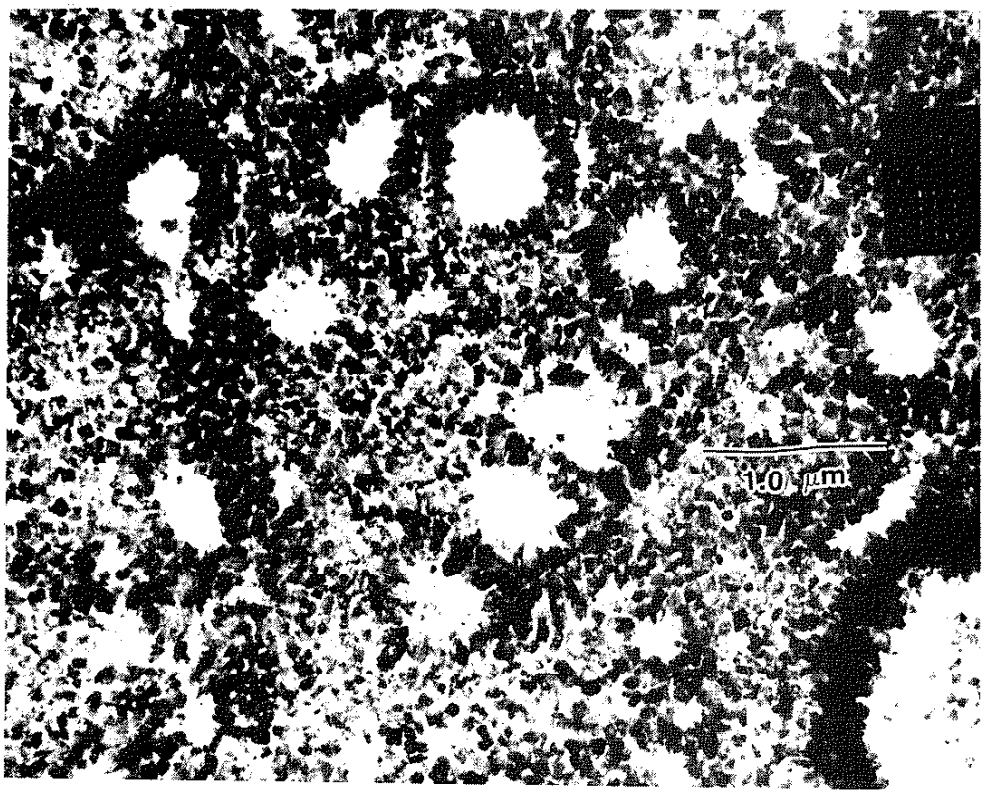

Figure 11. TEM bright field micrograph of evaporated aluminum on Formvar.

Figure 12. TEM dark field micrograph of aluminum ion plated onto sputter cleaned aluminum substrate with a 5 kV substrate bias.

coating grain size is much smaller than that of the substrate. 2) There is a damaged region characterized by a high density of point and line defects in the substrate adjacent to the coating/substrate interface with most of the defects being within the first 700 nm. 3) There is variability in the coating grain size such that the coating grain size closest to the interface is smaller than that away from the interface. 4) Coating growth is in a columnar fashion. 5) The coating surface appears relatively smooth; the column tops do not appear faceted. 6) It does not appear that any single grain extends from the interface completely through the coating. In comparison with figure (7), this indicates that there is a polycrystalline structure within the individual columns of the columnar structure. 6) In contrast with the substrate, very few point and line defects are visible in the coating.

Figure (13) is a very low magnification TEM micrograph of an Al coated and coiled copper foil specimen showing the numerous locations where it may be possible to have thin area in the coating and substrate simultaneously. Figure (14) is a higher magnification dark field view of one of the regions in figure (13) showing that is is not simple to attain electron transparency in the substrate and through the entire coating thickness for materials with different sputter yields.

Figure (15) is a dark field TEM micrograph of aluminum ion plated with a 5 kV substrate bias onto a sputter cleaned copper foil substrate. Significant features of this figure are: 1) The grain size of the "coating" grains is smaller than that of the substrate. 2) The "coating" grains are not pure aluminum; but rather, some compound

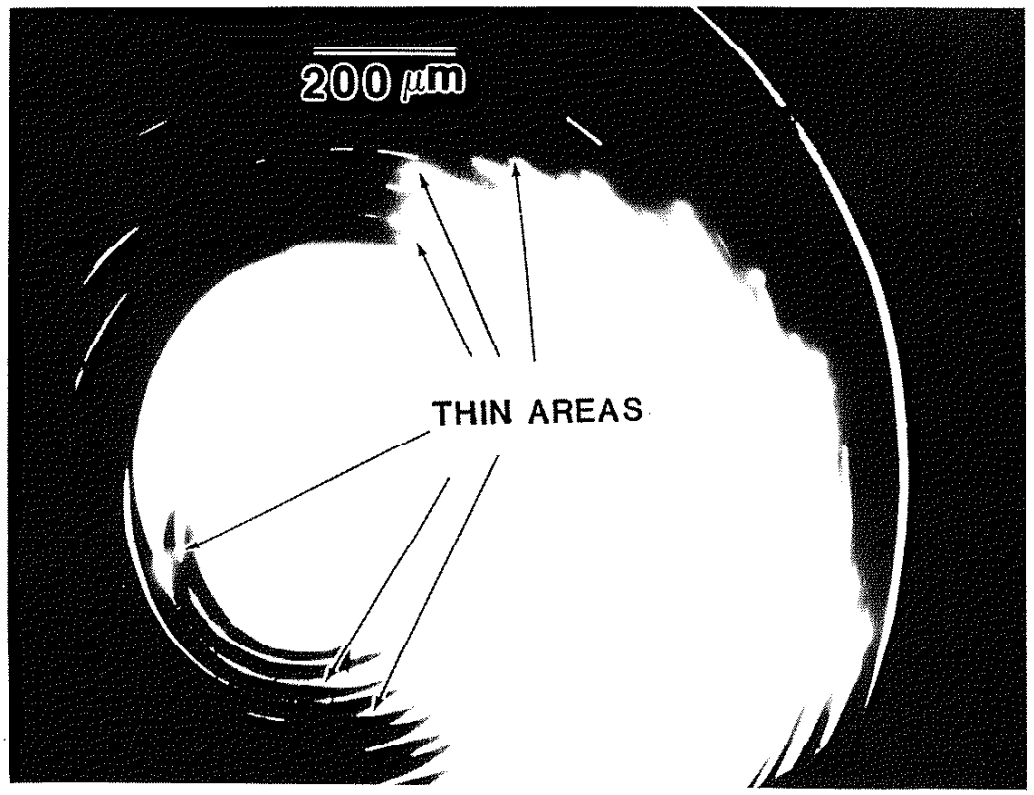

Figure 13. Low magnification TEM micrograph of aluminum coated and coiled copper foil specimen showing the numerous locations where it may be possible to have electron transparency in the coating and the substrate simultaneously. Aluminum ion plated at 5 kV substrate bias.

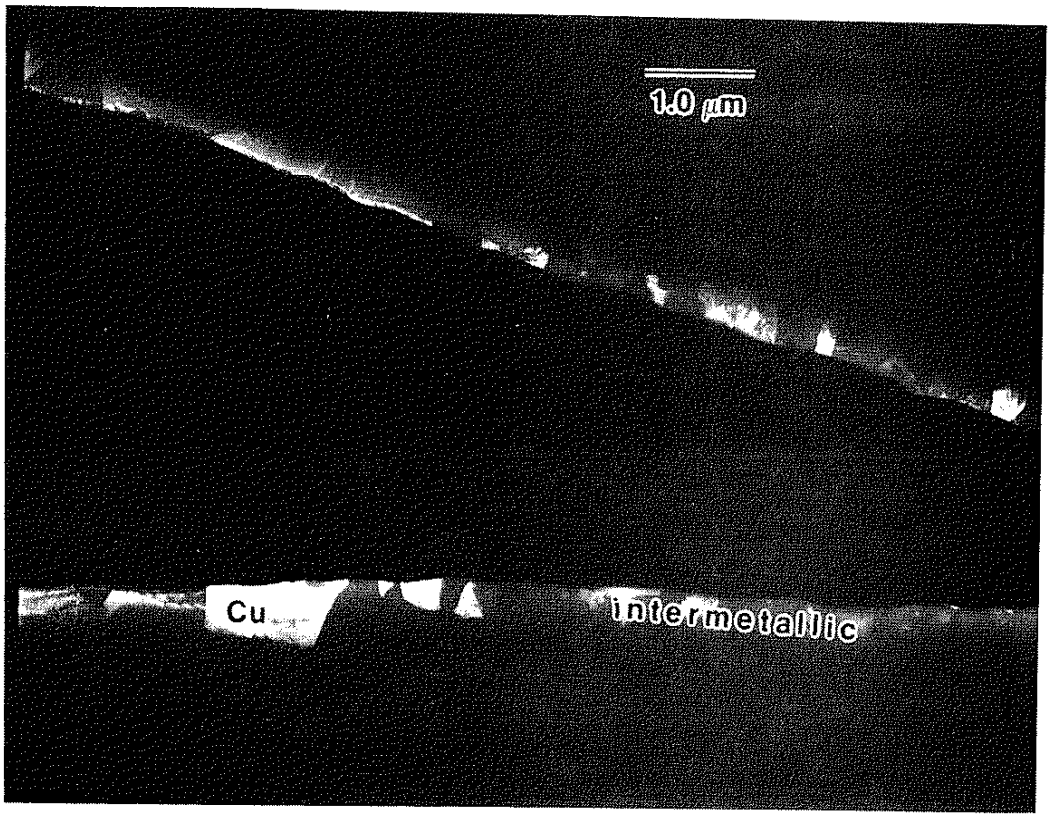

Figure 14. TEM dark field micrograph of ion plated aluminum on copper foil (5 kV substrate bias) showing that electron transparency does not occur at the interface and the full coating thickness in the same region.

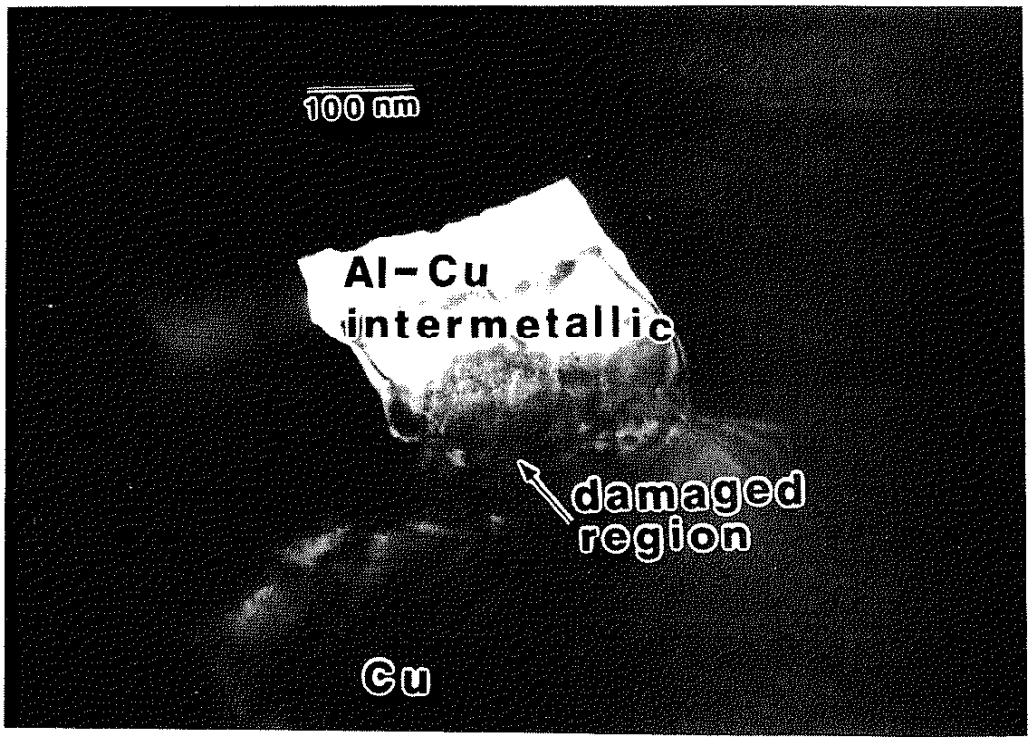

Figure 15. TEM dark field micrograph of aluminum ion plated onto a sputter cleaned copper foil substrate with a 5 kV substrate bias.

of aluminum and copper. 3) The thickness of this compound layer is at least an order of magnitude larger than could be formed by simple ion penetration indicating that some form of ion enhanced diffusion has occurred. 4) Point defects and line defects are visible in the interfacial region.

Figure (16) is a dark field TEM micrograph of ion plated aluminum onto a sputter cleaned copper foil substrate with a 5 kV substrate bias. Figure (16) was obtained by tilting and translating slightly from the region in figure (15). Figure (17) is a bright field of the same region. Figure (18) is a diffraction pattern taken from the same region indicating the low angle of tilt between individual grains of the coating. Diffraction patterns from the interfacial regions of these coatings do not all index simply to any known compound of aluminum and copper. The interfacial material may be a supersaturated compound due to the effects of ion bombardment during coating deposition.

Figures (19) and (20) are bright field and dark field TEM micrographs of evaporated aluminum on copper foil. Significant features of these figures are: 1) the coating/substrate interface is very abrupt. 2) The grain size of the coating is small compared to that of the substrate. 3) Line defects are visible in both the coating and the substrate. 4) There is no appreciable concentration of defects at the interface. 5) There is no appreciable evidence of a concentration of point defects in either the coating or the substrate.

Figure (21) is a dark field TEM micrograph of evaporated aluminum on NaCl. The sample was prepared by evaporation onto a freshly cleaved salt surface and then dissolving away the salt and

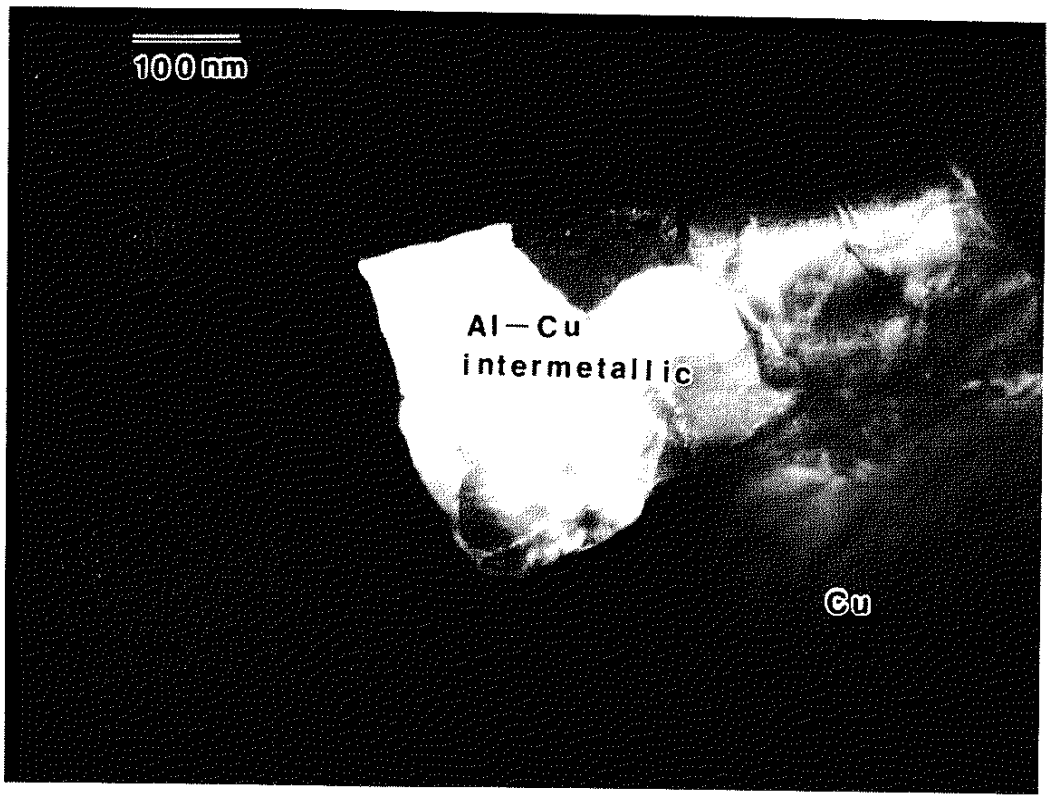

Figure 16. TEM dark field micrograph of aluminum ion plated onto a sputter cleaned copper foil substrate with a 5 kV substrate bias.

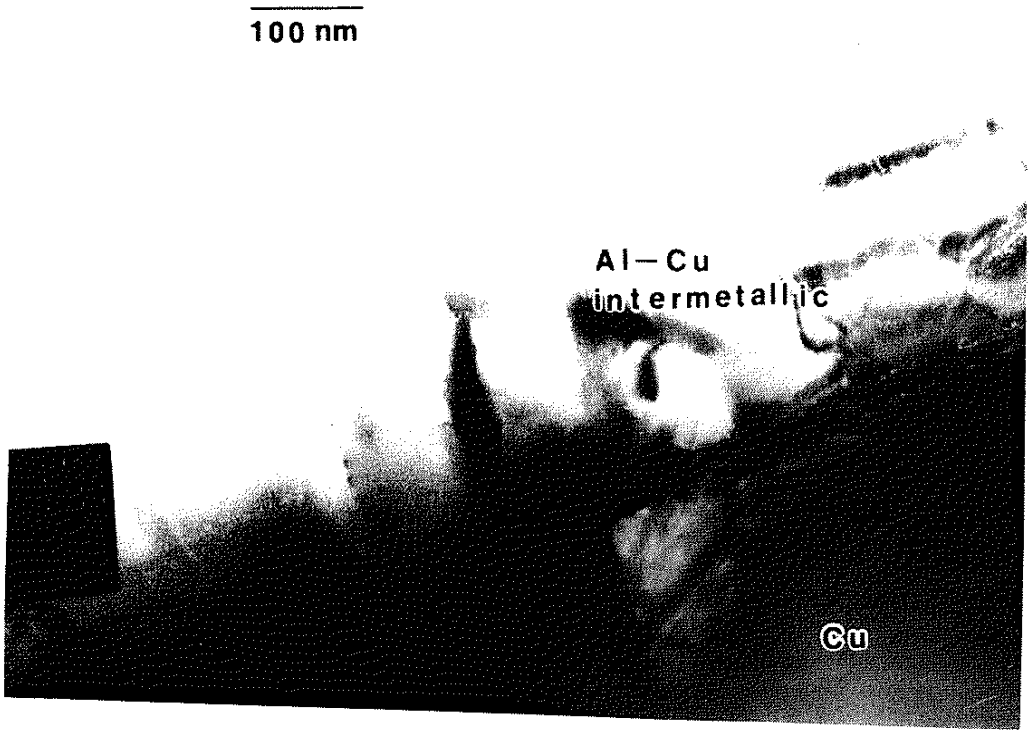

Figure 17. TEM bright field micrograph of same region as in figure (16).

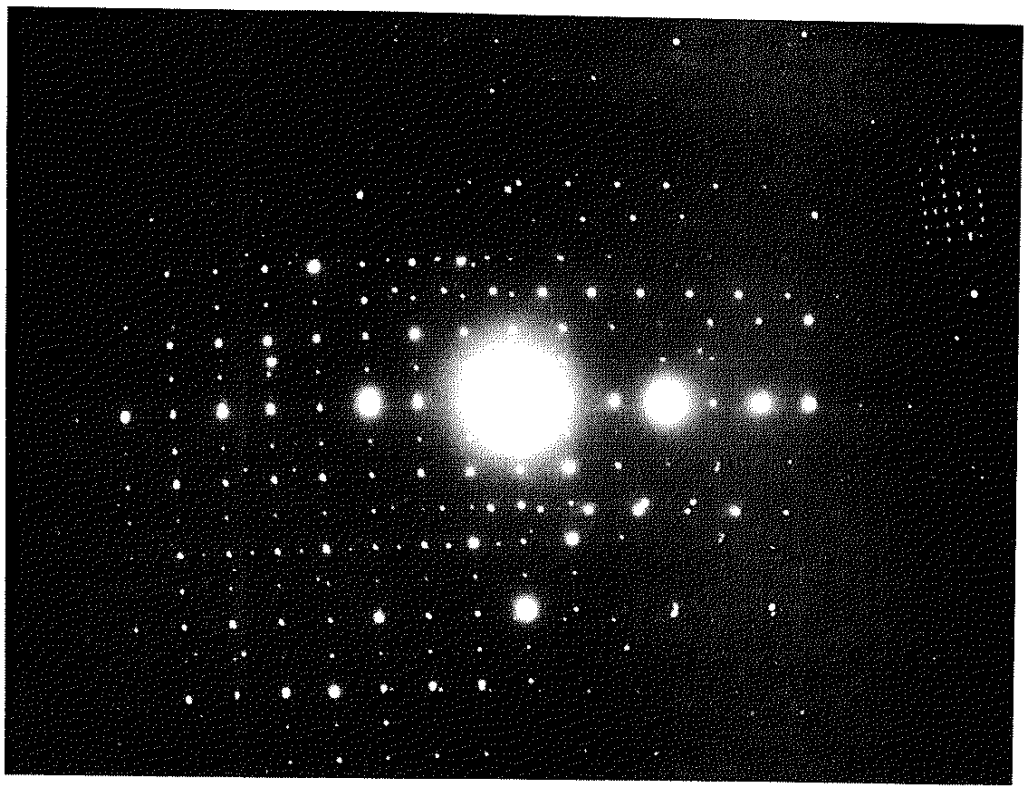

Figure 18. Electron diffraction pattern from region in figure (16) showing low angle tilt between intermetallic grains.

collecting the film with TEM screened grids. The maximum grain size in this figure appears to be about the same as that observed for evaporated aluminum on Formvar in figure (8).

Figure (22) is a dark field TEM micrograph of ion plated aluminum on NaCl. The maximum grain size in this case is larger than the corresponding ion plated coating on Formvar shown in figure (9). A possible explanation for this is the increased substrate current density that was observed for deposition on NaCl as compared with deposition on Formvar and metallic substrates under otherwise identical conditions. The average current density when depositing on the NaCl was at least 5 times that observed for depositing on other substrates. Average substrate holder current densities for several conditions are tabulated in table (15). The increased heating associated with the increased current density may allow recrystallization of the growing coating; in addition, the additional damage associated with an increase in the rate of ion bombardment may add a further driving force for recrystallization. Ion plated aluminum on NaCl appears to have a large distribution in grain sizes ranging from the fine grains observed in ion plated coatings on Formvar to the large recrystallized grains which are larger than any of the grains observed in evaporated coatings.

Figure (23) is a TEM micrograph of ion plated aluminum on NaCl showing the effects of arcing which occurred during the deposition on the coating structure. The arc paths generally occurred in three forms: 1) Fixed points which generally resulted in macroscopic holes (1 or more mm in diameter) being burned completely through the substrate. 2) Straight lines which seem to follow

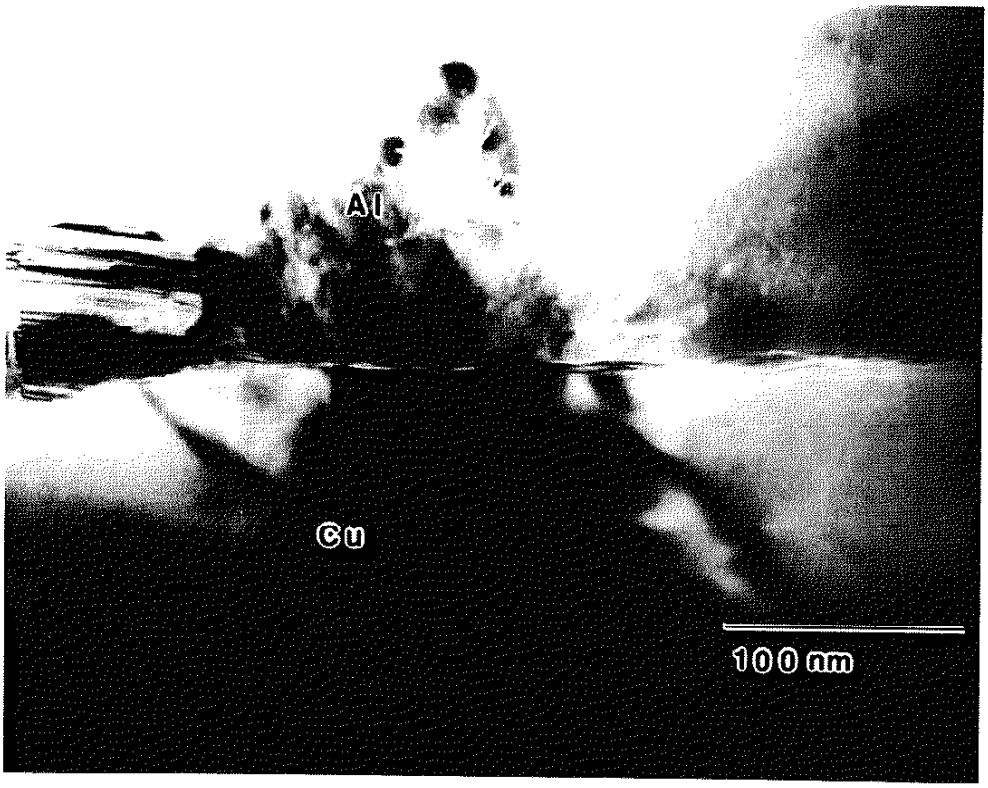

Figure 19. TEM bright field micrograph of evaporated aluminum on copper foil.

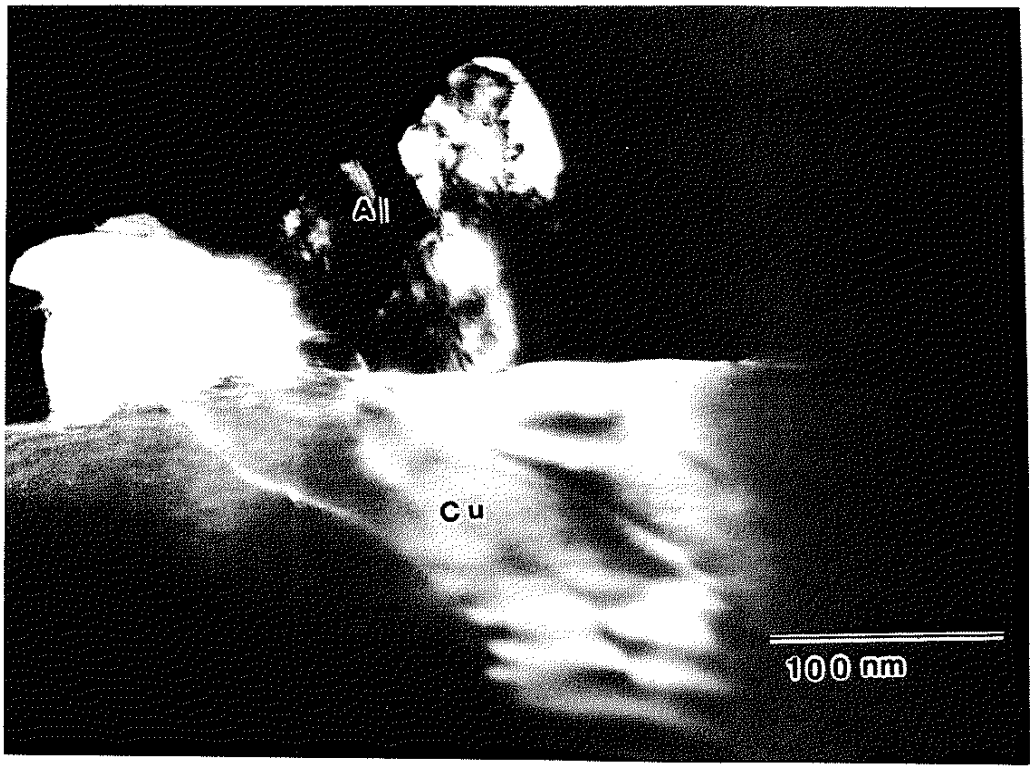

Figure 20. TEM dark field micrograph of evaporated aluminum on copper foil.

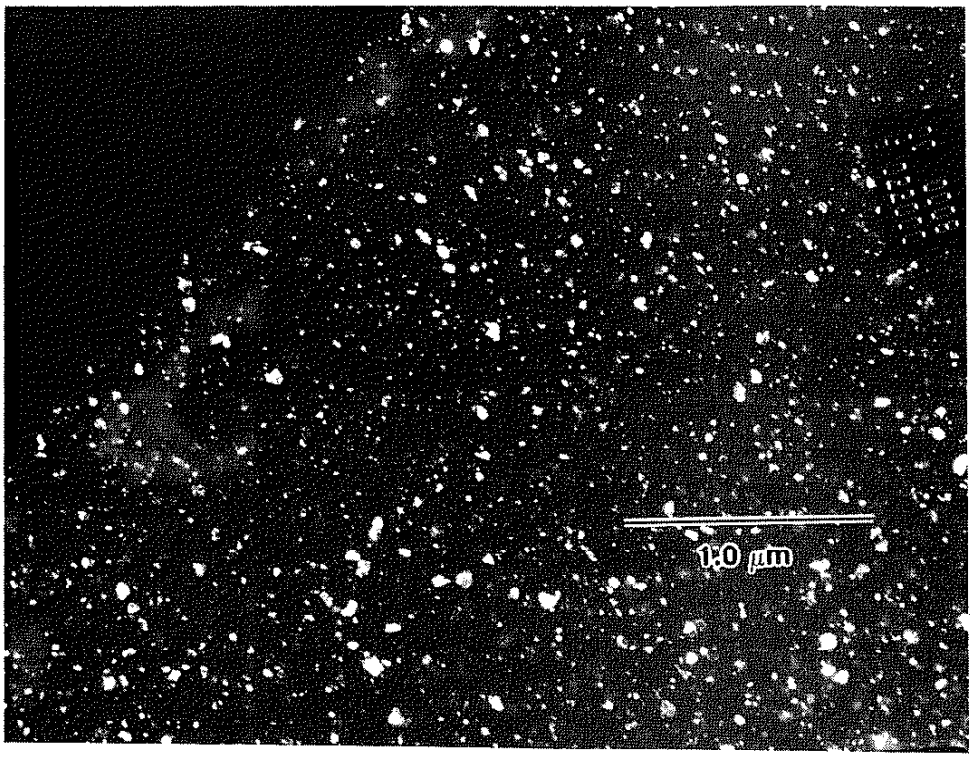

Figure 21. TEM dark field micrograph of evaporated aluminum on NaCl.

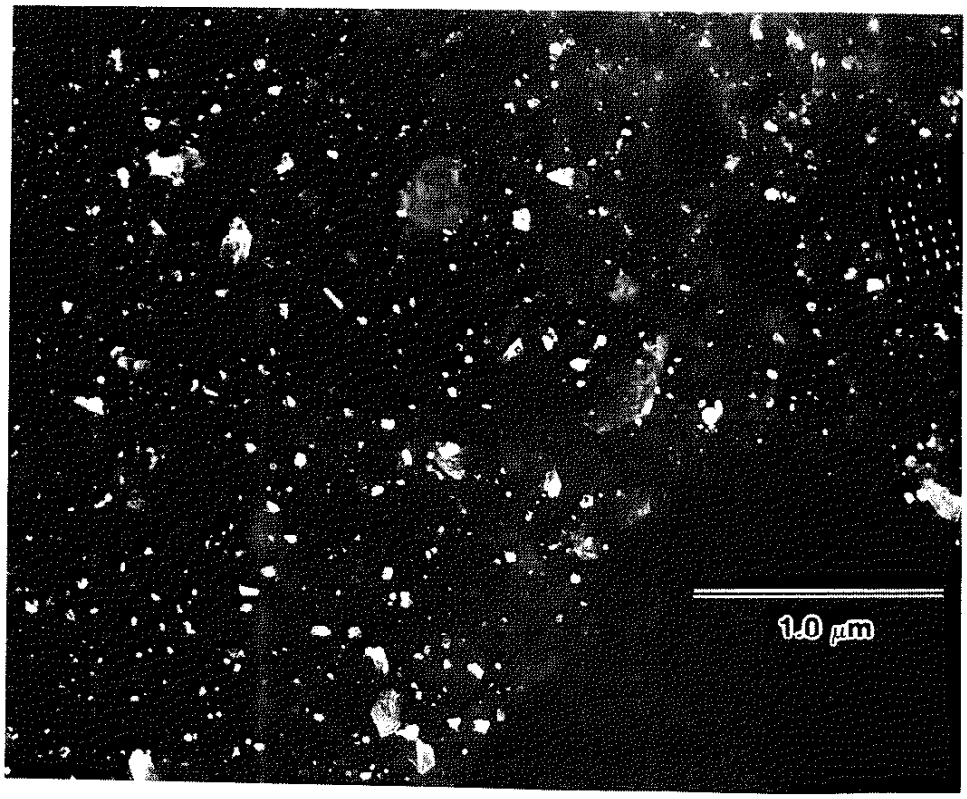

Figure 22. TEM dark field micrograph of aluminum ion plated onto NaCl with a 5 kV substrate bias.

Table 15. Table of average substrate current densities for indicated deposition conditions at 5 kV.

current density mA/cm^2	condition
0.65	-NaCl substrates
0.13	-Metal substrates
0.07	-Formvar coated substrates

Substrate holder area is approximately 153 cm^2

Figure 23. TEM bright field micrograph of aluminum ion plated onto NaCl with a 5 kV substrate bias.

crystallographic features of the substrate (possibly surface steps or cleavage cracks). and 3) Wavy lines which appear to run parallel to the straight lines. Examples of the straight and wavy paths can be seen in figure (23). The dark regions adjacent to the arc paths are thicker regions of the coating that coalesced due to surface tension forces when it was melted by the arc. A thinner region of coating at the bottom of the arc path arises due to coating deposition after the arc passed.

Figure (24) is a dark field micrograph of ion plated aluminum on NaCl showing low angle grain boundaries typical of a recrystallized grain. Notice also the large number of point defects present in the grains indicating that continued damage by ion bombardment was occurring simultaneously to coating recrystallization and grain growth during deposition.

Figure (25) is a dark field TEM micrograph of the tip of one of the pointed structures shown in figure (13) for ion plated aluminum on sputter cleaned copper foil. Comparing this figure with figure (14) it seems reasonable to assume that this material is at a significant depth below the coated surface of the substrate. Precipitates within the structure are visible. Moire fringe patterns indicate small deviations between contacting crystal faces. These patterns could arise from precipitates oriented parallel to the image plane or from aluminum being redeposited onto the copper surface during ion milling. The diffraction pattern shown in figure (26) which corresponds to the imaging conditions in figure (25) indicates that the features (most likely aluminum) giving rise to the Moire fringes are in strong alignment in at least one direction with the

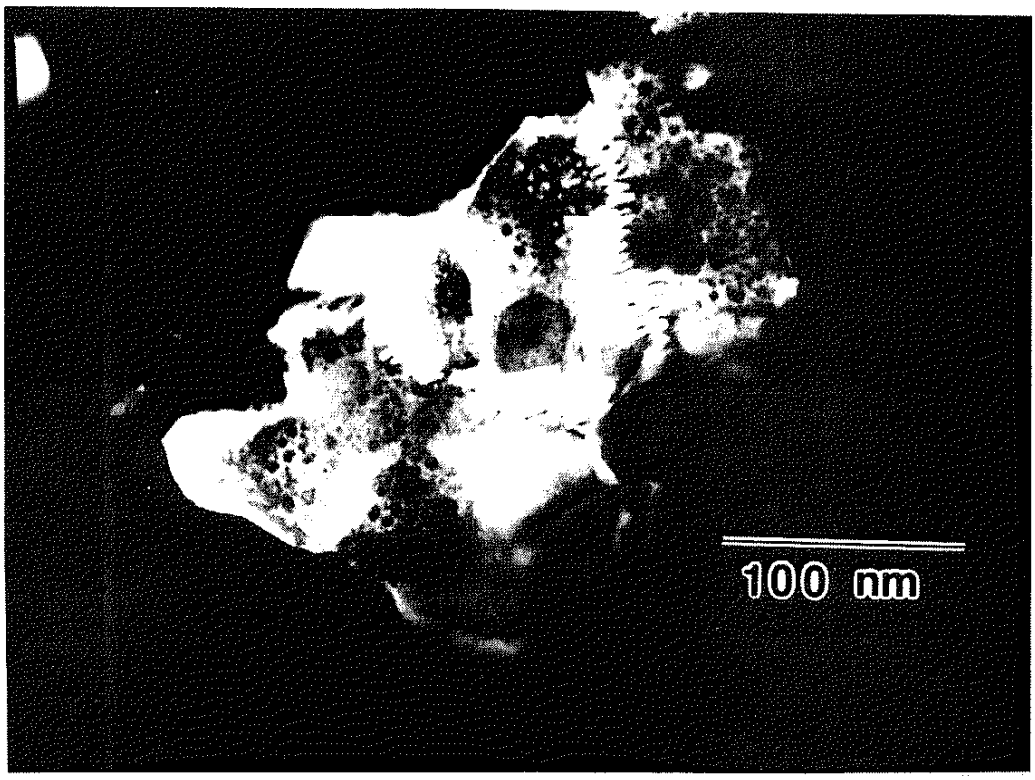

Figure 24. TEM dark field micrograph of ion plated aluminum on NaCl showing low angle grain boundaries typical of a recrystallized grain.

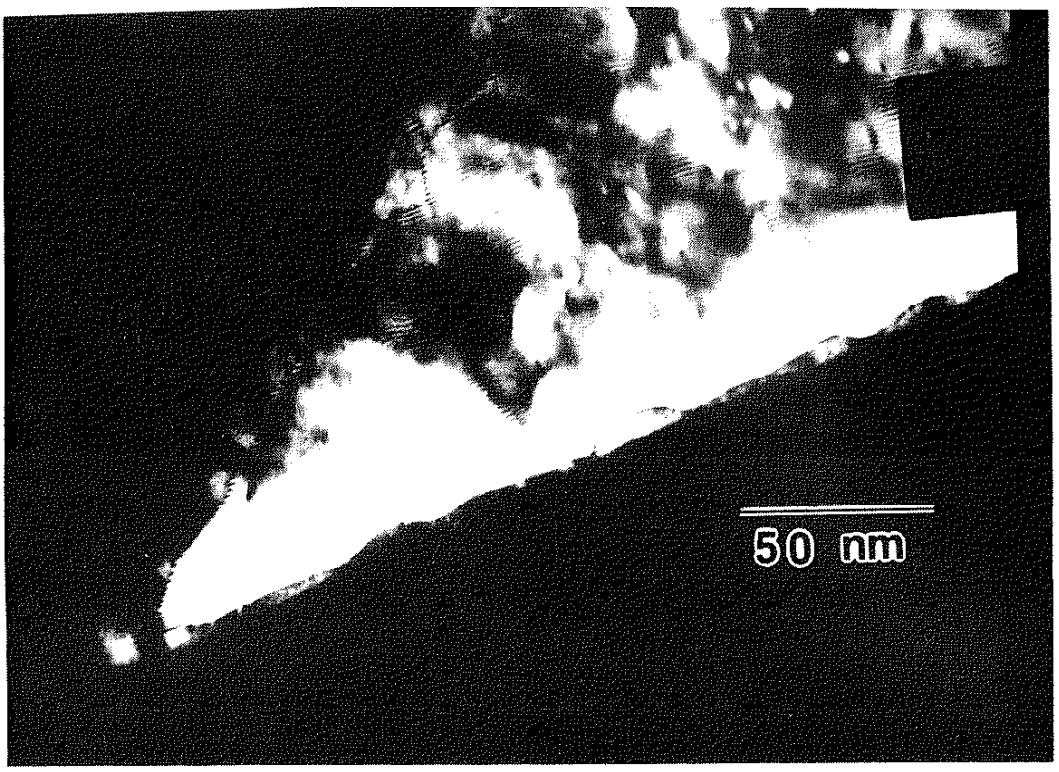

Figure 25. TEM dark field micrograph of ion plated aluminum on sputter cleaned copper foil.

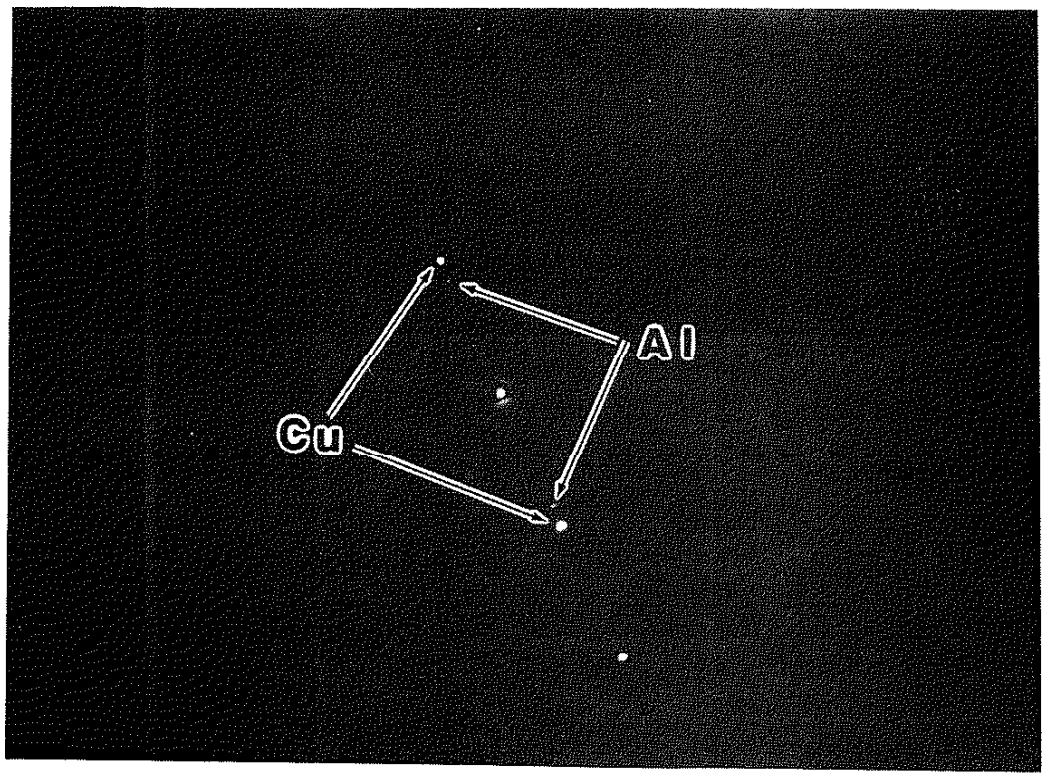

Figure 26. TEM electron diffraction pattern from ion plated aluminum on sputter cleaned copper foil showing imaging conditions from figure (25).

copper substrate. Tilting to the diffraction condition shown in figure (27) we see that all directions for the type 110 zone of the material giving rise to the moire fringes and the type 110 zone of the copper substrate are parallel.

IV.H. SURFACE CLEANLINESS (SPUTTER CLEANING)

Figure (28) shows Auger data for a silicon substrate "sputter cleaned" in the ion plating system. The upper scan is from the as-sputter-cleaned sample and the lower scan is after 3 minutes of cleaning with a xenon beam in the Auger apparatus. The upper scan shows contamination of the substrate surface by aluminum, carbon, and oxygen. The aluminum probably arises from redeposited material sputtered off of the substrate holding fixture; it was oxidized either by the ambient residual oxygen during processing, or by exposure to the atmosphere after processing. The carbon probably arises from the alcohol used to clean the sample before putting it in the Auger. The lower scan shows that the relatively thin layer of contaminant deposited by the "sputter cleaning process in the ion plater can be removed in a fairly short period of time by cleaning with an ion beam in the Auger spectrometer.

IV.I. INTERFACE WIDTH (ION BOMBARDMENT)

Figure (29) shows a SIMS depth profile of evaporated aluminum on copper foil. Figure (30) shows a SIMS depth profile of aluminum ion plated onto a copper foil with a 5 kV substrate bias. Significant features of a comparison of these figures include: 1) The ion plated sample shows an extended range of mixed composition between the

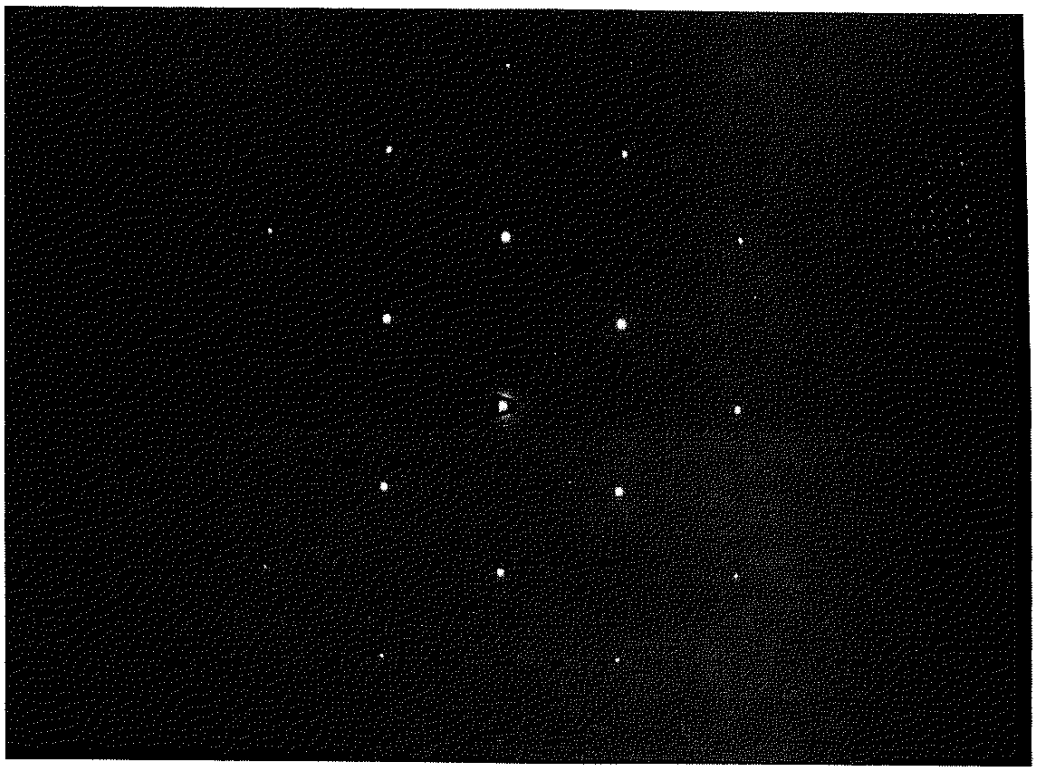

Figure 27. TEM electron diffraction pattern from ion plated aluminum on sputter cleaned copper foil after tilting region in figure (25) to type 110 zone.

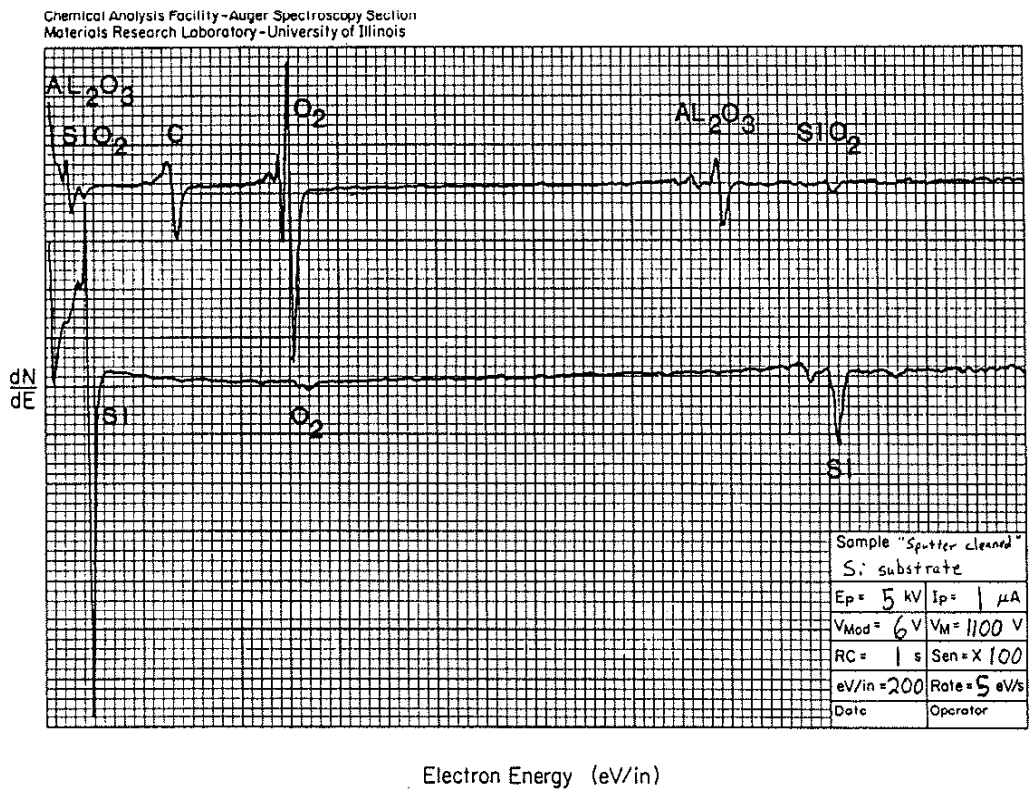

Figure 28. Auger data for silicon substrate "sputter cleaned" in the ion plating system. Upper line is as inserted in Auger, lower line is after cleaning for 3 minutes with a xenon ion beam in the Auger.

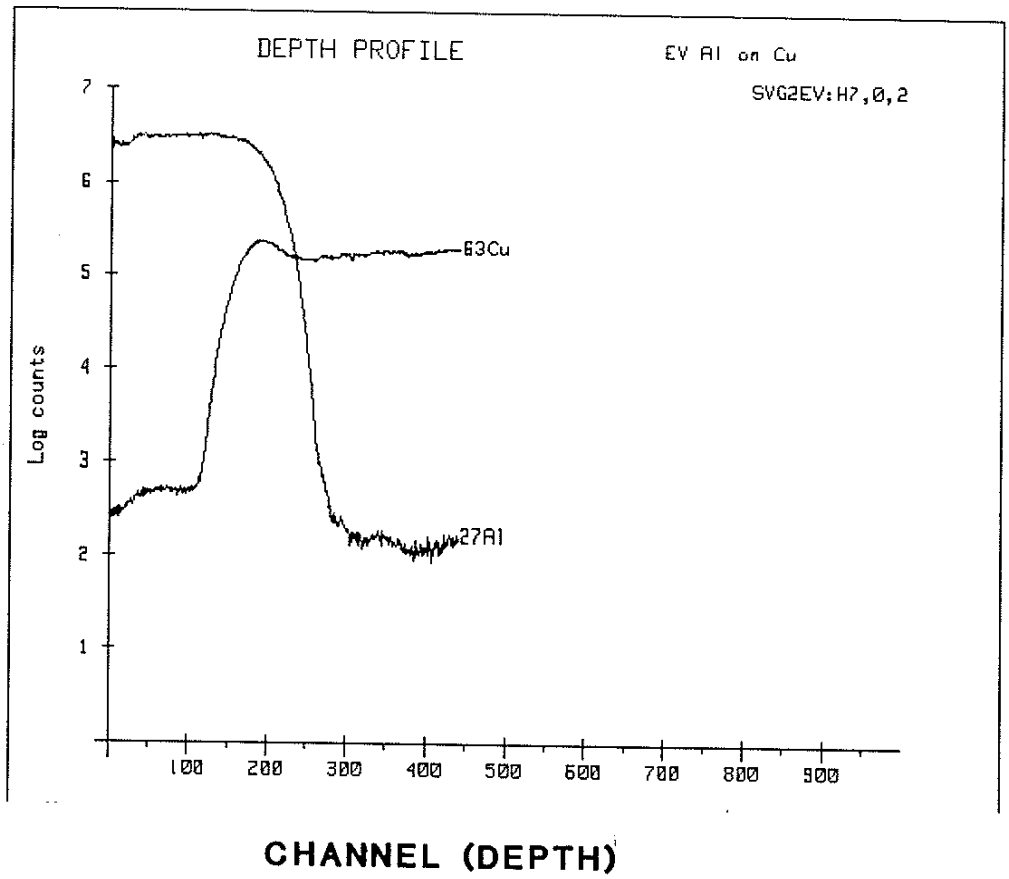

Figure 29. SIMS depth profile of evaporated aluminum on copper.

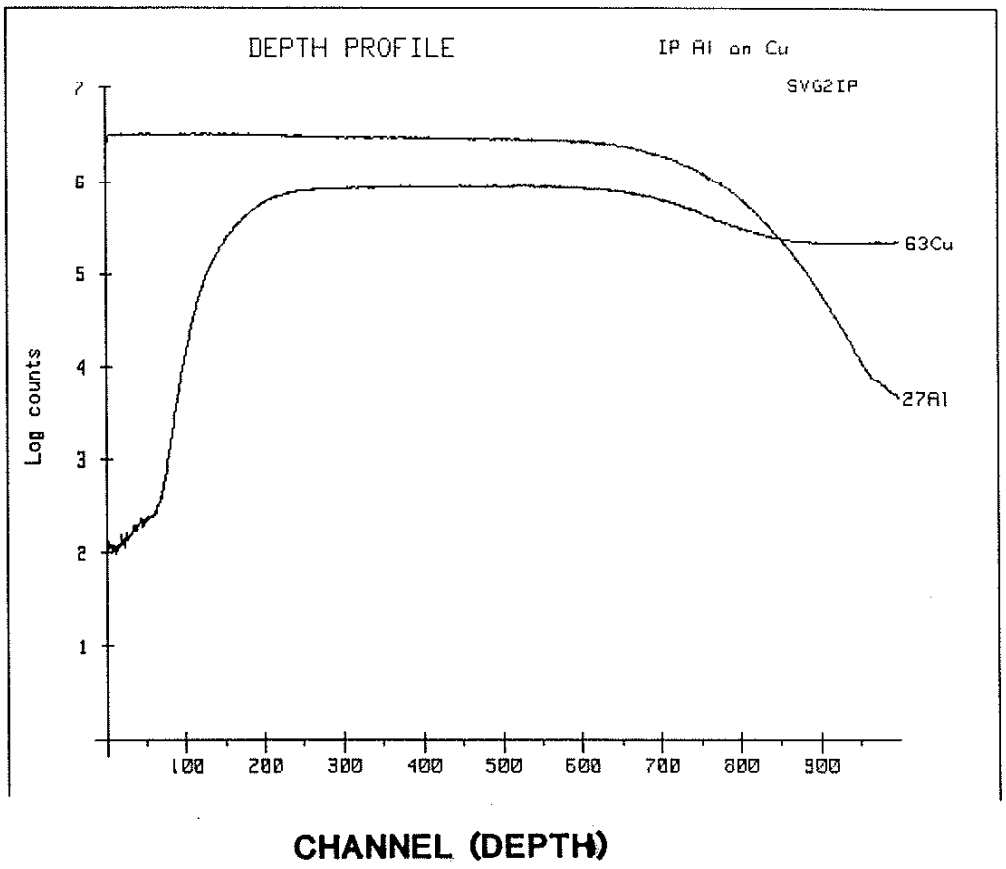

Figure 30. SIMS depth profile of aluminum ion plated onto copper foil with a 5 kV substrate bias.

aluminum coating and the copper substrate whereas the evaporated sample shows a rather abrupt interface. This region of mixed composition corresponds to the intermetallic like structure observed in figures (16), (17), and (18). 2) The sputter yield ionization of copper is increased in the presence of aluminum and the sputter yield ionization of aluminum is increased in the presence of copper. 3) The aluminum concentration in the substrate falls off to the background level at a much faster rate in the evaporated sample than in the ion plated sample.

IV.J. COATING TEXTURE (PRESSURE, BIAS)

A series of coatings was deposited onto single crystal silicon substrates and x-rayed using a single axis diffractometer to observe the effects of deposition parameters on deviations from a random texture. The deposition parameters are tabulated in table (16).

The integrated intensity of each of the peaks was calculated as the peak height above the background times the peak width at one half the maximum peak height above the background. The integrated intensities, in random units, are tabulated in table (17).

The deviation from a random texture can be observed by comparing the ratio of the intensity of a given peak to the intensity of the (111) peak and comparing that value with the same ratio for a random textured sample from the x-ray diffraction files. The intensity ratios are tabulated in table (18).

From this data we see that all the coatings show some deviation from a random texture. The tendency to have a nonrandom texture appears to be enhanced for deposition at low pressure and

Table 16. Table of deposition parameters for x-ray samples on Si substrates.

Pressure (mTorr (Pa))	Substrate bias (kV) 0	1	2.5
5 (0.67)	#15	#14	#13
20 (2.67)	#12	#10	#9

Table 17. Table of integrated intensities for x-ray samples on Si substrates.

	Sample #					
Peak	#9	#10	#12	#13	#14	#15
(111)	2	1.64	2+	0.26	0.27	0.2
(200)	0.65	0.43	0.99	0.15	0.85	2+
(220)	0.27	0.19	0.4	0.95	1.19	0.02
(311)	0.25	0.17	0.41	0.09	0.16	0.20
(222)	0.11	0.09	0.18	0	0	0
(400)	0.04	0.01	0.06	0	0.03	0.3
(331)	0.10	0.10	0.2	0.06	0.14	0
(420)	0.10	0.06	0.18	0.04	0.1	0.03

+ indicates that the peak went off scale.

Table 18. Table of intensity ratios I(hkl)/I(111) for x-ray samples on Si substrates.

	Sample #						
Peak	#9	#10	#12	#13	#14	#15	File
(111)	1	1	1	1	1	1	1
(200)	0.33	0.26	0.50	0.58	3.15	10	0.47
(220)	0.14	0.12	0.20	3.67	4.40	0.10	0.22
(311)	0.13	0.10	0.20	0.35	0.58	0.98	0.24
(222)	0.05	0.06	0.09	0	0	0	0.07
(400)	0.02	0.01	0.03	0	0.11	1.5	0.02
(331)	0.05	0.06	0.1	0.23	0.52	0	0.08
(420)	0.05	0.04	0.09	0.15	0.37	0.15	0.08 .

low bias for the range of parameters studied. Note: These data only indicate that there is a deviation from a random texture, the exact nature of the texture should not be inferred without the use of a more sophisticated diffractometer such as a double axis diffractometer.

V. DISCUSSION

The following section discusses the significant results of this work and compares this work to previous studies reviewed in the background literature. This section is divided into subsections covering substrates, deposition parameters, and properties of the coating/substrate composites. The first subsection, "substrates," is divided into discussions covering: substrate choice, substrate effects on coating properties, and substrate surface preparation. The second subsection, "deposition parameters," is divided into discussions covering: pressure, with its associated problems encountered with control and measurement, and evaporation rate, with its associated problems encountered with control and stability. The third subsection, "properties," is divided into discussions covering: coating thickness, coating adhesion, coating/substrate interface structure, and coating/substrate chemistry.

V.A. SUBSTRATES

V.A.1. SUBSTRATE CHOICE

A variety of substrate materials were chosen to provide a cross-section of possible glow discharge/coating/substrate interactions and to facilitate simplified specimen preparation and data analysis for the employed analytical techniques. Rationale for choice of individual substrates are discussed in the following paragraphs.

Aluminum substrates provide complete mutual solid solubility and no intermetallic formation with the aluminum coatings.

Aluminum foil substrates were chosen for: 1) TEM cross-section samples due to formability and low mismatch of sputter yields between coating and substrate during ion milling; 2) low thermal mass to enhance the effects of substrate heating during ion bombardment; and 3) ease of fabrication of substrate shapes and TEM specimens. Aluminum sheet substrates were chosen for: 1) TEM cross-section samples; 2) adequate strength for coating adhesion testing; 3) adherent thermal oxide formation; and 4) ease of fabrication.

Copper substrates provide limited mutual solid solubility with aluminum coatings and several intermetallics are present on the Al-Cu phase diagram. Oxygen free high conductivity (OFHC) copper is readily available in sheet and foil form. Copper foil substrates were chosen for their formability, which allowed fabrication of cross-section TEM samples by coiling into a tube, and smooth surface, which allowed meaningful SIMS data to be acquired on the apparent width of the coating/substrate interface. Copper sheet substrates were chosen for their adequate strength for coating adhesion testing.

Formvar coatings on substrates and NaCl substrates allowed simplified removal of films from substrates without necessitating the use of acids which may affect the coating structure. Pores in the formvar surface allow observations of the effects of local substrate surface orientation on coating growth without the difficulty of preparing cross-section samples for the TEM. Thin coatings on the formvar are electron transparent in the TEM and require no thinning by ion milling which may affect coating

structure. NaCl substrates provide simplified TEM sample preparation of the coatings since the substrate can simply be dissolved in water and the coating floated off onto grids.

Silicon substrates were chosen for their high purity which allows meaningful data to be collected on the nature of the impurities deposited during the sputter cleaning and coating deposition processes. The brittle nature of silicon allows ease in fabrication of fractured samples for SEM observation of coating fracture surfaces. The smoothness of the polished silicon substrate surfaces allows profilometry measurements of coating steps generated by an overlapping piece of silicon during coating deposition.

Titanium substrates provide limited mutual solid solubility with aluminum coatings. The Al-Ti phase diagram has several intermetallics present. Titanium sheet was also chosen for its strength suitable for adhesion testing.

V.A.2. SUBSTRATE EFFECTS ON COATING

Choice of substrate material was found to be important in light of the idea that the substrate must provide a suitable support for the coating during testing. Both of the below instances demonstrate less than optimum coating performance which is actually due to inadequacy in the substrate properties.

First, during adhesion testing of the aluminum coatings on oxidized aluminum substrates it was noted that loads which corresponded to high adhesion values often produced cupping of the substrate and premature failure of the epoxy due to shear stresses.

Apparently, the heat treatment that produced the heavily oxidized surface (several hours at 600 Celsius (873 K)) also excessively softened the material. A similar heat treatment to another material (full anneal) might not produce such low strength levels that there would be such excessive deformation at the stresses imposed by the adhesion testing. The problem of substrate softening could probably have been avoided by using a precipitation hardening grade of aluminum; this, however, may have greatly altered the nature of the oxide formed.

Second, the deformation characteristics of the substrate surface were found to have a significant effect on the behavior of the coating. SEM observations of severely bent samples indicated that when localized strain of the substrate (localized necking) occurred, the coating was not always able to accommodate the strain and localized failure of the coating across the strained region occurred. In the strongly adherent ion plated coatings, this failure was observed to occur without localized delamination of the coating from the less strained regions of the substrate as seen in figure (7). In evaporated coatings and poorly adherent ion plated coatings, this failure was accompanied by localized delamination of the coating from the less strained regions of the substrate as seen in figure (6).

V.A.3. SUBSTRATE SURFACE PREPARATION

Substrate surface preparation was found to have a major influence on the coating adherence for aluminum, copper, and titanium substrates. Adhesion values ranged from essentially zero

for coatings on tarnished substrates to tens of MPa for chemically and sputter cleaned substrates.

Tarnished surfaces in general gave the poorest coating adhesion performance. Tarnished substrates were "prepared" by giving the material a liberal exposure to fingerprints and normal "shop grime" during fabrication. No effort other than a light rinse with ethanol was made to clean the tarnished substrates prior to coating deposition. Although this surface preparation may not be exactly reproducible, it is believed to be representative of substrate surfaces for which little care has been taken to establish or maintain substrate surface cleanliness.

Chemically cleaned substrate surfaces (chemical polishing and chemical etching) in general gave an improvement in coating adhesion performance over tarnished surfaces. Chemical cleaning removes contaminants from the substrate surface and provides a surface that is relatively free of massive surface oxides. Some degree of surface reoxidation occurs after chemical cleaning due to atmospheric exposure. Chemical etching gave slightly higher adhesion values than chemical polishing on copper substrates. A possible explanation for this is that the etching process provides a faceted surface which produces a larger coating/substrate contact area and allows a greater degree of mechanical interlocking between the coating and substrate. The faceted surface also could increase the measured interfacial adhesive strength because while the applied stress will be normal to the macrosurface it is not normal to the individual surface facets. The stress resolved normal to the facets will be correspondingly reduced which will serve to increase

the macroscopic measured stress for interfacial adhesive failure of the coating. The faceted contact area may also allow better accommodation of property mismatches, such as thermal expansion coefficients, between the coating and substrate due to the short facet lengths.

The presence of a clean thermal oxide on the substrate surface appears to inhibit coating adhesion less than the presence of a heavy tarnish. Thermal treatment to the aluminum substrate to grow the oxide degraded the the substrate properties such that the observed reduction in adhesion properties was probably the result of deformation of the substrate. Aluminum is a special case since its oxide is naturally adherent. It is expected that substrate materials with less adherent oxides would exhibit reduced coating adhesion in the presence of an oxide layer irrespective of oxide cleanliness. Heat treatment of several copper substrates in air to develop a thick natural oxide resulted in explosive spalling of the oxide as the specimens cooled to room temperature. Coating adhesion to the oxidized copper substrates would be very poor due to the tendency of the intervening thick thermal oxide to delaminate from the substrate.

In-situ sputter cleaning of the substrate surfaces immediately prior to deposition appears to improve coating adhesion beyond that attainable by chemical cleaning alone. The additional substrate heating during sputter cleaning may contribute to degradation of substrate properties in the near surface region. Evidence of substrate property degradation was not observed or sought in this work; however, the author has observed softening of 6061 T6

Aluminum substrates during ion plating with Ti_xN_{1-x}. The increase in adherence due to sputter cleaning prior to deposition is especially noticeable in the evaporated coatings. Sputter cleaning of the substrate surface was first described as an intrinsic step of the ion plating process by Mattox (20) and its effectiveness in improving coating adhesion is clearly demonstrated by the data generated for this thesis.

From the above discussion, it appears that the closer one can get to an atomically clean substrate surface prior to coating deposition, the better the adhesion of the coating will be.

V.B. DEPOSITION PARAMETERS

The deposition parameters used in this study were not as reproducible as would be desirable. The easily controlled parameters were substrate bias and support gas inlet flow rate. The parameters which were found to be the most difficult to control were chamber pressure, evaporation rate, and substrate temperature; these are discussed briefly below.

V.B.1. PRESSURE

The chamber pressure was controlled manually by adjusting the flow rate of argon through the mass flow controllers. The mass flow controllers work very well for maintaining a constant influx of gas to the chamber; but, they are a very awkward means of establishing and maintaining a constant pressure in the chamber. Chamber pressure actually fluctuated about some nominal value that was selected for the particular deposition run. Typical values are

plus or minus 2 microns (0.27 PA) about a nominal value of 5 microns (0.67 Pa).

Another difficulty with the pressure was with its actual measurement. Thermocouple guages are generally calibrated for a specific gas (air) and the tc gauge used for this work was actually measuring a mixture of argon with a small amount of air. (The air leaked into the system through the many o-ring seals. The leak rate is changed every time the seals are disturbed by opening and closing the system and is important for operation at high vacuum conditions such as conventional evaporation. An operating pressure of 8.0×10^{-5} Torr (1.1×10^{-2} Pa) corresponds to an argon flow rate of 25 sccm when the base pressurre is 5.0×10^{-7} Torr (6.67×10^{-5}Pa). Typically the system only pumps down to 10^{-5} or 10^{-6} Torr (1.33×10^{-3} or 1.33×10^{-4} Pa) which corresponds to a leak rate from wall outgassing, seals, and other sources of 2 to 4 sccm. Upper chamber pressure during operation is on the order of 10^{-3} Torr (0.13 Pa) so the pressure contribution of leak gasses is probably less than a few percent of the total. A capacitance manometer was also available for measurement of pressure; this, however, functioned poorly and tended to drift with time even when the pressure was stabilized.

Chamber pressure is a fundamentally desirable parameter to control since it affects the properties of the glow discharge during ion plating and the amount of collisions and scattering that depositing coating atoms and ions undergo before arriving at the substrate. Results of this work have indicated that decreasing argon pressure during ion plating increases the tendency for coating texturing and decreases argon incorporation in the growing coating.

An explanation for this is that an increased support gas pressure promotes a more intense glow discharge with subsequent higher substrate surface power density and heating. These factors stimulate the production of more nucleation sites and cause substrate heating to the point that recrystallization of the deposited coating may occur (recrystallization is sufficiently random that any existing texture would tend to be reduced). Elevated argon pressure also increases the incident argon atom to depositing coating atom flux ratio at the substrate surface which increases the probability that argon will be incorporated into the growing coating. The effects of pressure on coating microstructure for sputter deposited coatings are demonstrated by the Thornton diagram in figure (3). This is further discussed in the structure section.

V.B.2. EVAPORATION RATE

The evaporation rate was controlled manually by adjusting the beam current of the electron beam evaporation source. The beam current has a tendency to drift with time as the tungsten (electron source) filaments age with use. The evaporation rate also fluctuates with time as the source material in the water cooled crucible is gradually depleted. The evaporation rate is coupled to the chamber pressure since an emitted atom may be reflected back into the melt if the mean free path above the melt surface is too short. High evaporation rates were observed to result in the generation of a metal ion plasma due to interactions between the

emerging evaporant atoms and the electron beam supplying heat to the evaporation source.

Stability of the evaporation source seemed to be promoted by using high beam power levels (approximately 9 kW); this unfortunately allowed evaporation from only one source at a time since the electron beam power supply is only rated for 14 kW. A possible explanation for the increased stability at high power levels is that complete melting of the material is maintained during deposition. At lower power levels, the source material is only partially melted and as the evaporation progresses, more source material is melted and occluded gas pockets and contaminants are released into the melt to cause spitting and in some cases expulsion of a significant portion of the melt from the crucible. Contaminant scales in the crucible can cause similar problems even at high power levels. Premelting of the source material at high power levels prior to substrate loading and coating deposition is an important step toward ensuring good evaporation source stability during deposition.

Evaporation rate is a fundamentally desirable parameter to control since it is directly coupled to the deposition rate. For a constant ion bombardment rate at the substrate, a variation in the deposition rate translates into a variation in the ratio of bombarding ions to depositing coating atoms. Modification of this ratio by use of an extra anode for plasma density enhancement was seen to increase coating adhesion. Increasing the ion to depositing atom ratio at constant depositing atom rate gives a net decrease in the deposition rate due to increased sputtering of the depositing atoms. Increasing the ion to depositing atom ratio was found to cause a

transition from loosely bound zone 1 and zone t structures to more dense zone 2 and zone 3 structures. The coupling of evaporation rate and bombarding ion to depositing atom ratio for this work are in agreement with the trends observed by Egert and Scott (126) who ion plated aluminum onto uranium.

The ion to depositing atom ratio can be estimated as follows. The surface density for a close packed plane of aluminum atoms is about 1.41×10^{15} atoms/cm^2 and has an average thickness of 2.34 angstroms per monolayer. For a 1.2 micron per hour deposition rate, this corresponds to a deposition rate of 2×10^{14} atoms per square centimeter per second. A current of 10 mA on an area of 150 cm^2 corresponds to 4.2×10^{14} charges per cm^2 per second. If half the current is ions (the other half is secondary electrons) then the ion bombardment rate is 2.1 ions/cm^{2}sec and the ion to depositing atom ratio is about 1 to 1. In actuality, the ratio is probably lower since the estimate does not account for resputtering of atoms and secondary electron generation due to impacting energetic neutrals. If the probability of secondary electron generation is about equal for both ions and energetic neutrals and ions comprise less than 1% of the plasma, then the bombarding ion to depositing atom ratio is probably 1:100 or less.

V.B.3. TEMPERATURE

The bulk substrate temperature was controlled by mounting the substrates on a water cooled substrate holder. The operator has a choice of either hot or cold water circulating through the substrate holder. The actual temperature of the water varies with

the time of day and the season so that it is not reasonable to assume any constant quantitative value for either the hot or cold temperature. The hot water temperature oscillates approximately plus or minus 20 degrees Celsius (20° K) about an average value of about 50 degrees Celsius (323 K). The cold water temperature oscillates approximately plus or minus 5 degrees Celsius (5° K) about an average value of about 20 Celsius (293 K). The actual temperature of the substrate depends on how well it is thermally contacted to the substrate holder and the thermal loading caused by the deposition conditions. Optimally, it would be desirable to be able to fix the substrate temperature at a chosen value and keep it constant for the duration of the experiment.

The effects of the nominal substrate temperature during deposition are well demonstrated by the diagrams of Movchan and Demchishin (figure (31)) and Thornton (figure (3)). The term "nominal substrate temperature" is used because the work for this thesis and work by Lardon, et al. (46) indicates that the use of increasing applied substrate bias causes a transition to elevated temperature structures, as indicated by the diagram of Movchan and Demchishin (figure (31)), even though the bulk substrate temperature is much lower than that necessary to obtain such structures. In general, this research showed that increasing the nominal substrate temperature during deposition promotes bulk-like structures and properties of the coating material. Effects of increasing nominal substrate temperature by ion bombardment are further discussed in the structure section.

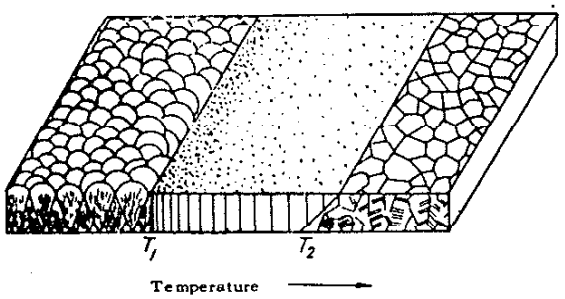

Figure 31. Diagram of structural zones of condensates as a function of temperature. From Movchan and Demchishin (45).

V.C. PROPERTIES

The "properties" section that follows is divided into subsections covering thickness, adhesion, structure, and chemistry. The first subsection, "thickness," is divided into discussions covering: measurement methods optimization, and the Q value (uniformity of coating thickness). The second subsection, "adhesion," is divided into discussions covering: conditions promoting optimal adhesion; limitations of the Sebastion adherence test; and, qualitative evaluation of adherence by SEM. The third subsection, "structure," is divided into discussions covering: effects of argon pressure and applied substrate bias on structure; ion plated aluminum on aluminum; evaporated aluminum on copper; ion plated aluminum on copper; directional columnar growth; and effects of applied substrate bias and pressure during deposition on coating texture. The fourth subsection, "chemistry," is divided into discussions covering: Auger analysis of "sputter cleaned" substrates; EDX of argon incorporation; and, SIMS profiling through coating/substrate interfaces.

V.C.1. THICKNESS

V.C.1.a. MEASUREMENT OPTIMIZATION

Thicknesses of the coatings were evaluated using surface profilometry, SEM observation, and TEM observation; none of these methods were found to be without potential sources of error. Surface profilometry was limited to measuring step heights generated by coating overlapping pieces of silicon. Attempts at

measuring step heights on other substrates were aborted because the coating thickness was on the order of or less than the substrate surface roughness. SEM and TEM measurements were subject to error in determining the actual magnification of the image. All of the methods were subject to errors due to nonuniformity in the deposited coating thickness arising from geometrical, shadowing, pressure, and resputtering effects during deposition. TEM is probably the optimal method for thickness determination since it allows a direct observation of the coating thickness and the width of the reaction zone between the coating and substrate. The TEM method works best on thin films (less than 1 micron) when the coating, reaction zone, and substrate can be thinned to electron transparency in the same area while leaving the coating thickness intact (134).

V.C.1.b. THE Q VALUE

The "Q" value, devised in this study to quantify coating thickness uniformity, showed that deposition with an applied substrate bias slightly enhanced coating uniformity in comparison to that for an evaporated coating deposited at the same pressure (Q for ion plating is 2.839; Q for evaporation is 2.677; about a 6% improvement for ion plating over evaporation). The percentage improvement in Q attained by ion plating using the data of Chevallier data (63) was greater than that attained in this work (Q for ion plating is 1.6041; Q for evaporation is 1.2456; about a 28% improvement for ion plating over evaporation).

However, the absolute values of the Qs for Chevalliers data are lower than for this work. This can be explained in terms of pressure and geometrical effects. Most evaporation runs are carried out at low pressures to maximize the mean free path, thus allowing an evaporant atom to travel in a straight line from the source to the substrate without encountering significant gas scattering. In this work, the same pressure was used for both evaporation and the plating to more clearly see the effects of the plasma discharge on scattering of coating atoms between the source and the substrate. The use of increased chamber pressure during coating deposition promotes the formation of a more uniform coating (higher Q) by scattering the coating vapor to allow deposition of material on surfaces which are not within direct line of sight of the vapor source. Geometrical effects arise from the size and shape of the substrate which causes it to intercept at different surface locations a distribution of deposition rates. The substrate shape also modifies the deposition rates by shadowing and by variations in the projected area of different surface locations. Chevallier's data came from a large geometrically tortuous substrate subtending a significant angle of the source which should naturally give rise to a lower value of Q than the flat substrates subtending a small angle of the source used for this work. An ideal and perfectly uniform coating would have a Q of infinity.

V.C.2. ADHESION

V.C.2.a. CONDITIONS PROMOTING

This research showed that coating adhesion was generally enhanced with increasing substrate cleanliness obtained by chemical and sputter cleaning prior to deposition (see tables (7) and (10)). Adhesion was also improved with increasing deposition energy obtained by increasing the substrate bias or by using enhancement to increase the bombarding ion to depositing atom ratio (see table (7)). Increased coating adhesion produced by energetic ion/neutral bombardment during the ion plating process is generally believed to be the result of a chemically and structurally graded interface and increased active coating nucleation sites, Mattox and McDonald (20).

Mattox and McDonald (20) observed increased adherence of Cd to Fe in the presence of a 4kV argon glow discharge during deposition. Steube and McCrary (57) observed that IVD aluminum coatings exhibit improved adhesion to aerospace parts over evaporated coatings. Dugdale (64) deposited metals and ceramics via evaporation and sputtering onto biased and unbiased substrates and observed that substrate cleaning by ion bombardment prior to coating deposition improved coating adhesion. Coad et al. (19) observed that organic and other contaminants on the substrate surface may cause degraded coating adhesion and that removal of these contaminants is beneficial to coating adhesion; they noted that although ion cleaning has a number of disadvantages, it is useful as a means of heating the substrate to drive off contaminants. Hurley and Williams (10) observed that ion plating

produced improved adhesion of metals to polymers over that produced by evaporation. Vogel and Bergmann (121) observed that difficulties in adhesion of ion plated industrial TiN coatings are encountered due to substrate contamination during cleaning processes. Scott (133) observed an increase in coating adhesion with increasing applied substrate bias for copper coatings deposited on ceramic substrates.

The adhesion results of this work, as explained above, appear to be in excellent agreement with the literature chronologically reviewed in appendix B of this thesis.

V.C.2.b. LIMITATIONS OF TEST

The Sebastian adhesion test used to determine adhesion strengths for this work provided useful data for qualitative comparison of the effects of the deposition parameters and substrate treatments on coating adhesion. However, limitations of the method and materials prevented the generation of accurate quantitative data. Limitations of this test include the following parameters. 1) The epoxy used to bond the pull stub to the sample must be thermally cycled to be cured. This thermal treatment may have significant effects on the coating and or substrate so as to modify the actual adhesion value. 2) Alignment difficulties were experienced with mounting the epoxy coated aluminum stubs onto the substrate. This misalignment results in incomplete bonding of the stub to the substrate and failure at an artificially low stress. 3) Alignment difficulties were experienced with mounting the specimen into the pulling fixture; possibly resulting in failures at

artificially low stresses. 4) The epoxy used to bond the stubs to the coatings did not appear to have reliably adequate strength over the force range of the test fixture. 5) The upper limit of the test is about 10.5 ksi. 6) There appears to be quite a bit of scatter in the test results due to alignment problems. The greatest value in each data set is probably most representative of the actual adhesion; however, there is no way of knowing whether any or all of the samples in a given set is actually properly aligned. The average of each data set appears to be an underestimate of the actual adhesion value.

Shah (134) observed the epoxy strength as a limiting factor and observed scatter in the data even at low strength levels for tests on the same instrument used for this work. Chapman (13) in a review of measurements of thin film adhesion points out that it would be more practical to design tests of durability under service conditions rather than tests of adhesion in reference to the difficulties encountered with the various adhesion tests. Specifically, for the pull test, Chapman (13) lists the difficulties as (i) applying a normal pull force rather than a peel force and (ii) soldering (or any other attachment process in similar tests without grossly affecting the film under test. Weaver (14) in a review of adhesion of thin films pointed our that adhesion measurements are limited by two fundamental difficulties; (i) being able to obtain perfect contact (or even a known area of perfect contact) and (ii) being able to apply stress in such a way that the force (or energy) required to separate the two materials may be accurately determined. The limitations observed for the adherence test used in

this thesis appear to be in agreement with the limitations of adherence tests mentioned in the literature in the chronological review in an earlier section of this thesis.

V.C.2.c. QUALITATIVE EVALUATION

Qualitative evaluation of coating cohesive and adhesive strength by SEM observation of severely bent substrates indicates that for evaporated aluminum coatings the cohesive strength is significantly higher than the adhesive strength based on the observed failure modes. This was visible as delamination of the coating from the substrate. Coating fracture in the evaporated case is clean with little evidence of plastic deformation at the fracture surface between the column boundaries. SEM observation of ion plated aluminum on aluminum (see figure (7)) indicated that both the cohesive and adhesive strengths were significantly higher than the evaporated case (see figure (6)). No delamination of the ion plated coating from the substrate was observed and there was extensive plastic deformation at the fracture surface between column boundaries indicating significant cohesive strength.

Movchan and Demchishin (45) in developing their temperature-structure zone model concluded that mechanical properties such as microhardness, strength and ductility of the condensates are determined by the structural features of the zones. The increased ductility observed for the ion plated versus evaporated coatings in this work is apparently due to the structural differences between the coatings. In agreement with the generalized structure zone model (45) the evaporated coatings consisted of porous columnar

grains and the ion plated coatings exhibited a dense recrystallized structure.

V.C.3. STRUCTURE

V.C.3.a. EFFECTS OF PRESSURE AND BIAS

SEM and TEM observation of the coatings indicated a transition from a well defined columnar structure with domed tops (zone 1) at zero bias and 20 microns (2.67 Pa) argon pressure to a dense structure with significant evidence of recrystallization (zone 3) with decreasing pressure and increasing energy of deposition. This is, for the most part, in agreement with the work by Lardon and coworkers (46) which indicated that the effect of applied substrate bias on the Movchan and Demchishin (45) model is a shift of elevated temperature structures to lower temperatures with increasing substrate bias. The effect of increasing deposition energy by increasing applied substrate bias and using enhancement in this work was to allow coating grains to recrystallize and grow; however, a large number of smaller grains were also observed due to the continuous nucleation of new coating grains stimulated by ion bombardment during coating deposition. In general, it was observed in this thesis research, that the use of applied substrate bias during deposition produced coatings with finer grain sizes than the evaporated case until the energy of deposition was increased such that recrystallization and growth of the coating grains could occur. At this point there is a transition to a structure consisting of a mixture of very fine grains (finer than the evaporated case) mixed

with large grains (larger than the evaporated case) which often displayed ion bombardment induced damage and accumulations of point defects after growth. The effects of pressure on coating structure in this work (observed in specimens examined for argon incorporation) are in agreement with the effects described by Thornton (18). For this work it was observed that increasing argon pressure stabilized the zone 1 and zone t structures to higher effective substrate temperatures.

V.C.3.b. ION PLATED Al ON Al

TEM observation of aluminum ion plated with a 5 kV bias onto a sputter cleaned aluminum substrate indicated a high density of point and line defects in the substrate near the interface, while the coating was observed to have a relatively low defect density, see figure (12). A simple explanation for these radiation - induced defects is that the fine grain size of the coating provides numerous grain boundaries to act as defect sinks while the relatively massive grain size of the substrate does not provide adequate grain boundary area per unit volume to absorb the defects.

Variation in the coating grain size with coating thickness, as observed in figure (12), can be explained in terms of the deposition parameters as follows. 1) Initially the substrate is subjected to ion bombardment in a glow discharge in order to sputter clean the surface. This cleaning of the surface, activates a large number of nucleation sites, introduces a large number of defects to the surface region of the substrate (in agreement with Mattox and McDonald (20)), and begins heating the substrate surface. 2) The electron

beam evaporation source is turned on, and over a finite time it warms up the evaporant charge. Initially the evaporation rate is very low, and the ratio of bombarding ions and energetic neutrals to depositing atoms is relatively high. Also the initial flux of coating atoms sees a high density of nucleation sites on the sputter cleaned surface so a large number of grains are formed. As the vapor flux increases, the bombarding ion to depositing atom ratio drops so fewer new grains are nucleated and some of the favorably oriented grains grow into columnar grains at the expense of less favorably oriented grains. This is in agreement with the work of Egert and Scott (126) who indicated that the ratio of the energetic particle bombardment rate to the coating atom arrival rate has an influence on the aluminum coating structure such that increasing energetic particle bombardment promotes the formation of elevated temperature structures.

Growth in the above sense refers to having a more favorable surface orientation for adatom absorption in the boundary region than the adjacent column or grain such that an atom arriving on the surface of the unfavored grain near the boundary has a significant probability of migrating to the boundary and being incorporated in the favored grain while the atoms arriving on the favored grain are less likely to migrate and be absorbed by the unfavored grain. This sort of growth is by deprivation of adjacent grains of adatoms and not by consumption of adjacent grains as is observed in recrystallization and growth processes.

3) As the system approaches steady state (substrate temperature, bombarding ion to depositing atom ratio, and

deposition rate) a steady state columnar grain size is established. Grain size at this point is limited by the accumulation of strain energy in the grains due the continued ion bombardment during deposition.

A strain energy limitation on grain size occurs because defects created by ion bombardment are only able to migrate a finite distance to be absorbed at a grain boundary. Grain sizes much larger than this migration distance will accumulate strain energy due to the defects which will cause clustering of the defects or nucleation of new grains to reduce the strain energy. The grain size depends on temperature (homologous temperature, defined as the actual or effective absolute temperature divided by the absolute melting point of the material), applied substrate bias, bombarding ion to depositing atom ratio, coating material and ion chemistry, coating growth rate, bombarding ion and neutral energies and energy distributions, and coating crystal structure.

V.C.3.c. EVAPORATED Al ON Cu

TEM observations of evaporated aluminum on copper indicated an abrupt coating/substrate interface with no appreciable concentrations of point defects in either the coating or the substrates as seen in figures (19) and (20). This is the anticipated result since the conditions of ion plating (ion bombardment and sputter cleaning) described by Mattox and McDonald (20) as promoting an extended interfacial region are not present. The absence of concentrations of point defects is expected since ion bombardment is not present to create them. The relatively low

temperature of the substrate during deposition prevented the formation of an extended interface by normal diffusional mechanisms.

V.C.3.d. ION PLATED Al ON Cu

TEM observations of aluminum ion plated with a 5 kV substrate bias onto a sputter cleaned copper foil substrate indicated the formation of a damaged region and an extended interfacial reaction zone as seen in figures (16), (17), (25), and (27). The width of this reaction zone is at least an order of magnitude greater than could be formed by simple ion penetration as demonstrated by the numbers in tables (13) and (14) (calculated using TRIM, reference (41)) in comparison with the dimensions of the intermetallic region in the above TEM micrographs. With the large number of defects being created by ion bombardment, it is not unreasonable to assume that ion enhanced diffusion is occurring and is responsible for the chemically mixed interfacial layer observed for this system.

Electron diffraction patterns from the reaction zone indicate that some form of intermetallic compound of aluminum and copper has formed with a crystalline structure. However, some of the electron diffraction patterns cannot readily be indexed to any of the known compounds of aluminum and copper. A possible explanation for this is that the compounds exist over a significant composition range on the phase diagram and energetic particle bombardment during deposition may further extend this composition range with some metastable variation of the equilibrium crystal structure to accommodate the nonequilibrium chemistry. The metastable phase

in this case may be some form of tetragonal structure indicating preferential accommodation of one of the atom species along specific planes of the intermetallic, similar to the accommodation of increasing amounts of carbon leading to a lattice parameter shift along a crystallographic direction in iron carbon martensitic steels. The possibility of a metastable phase is supported by the observation of Munz (116) that the substitutional incorporation of aluminum in the TiN lattice may form a metastable phase. Sundgren and Hentzell (119) in their review of hard coatings indicated that metastable phases and metastable atom positions are often observed in thin refractory films. Pandey, Gangopadhyay, and Suryanarayana (130) observed the formation of a series of metastable phases in the Al-Zr system by annealing evaporated films which were deposited as supersaturated solid solutions. The formation of an intermetallic and an extended interfacial zone is in agreement with the work by Teer and Salem (8) who found that the formation of intermetallics and an extended reaction zone in the aluminum - titanium system is promoted by ion plating at high power (5kV in 10 to 50 microns (1.33 to 6.67 Pa) argon pressure).

V.C.3.e. COLUMNAR GROWTH

TEM observations of evaporated and ion plated coatings indicated that columnar coating growth was not in the direction of the vapor flux; but, rather in some direction between the local surface normal and the direction of coating vapor flux. This deviation is most noticeable at the inward pointed columnar coating grains around holes and depressions in the formvar substrates in

figures (8) and (9). The exact nature of the relationship between coating columns, substrate surface normal, and coating vapor flux was not determined. However, at first glance, it appears that the columnar growth follows the tangent rule described by Dirks and Leamy (25) and reviewed in detail in the chronological review section. More specific experiments would need to be performed to verify that the tangent rule applies and to determine the effects of ion bombardment on the relationship.

V.C.3.f. COATING TEXTURE

The coating texture was determined to be nonrandom by comparison of relative x-ray peak intensities with those of the powder file. This is in agreement with the literature previously discussed in the chronological review. Results of this work were presented in tables (16) and (17). Specific references involving nonrandom texture in vapor deposited aluminum coatings include the following: Dobson and Hopkins (48) observed a strong {111} fiber orientation for low melting point fcc metals deposited at 300K. Dhere, et al. (29) observed a {111} texture orientation at low thicknesses transforming to a {311} texture at higher thicknesses for evaporated aluminum films over the range of 15 - 200 μm. Dhere, et al. (30) observed {111} and {311} textures in evaporated aluminum films in the thickness range 7 - 65 μm. Yamada and co-workers (105) observed specific orientational relationships between epitaxial aluminum and a silicon substrate using ionized cluster beam (ICB) deposition. Roberts and Dobson (117) observed a <111> fiber texture in evaporated aluminum films on SiO_2 substrates.

The x-ray data for the current work indicate a general trend toward random coating texture with increasing argon pressure and applied substrate bias. From these trends, it appears that high power deposition conditions which promote the recrystallization and growth of grains within the coating promote the formation of a random coating texture.

V.C.4. CHEMISTRY

V.C.4.a. AUGER STUDY OF SPUTTER CLEANING

Auger studies of a "sputter cleaned" substrate indicated that a detectable amount of contamination of the substrate surface occurs due to redeposition of material sputtered off the adjacent substrate support fixtures as shown in figure (28). This indicates that precoating the fixtures in the system is an important step toward minimizing coating and substrate contamination due to sputter redeposition. The results here are in agreement with the findings of Love and Bower (33) who found that materials sputtered off the high voltage leads to the electron beam source acted as contaminants in evaporated aluminum films. Slusser and MacDowell (135) indicated that surface contamination of ion implanted specimens may occur due to sputtering of lenses, platens, and other fixtures in the ion implanter. Contributions to contamination from the high voltage leads to the electron beam source in the present work are somewhat limited by the baffle plate used to generate a differential pressure between the upper chamber where the coatings are deposited and the

lower chamber where the electron beam filament assemblies are located.

V.C.4.b. EDX STUDY OF ARGON INCORPORATION

EDX studies of argon incorporation in the growing coating indicated that argon incorporation in the aluminum coatings increases with increasing substrate bias and argon chamber pressure. This trend of parameters was also found to promote recrystallization and zone 3 structures, and it is not unreasonable to assume that the amount of argon incorporated should level off or decrease due to substrate heating (thermal diffusion) and ion enhanced diffusion at higher deposition energies which would allow argon to diffuse out of the material as fast as it is being incorporated. The argon content of the coatings for all the deposition conditions used was less than 1 at %. This is in agreement with the work of Walls and co- workers (78) who used AES to study ion plated Cu and Ag coatings on Ni substrates and found that the argon content is less than 1%.

V.C.4.c. SIMS DEPTH PROFILING

SIMS depth profiles through the coating/substrate interface for evaporated (figure (29)) and ion plated (figure (30)) aluminum on copper showed that ion plating resulted in the formation of a greatly extended range of chemically mixed coating/substrate interface region in comparison with the evaporated case. This result is similar to that of the work by Teer and Salem (8) which showed an extended region of mixed composition in the titanium - aluminum

system using microprobe analysis. Walls and co-workers (78), using AES depth profiling, observed a chemically graded interface between ion plated Cu and Ag coatings on Ni substrates.

The SIMS observation of an extended region of relatively constant chemistry in the ion plated case is in good agreement with the observation of an extended region of intermetallic compound in the TEM. Although no determination of the composition of the interfacial material was done in the present work, the composition of the intermetallic may possibly be determined from the relative fluxes of the secondary ions compared and adjusted for sputter yield and ionization efficiencies by calculation or by comparison with standards of known composition and structure. Standards may need to be single crystals with an orientation similar to the coating texture since crystal orientation is known to affect sputter yields. Variations in orientation and chemistry may give rise to nonlinear variations in sputter yield and secondary ionization efficiency. No comparisons with separate standards were made in this work; however the presence of a relatively pure aluminum coating at the outermost surface and relatively pure copper substrate may provide an internal standard for the extremes of the composition range and allow a calibration or calculation of composition in future work.

VI. CONCLUSIONS

This research has investigated the mechanical, microstructural, and chemical properties of evaporated and ion plated aluminum coatings on aluminum, copper, formvar, NaCl, silicon, and titanium substrates. Several significant conclusions have been reached as a result of this work:

Increasing the substrate cleanliness by chemical etching, chemical polishing, or in-situ sputter cleaning prior to deposition causes a significant increase in coating adhesion strength for both evaporated and ion plated coatings. For example, on titanium substrates, the adhesion for the no bias case went from zero for a tarnished substrate with no sputter cleaning to 7 ksi (48.1 MPa) or more for chemical and sputter cleaning prior to deposition.

The sputter cleaning process provides a significant increase in coating adhesion; however, it has also been found to cause potential contamination of the substrate due to redeposition of materials sputtered off of adjacent biased fixtures as was demonstrated in figure (28). Therefore, it is important to precoat all biased fixtures with a suitable material (aluminum foil worked nicely in this work) to minimize adverse contamination of the substrate and coating source material during the sputter cleaning process.

Increasing the deposition energy through the use of increased applied substrate bias and a discharge current enhancement system was found to increase coating adhesion strength. For example, on chemically etched copper substrates, the maximum observed adhesion of aluminum coatings increased from 0.09 ksi in the evaporated case (0 kV) to 9.89 ksi (68.0 MPa) for 5 kV substrate bias

and to and excess of 10.42 ksi (71.6 MPa) for 5 kV bias with discharge current enhancement.

Coating texture is nonrandom with a tendency toward a random texture at increasing deposition energy as shown in table (18).

Coating microstructures were observed to range from zone 1 structures observed in evaporated coatings to zone 3 structures observed in coatings deposited with high deposition energies.

An extended interfacial region of graded chemistry and intermetallic compound forms between the coating and substrate when the coating is deposited at increased deposition energy. The extent of this region is beyond what may be formed by simple ion penetration so it is evident that ion bombardment somehow enhances diffusion. Calculated ion ranges are on the order of 10 nm as seen in tables (13) and (14); the extent of the interfacial reaction zone is on the order of 100 nm or more as seen in figure (12).

Coating thickness uniformity increases with the use of applied substrate bias during deposition. This was demonstrated by a 6% increase in Q (2.667 evaporated to 2.839 ion plated with 5 kV bias) for the ion plated (as opposed to evaporated) coatings in the present work on a non geometrically tortuous substrate and a 28% increase in Q (1.2456 evaporated to 1.6041 ion plated) for the ion plated coating in the work of Chevallier (63) on a larger, more geometrically tortuous substrate. It should also be noted that more geometrically tortuous substrates with larger areas give a lower value of Q than simple substrates with small area since the smaller substrate will intersect a smaller portion of the thickness distribution.

Argon incorporation into the coating increases with increasing applied substrate bias and argon pressure over the range of parameters studied. As seen in table (12), all the values were less than 1 atomic %.

Coating columnar growth is not along the direction of the vapor flux, but rather is in a direction between the local substrate surface normal and the vapor flux direction. This was observed as inward pointed columnar structures of the aluminum coatings in the surface voids of formvar substrate surfaces as seen in figures (8) and (9).

VII. APPENDIX

VII.A. ION PLATING

The following is a discussion of ion plating as relevant to the electron beam source evaporation/ion plating unit at the U. S. Army Construction Engineering Research Laboratory (USA-CERL) in Champaign Illinois.

Ion plating, a plasma-assisted physical vapor deposition process, was first described by Mattox (20) in 1963 as a means of improving coating adhesion to levels above those attainable by electroplating, vacuum evaporation, and sputter deposition. The ion plating technique involves making the substrate the cathode of a high voltage glow discharge to sputter clean the substrate surface and then exposing the substrate to a flux of vapor phase coating material to be deposited on the surface. The glow discharge is continued during deposition so that there is simultaneous deposition and resputtering. To ensure net coating growth, the rate of condensation of vapor phase coating material at the substrate surface must be greater than the rate of resputtering from the substrate surface. Some fundamental considerations of the ion plating process are: 1) the vacuum; 2) the glow discharge; 3) energetic particle bombardment of the substrate; 4) the effects of ion bombardment on the substrate; 5) evaporation of the coating material; and 6) condensation of the evaporant onto the substrate.

VII.A.1. VACUUM

The quality of the vacuum is a primary consideration in any

vacuum deposition process. The residual gas composition and pressure will determine the mean free path of atoms in the system and the relative fluxes of coating and residual gas atoms incident on the substrate. The ultimate vacuum attainable by a vacuum system will depend on many factors including construction materials, pumping arrangement, and cleanliness.

The mean free path of an atom is the average distance that atom travels between collisions with other atoms. Mean free path increases with decreasing pressure and atom size. The mean free path L can be estimated as follows (21): If a gas atom has diameter D, then it will undergo a collision if its center comes within a distance D of the center of another atom. The collision area has radius D and area $A = 2\pi D^2$ and sweeps out a volume as the atom moves through the gas. If at a given pressure there is 1/V atoms/cm^3 then there is one atom in each V cm^3. The average distance L that an atom of collision area A must move to sweep out a volume of V is L = V/A. At room temperature and 1 mtorr pressure the mean free path of argon is about 8 cm. The probability of an atom traveling a distance x without making a collision is given by the expression (21):

$$P(x) = \exp(-x/L) \qquad (2)$$

From this expression we can see that when x = L, P(x) = 0.37 so there is still a reasonable probability of the atom travelling the distance without undergoing a collision.

The impingement flux of residual gas atoms on the chamber walls is given by (21):

$$\text{Flux} = nc/4 \tag{3}$$

where n is the number of atoms given by

$$n = PV/kT \tag{4}$$

and c is the mean speed of the atoms given by (21):

$$c = \text{sqrt}(8kT/(\pi m)) \tag{5}$$

where m is the mass of the atom. For argon at 1 mtorr and 20° Celsius (293 K) this is about 3.6×10^{17} atoms per square centimeter per second. If we assume that there are about 10^{15} atoms per square centimeter on a typical surface, we can calculate that each of these sites will be struck once a second at a pressure of about 10^{-6} Torr (1.33×10^{-4} Pa) (21). If each of these atoms stuck (a sticking coefficient of unity), this would correspond to formation of 1 monolayer per second at 10^{-6} Torr (1.33×10^{-4} Pa) (21).

The materials used in the construction of a vacuum system are an important consideration from the standpoints of outgassing and permeability. Outgassing is the desorption of contaminants on the vacuum system surfaces into the vacuum. Since desorption is a thermally activated process, outgassing can be accelerated by

heating up the surfaces, "baking out" the system. Permeation is the diffusion of gas atoms through the openings in the structure of the construction material. Permeation is a function of both temperature and pressure gradient, so it obeys Fick's diffusion laws. Metals and glasses (ceramics) generally have lower permeabilities and outgassing rates than polymers. Detailed data for specific materials can be found in Glang et al.(35).

Evacuation of the deposition system is accomplished by using a system of vacuum pumps. These pumps may include: mechanical pumps, diffusion pumps, cryogenic pumps, cryosorption pumps, and getter pumps (35). Oil-sealed rotary mechanical pumps and diffusion pumps are most relevant to this work; details on other pumps may be found in Glang et al. (35).

Mechanical pumps move gases by using the cyclic motion of an arrangement of mechanical parts as shown in figure (32). Mechanical pumps can evacuate chambers relatively quickly down to pressures of several mtorr; but, their pumping efficiency rapidly declines at pressures below this as shown in figure (33). Mechanical pumps are used largely to rough out systems and to back diffusion type pumps. A common problem with oil sealed mechanical pumps is back streaming of pump oil into the vacuum system. Backstreaming can be minimized by not operating at base pressures and by installing a foreline trap similar to the one shown in figure (34).

Diffusion pumps operate on the principle of momentum transfer from streaming oil molecules to gas atoms/molecules as shown schematically in figure (35). Diffusion pumps are backstreaming limited (at their base operating pressure they emit

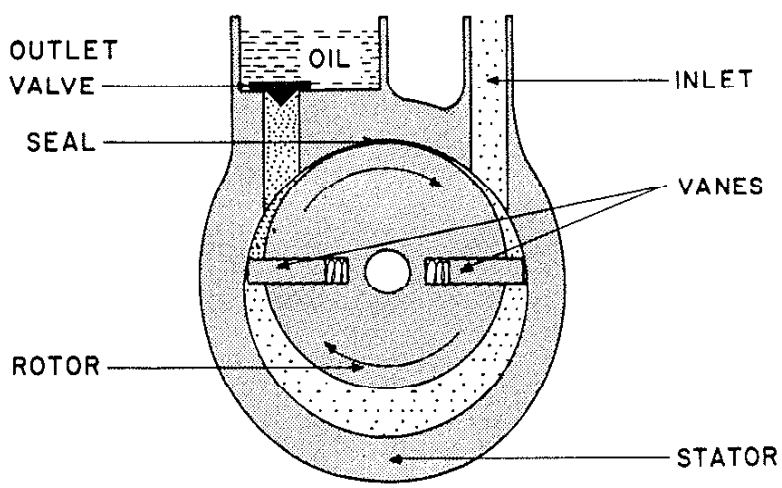

Figure 32. Schematic of vane-type rotary oil mechanical pump. From Glang, et al. (35)

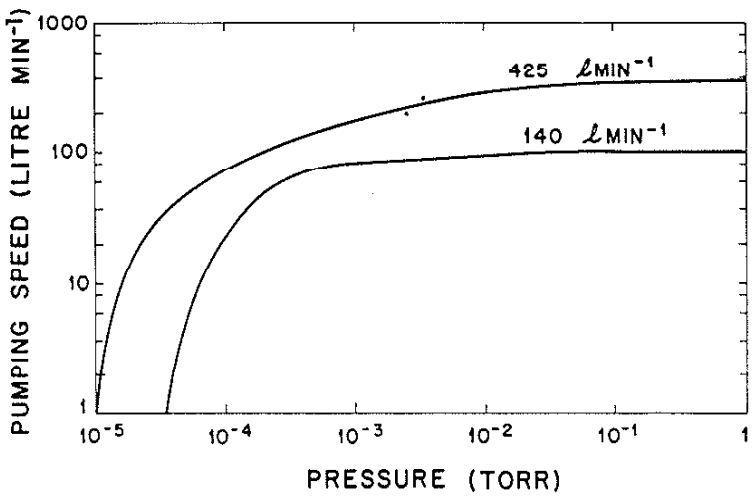

Figure 33. Pumping speed of rotary oil mechanical pumps as a function of chamber pressure. From Glang, et al. (35).

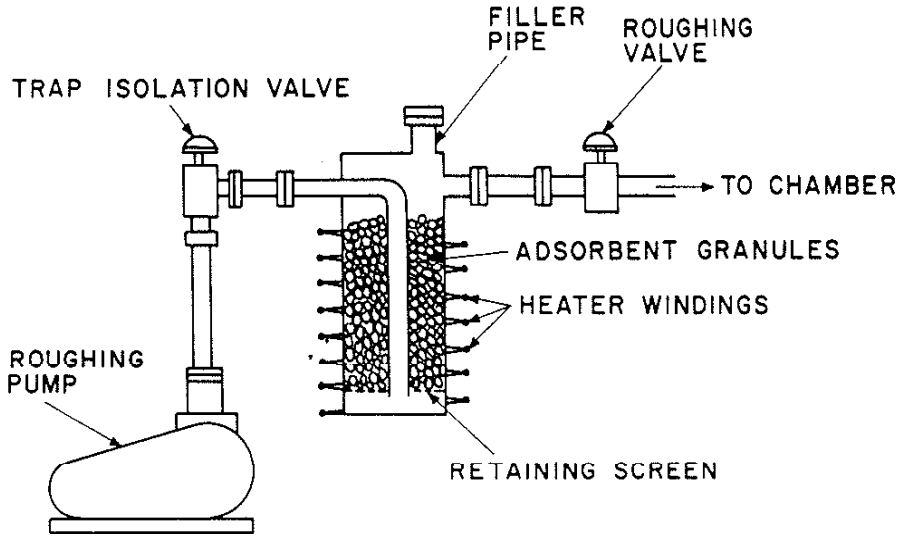

Figure 34. Schematic of foreline trap for reduction of backstreaming of mechanical pump oil. From Glang, et al. (35).

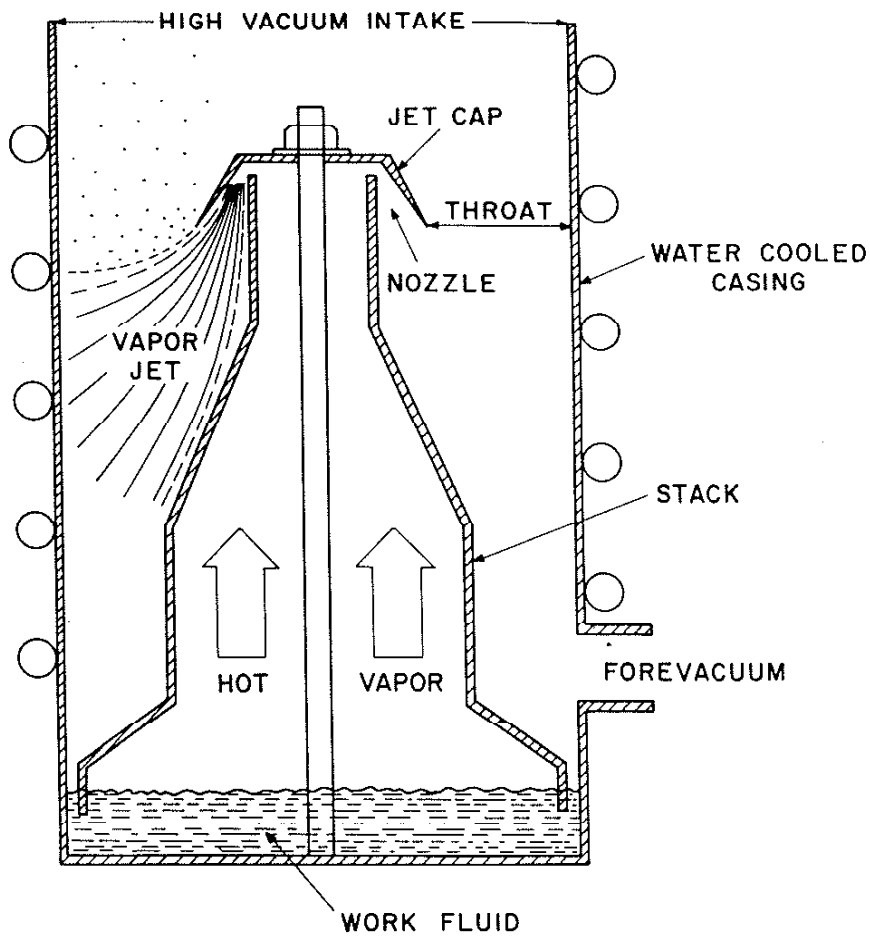

Figure 35. Schematic diagram of basic elements and operation of a diffusion pump. From Glang, et al. (35).

as much contamination gas as they remove) at pressure in the region of 10^{-7} to 10^{-8} Torr (1.33×10^{-5} to 1.33×10^{-6} Pa) (35). Oil films accumulating on substrates prior to coating deposition in diffusion pumped systems can contribute to poor film adhesion (35). The use of optically opaque liquid nitrogen cooled and adsorbent traps can reduce backstreaming and give ultimate pressures in the 10^{-9} to 10^{-10} Torr (1.33×10^{-7} to 1.33×10^{-8} Pa) range. Details of the various arrangements of traps and baffles and the performance of various diffusion pump fluids are discussed in Glang et al. (35).

Cleanliness is an important consideration in attaining a good vacuum in a reasonable amount of time. Fingerprints contain water, body oils and hydrated salts which can contribute to off gassing. Evaporated coatings deposited on chamber walls and fixtures often have porous structures characteristic of low temperature deposition (see figure (3)). These open structures can accumulate large quantities of adsorbed water vapor and other atmospheric contaminants when exposed to atmospheric pressure. Cold surfaces such as cold traps and water cooled chamber walls or evaporation hearths are also subject to condensation of water vapor when exposed to atmosphere; the presence of porous coatings on these surfaces will enhance this problem. Vacuum systems should be designed to facilitate easy cleaning; this can sometimes be effected by covering surfaces exposed to vapor fluxes with aluminum foil which can easily be replaced when it becomes contaminated.

Vacuum requirements during ion plating are typically on the order of several millitorr (7.5 mtorr = 1 Pa). We can attain this

pressure by considering an ideal (no leaks) and a nonideal (leaks) vacuum system.

In the ideal vacuum system, the work chamber can be evacuated to a high vacuum (much less than a millitorr) and then backfilled to the desired pressure with an inert gas such as argon. Deposition could then start and the pressure could be expected to remain constant. In actuality, the pressure could show a decrease due to incorporation of gas atoms into the growing coating according to equation (1) or an increase due to heating of the gas during deposition and the ideal gas law.

In the non-ideal vacuum system there will be real and virtual leaks of magnitude q present which will limit the base pressure that the chamber can be evacuated to according to the equation:

$$q = p_0 s \tag{6}$$

where p_0 is the base pressure and s is the pump speed. Real leaks arise from imperfections in seals or flaws in the vacuum chamber, virtual leaks arise from off gassing, porous materials, cold traps, backstreaming, pump fluids, etc. Since leaks are present, the chamber cannot be isolated from the pumps without losing control over the pressure. In this case, pumping must be continued and an adequate flow of inert gas maintained to achieve the desired working pressure. The working pressure p_1 is given by the equation:

$$p_1 = (q + Q)/s \tag{7}$$

where Q is the inert gas flow rate. To minimize coating contamination, it is desirable to have Q>>q.

In oil diffusion pumped systems it is desirable to keep the working pressure p_1 that the pump sees below 1 mtorr to be within the efficient working range of the pump. If an operating pressure p_2 higher than p_1 is desired, this can be accomplished by adding a limiting conductance F to the throat of the pump and using equation (8) to achieve the desired working pressure p_2.

$$p_2 - p_1 = F(Q + q) \tag{8}$$

Illustrations of these pressure - flow relationships are shown in figure (36) from Chapman (21).

VII.A.2. GLOW DISCHARGE

The "glow discharge" used in ion plating processes is a weakly ionized plasma similar to those found in fluorescent and "neon" lamps. The majority of the following discussion on the glow discharge is taken from Chapman (21). DC glow discharges consist of a series of luminous and dark regions similar to those shown in figure (37). These distinct regions may or may not be visible in actual ion plating systems due to the effects of system geometry on the electric field and the low relative intensity of the discharge in comparison with illumination from the vapor source.

The region of the discharge that most resembles a plasma is the positive column (21). As the distance between the electrodes is reduced, the positive column shrinks and the cathode dark space and

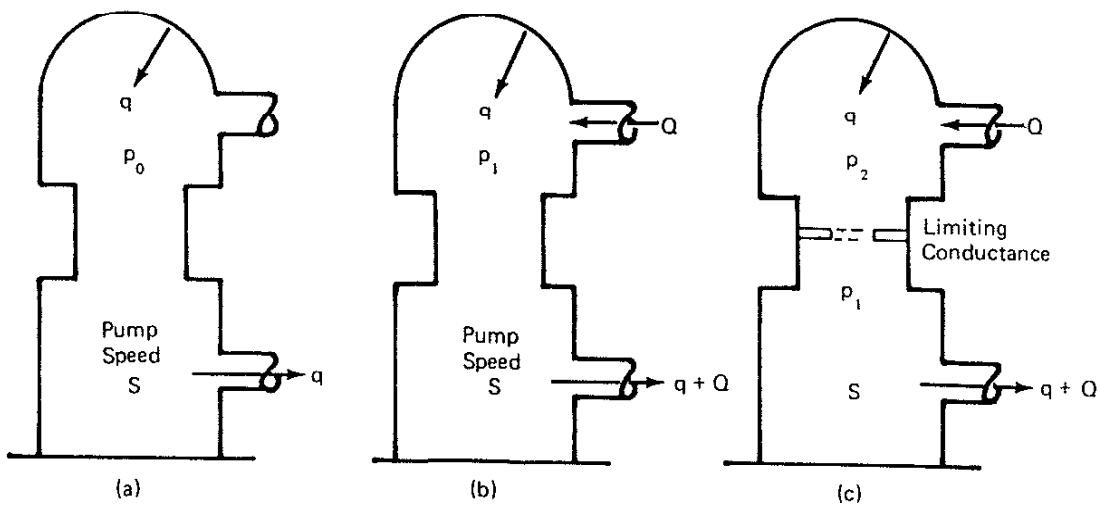

(a) At base pressure p_0, $q = p_0 S$

(b) Now add required gas flow Q, $q + Q = p_1 S$

(c) Then throttle to establish required pressure p_2, $q + Q = F(p_2 - p_1)$

Figure 36. Pressure - flow relationships. From Chapman (21).

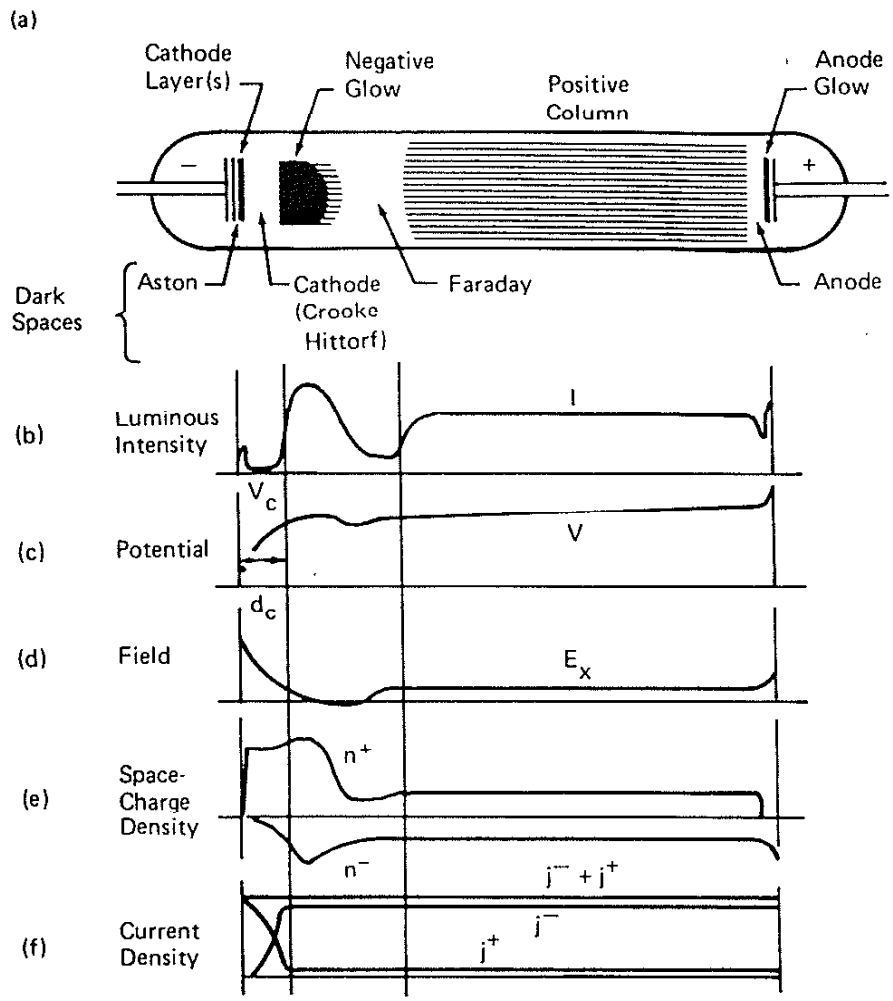

Figure 37. Schematic of glow discharge showing luminous and dark regions. From Chapman (21).

negative glow are unaffected (21). When the distance is further reduced the positive column and then the faraday dark space will be extinguished to leave only the negative glow and the dark spaces adjacent to each electrode (21). The discharge is extinguished when the electrode separation distance is less than about twice the dark space thickness (21).

To sustain the glow discharge, electron and ion loss processes must be balanced against electron and ion generation processes (21). According to Chapman (21), loss processes include electron-ion recombination at the walls, ion neutralization by Auger emission at the cathode, and an equivalent electron loss to the external circuit at the anode. Energy is also lost from the discharge in the form of photons and heating of electrodes and chamber walls of the system; energy input to the discharge must be balanced against energy loss to maintain a steady state discharge (21). The simplest explanation of how ionization (electron - ion pair creation) and energy requirements are met is that the applied electric field accelerates electrons, giving them sufficient energy to ionize gas atoms (21). The charged particles resulting from the ionization are then accelerated by the field to create further ionizations and the discharge is thus sustained. The motion of ions in the electric field eventually brings them to the cathode where they can be neutralized by combination with Auger electrons and the motion of electrons in the electric field eventually brings them to the anode where they can be lost to the external circuit; the net result of both these processes is a current in the external circuit which varies with gas

pressure and discharge voltage as shown in figure (38) from Chapman (21).

The above discussion accounts for ionization, recombination, and external current very nicely; unfortunately, it predicts a linear voltage distribution between the two electrodes which would result in a uniform discharge between the electrodes. From the earlier discussion, we know that the discharge consists of a series of luminous and dark regions between the electrodes which indicates nonuniform ionization and recombination between the electrodes; apparently, we need to account for the difference. Much of the difference can be explained in terms of the mass of an electron being much less than the mass of an ion and space charge limited current at the electrodes.

If we look at figure (39) from Chapman (21) and compare it with figure (37) we see, according to Chapman (21): 1. The discharge does not take a potential intermediate between those of the electrodes; the positive column is the most positive region of the discharge. 2. The electric fields in the system are restricted to sheaths (dark spaces) at each of the electrodes. 3. The sheath fields are such as to repel electrons trying to reach either electrode.

The positive charge on the positive column arises because electrons with their lower mass than ions are more mobile than ions. Electrons are also smaller than ions, so they are able to traverse a greater distance in the discharge without encountering a collision with a gas atom. In the positive column, the electron and ion densities are approximately equal, giving the plasma an approximately neutral charge. In the presence of an electrode such

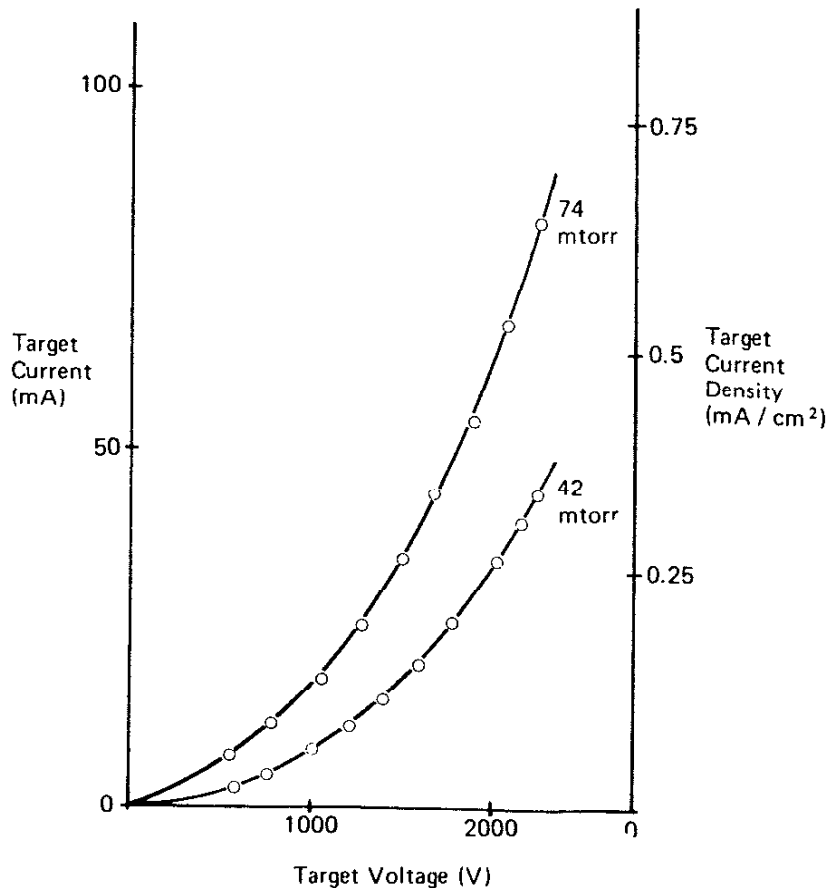

Figure 38. Variation of target current with discharge (target) voltage and gas pressure. From Chapman (21).

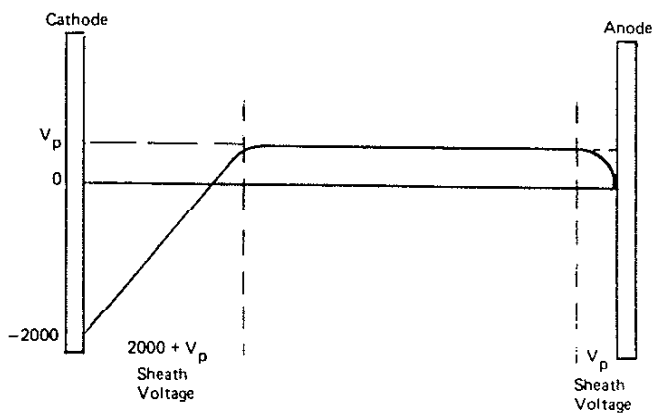

Figure 39. Voltage distribution in a DC glow discharge process. From Chapman (21).

as the cathode or anode, this equilibrium is disrupted. In the case of the anode, electrons can be rapidly drained from the nearby plasma, resulting in an excess of positive charge in the nearby region. Electrons within the discharge redistribute themselves in an attempt to balance the excess positive charge; since there is not enough of them, the body of the discharge will have a net positive charge. The slight positive charge relative to the anode slows the drain of low energy electrons to the anode (only high energy electrons accelerated from the cathode and passing through the discharge will be able to cross the barrier at the anode), causes nearby positive ions to be drawn to the anode, and causes low energy secondary electrons from the anode to be drawn to the positive column.

In the case of the cathode, the situation is similar. Electrons are repelled from the cathode to such a distance as the voltage of the cathode is screened by the positive ions that are moving toward it. The relatively slow motion of ions relative to electrons causes a slight buildup of positive charge. The low energy electrons in the body of the plasma attempt to neutralize; but there are not enough of them so a net positive charge of the discharge results.

The balancing processes at the anode and cathode that result in sheath or "dark space" formations occur very quickly so that the system rapidly achieves a steady state.

In an ion plating glow discharge, the substrates are made the cathode of the discharge; so, it is relevant to discuss the cathode region in greater detail. The basis for this discussion comes largely from Chapman (21) and Hurley (36).

The behavior of the discharge at the cathode characterizes the discharge as either a "normal glow discharge" or an "abnormal glow discharge". A "normal glow discharge" occurs at low voltages and low currents such that the discharge occurs at constant voltage and constant current density with an increase in power to the system being utilized by increasing the size of the region of the cathode carrying current until the whole cathode is utilized (21). If more power is added to the system beyond the point at which the whole cathode is utilized, the discharge becomes abnormal and both the current density and the voltage increase with increased power to the system (21). The discharges used in ion plating processes are "abnormal glow discharges".

Particles in the discharge adjacent to the cathode include neutrals, metastables, positive ions, negative ions, electrons, and photons (36). The relative importance of these particles as far as their interaction with the substrate (cathode) depends on their energy distribution (36).

Neutrals near the cathode occur in several forms and arise from several sources. Thermal neutrals arise from the background gas including all sources of impurities; they have a Maxwell-Boltzman energy distribution and occur in concentrations of approximately 3×10^{13} /cm^{3}mtorr (2.25×10^{14} /cm^{3}Pa) (36). Energetic neutrals near the cathode arise from charge exchange collisions in the dark space and neutralization of ions at the cathode (36). Their energy increases with increasing voltage and decreasing pressure; the energy of energetic neutrals is reduced when they encounter collisions with background gas atoms (36). Neutrals may

undergo significant reactions with impurity gas atoms at higher pressures (36).

Metastables are excited atoms with very long lifetimes which arise because selection rules forbid relaxation to the ground state or make the transition to the ground state unlikely (21). Argon, which is commonly used as a background gas in ion plating, has metastables at 11.5 eV and 11.7 eV (21). Metastables can undergo interactions with other metastables, neutrals, and electrons (21). Penning ionization occurs when a metastable atom collides with a neutral atom with an ionization energy less than the excitation energy of the excited atom and the neutral is ionized (21). Metastables colliding with one another may result in the ionization of one of the pair; two argon metastables of energy 11.55 eV could interact to overcome the 15.76 eV ionization threshold of one of the pair (21). Electron impact with a metastable may lead to ionization of the metastable (21). In the case of argon, the threshold for ionization of a ground state atom is 15.76 eV whereas for an 11.55 eV metastable the threshold would only be 4.21 eV; therefore, it is reasonable to assume that there are many more electrons in the discharge capable of ionizing metastables than there are capable of ionizing ground state atoms (21). The potential energy of metastable states may promote chemical and physical interactions near the cathode which ground state atoms are not energetically favored to undergo (36). Metastable density in a discharge has been estimated at $10^{10}/cm^3$ (21).

Positive ions near the cathode may be formed by metastable - neutral and metastable - electron interactions as discussed above;

they may also be formed by electron - neutral and ion - neutral interactions (21). The current density of positive ions is approximately $j_+ = n_+ e v_+/4$ where v_+ is the mean velocity and n_+ is the ion density of the species of interest (36). For argon in ion plating discharges, n_+ is on the order of 10^9 - $10^{10}/cm^3$ (36). Ionized combinations of atoms may occur involving interactions between inert gas atoms, impurities, and coating atoms; this may lead to the formation of multiply charged species (36). The energy distribution of positive ions near the cathode is determined by collisions with other species (mostly neutrals) in the dark space and thus will be pressure and voltage dependent (36).

Negative ions are of importance in chemically reactive plasmas and may also be of importance in inert gas discharges (36). Negative ions may arise from the background gas, pumping oils, sealing materials, chamber walls and fittings, coating and substrate materials (36). In general, negative ions are accelerated away from the cathode region of the discharge by the electric field; so, their formation by impurities tends to reduce impurity incorporation in the growing coating (36). Negative ions may be formed by the same mechanisms described for positive ions.

Electron - neutral collisions leading to ionization (electron impact ionization) in the region near the cathode occur when secondary electrons emitted from the cathode are accelerated by the electric field in the dark space to attain sufficient energy to cause ionization before colliding with a neutral atom (21). The electron or electrons liberated from the ionized atom may then traverse the electric field and cause further ionizations before entering the

positive column where there is no longer an electric field to cause acceleration of any more electrons produced (21). Some electrons may be accelerated from the cathode and traverse the entire discharge to impact on the anode without encountering a collision; the probability of this occurring decreases with increasing pressure and increasing distance between the electrodes (21).

Ion - neutral collisions leading to ionization (ion impact ionization), in the region near the cathode occur when ions extracted from the positive column or generated by electron impact ionization are accelerated by the electric field near the cathode and acquire sufficient energy to cause ionization or neutral atoms they collide with (21). Ion impact ionization is a less efficient process for ion production than electron impact ionization (21). Maximum possible ion production rates by these processes in a 600 V 60 mtorr (8 Pa) argon discharge have been quoted as 0.15 ions per ion for ion impact ionization and 0.24 ions per ion for electron impact ionization (21).

Electrons in the region adjacent to the cathode arise from secondary emission and photoemission at surfaces within the chamber and from ionizing collisions in the plasma or the dark space (36). In sputtering systems where the target potential (cathode) is high relative to the substrate bias potential (anode), target secondary electrons may induce polymerization of unwanted hydrocarbon contaminants on the substrates; in the case of ion plating, the substrates are the cathode and the chamber walls are the anode so unwanted hydrocarbons may be polymerized on the chamber walls, effectively reducing their probability of being incorporated into the growing coating (36).

The density of electrons in the discharge is on the order of the density of ion to maintain the approximate charge neutrality of the discharge (21). The density of electrons and ions in the discharge is generally less than one tenth of one percent of the density of neutrals in the system (21). Mechanism of ionization enhancement can be used to increase the density of electrons and ions relative to that of neutrals. These mechanisms most commonly include: 1) use of magnetic fields to increase the path length of electrons before they collide with the anode; 2) using the inherent ionization enhancement provided by RF excitation; and 3) pumping more electrons into the discharge by using a hot filament as an electron source (21). Method 3 is most relevant to ion plating discharges in which case it is implemented in a triode configuration (21). In the triode an anode is provided and/or the hot filament is biased negatively to overcome the space charge limitation imposed on thermionic emission given by the Richardson - Dushman equation (equation (9)) (21).

$$j = AT^2 \exp(-e\phi/kT) \qquad (9)$$

where j is the electron current, ϕ is the work function of the metal, T is the temperature of the filament, and A is a constant equal to 120 A/cm^2deg^2 (21).

Photons in the cathode region of the discharge arise from particle-particle interactions, recombinations at the cathode surface, and electron impact on metal surfaces such as in electron beam evaporation sources (36). Photon energies range from the

visible up into the x-ray region (36) The wavelength of the most energetic photon in the system is given by equation (10) from reference (37).

$$w_{swl} = 1240/V \tag{10}$$

where V is the greatest potential difference in the system in kV and w is in angstroms (37). In electron beam evaporator sourced ion plating systems, the greatest potential difference is generally due to the evaporation source and is on the order of 10 kV. Energy transfer by photons may promote physical and chemical reactions within the discharge and at surfaces (36). Detection of photons from a discharge may be difficult due to gas absorption; this may lead to difficulty in quantifying information carried by the photons although a qualitative understanding of the species present may be obtained from the characteristic wavelengths (36).

VII.A.3. ENERGETIC PARTICLE BOMBARDMENT

Realistically, any particle except electrons in the discharge adjacent to the cathode is a candidate for bombardment of the substrate (cathode). Of primary interest in this work are ions and energetic neutrals since they are believed to cause the differences observed between ion plated and evaporated coatings. Chapman (21) gives a good review of the interactions of ions with surfaces and sputtering kinetics; however, he does not discuss the interactions of energetic neutrals with the cathode. Thornton (18) and Hagstrom (38) discuss the neutralization of ions as they approach the surface

by Auger electrons emitted from the surface as the ions get close. From this, it is not unreasonable to assume that energetic neutrals with energies approaching those of the ions will interact with the cathode similarly to the ions.

The extent of interactions between bombarding ions and neutrals and the bombarded surface is dependent on incident particle energy for a given substrate voltage. Due to collision processes in the glow discharge, ions incident on the substrate (cathode) are not monoenergetic; but, rather, there is a distribution of ion energies with the peak in the distribution at less than one half the discharge voltage. The distributions of ion energies incident on the cathode in a glow discharge has been described by Davis and Vanderslice (39), Hurley (36), Armour et al. (40), Chapman (21), and others. The nature of the plasma is strongly dependent on electric fields, magnetic fields, working gas pressure, residual gas composition, geometry of the vacuum system, and the composition of material being sputtered off the substrate holder and chamber walls. There is not exact agreement as to the peak energy in the energy distribution of singly ionized species impacting the substrate. The work by Davis and Vanderslice (39) for singly ionized argon indicates a maximum number of ions at energies less than 15 percent of the applied voltage as shown in figure (40). The main energy peak in the work cited by Hurley (36) and the work by Armour and co workers (40) was at about 25 percent of the applied voltages as shown in figure (41). In general, it could be said that the majority of singly ionized argon atoms bombarding the substrate would have energies of less than 30 percent of the applied voltage.

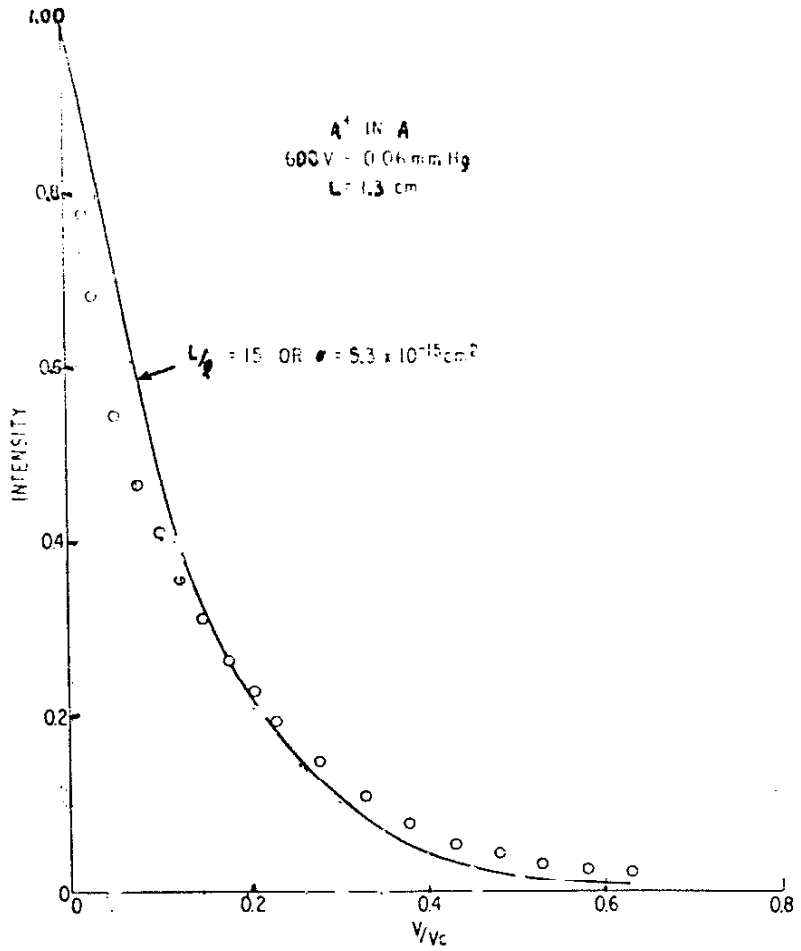

Figure 40. Energy distribution for Ar^+ from an argon discharge. From Davis and Vanderslice (39).

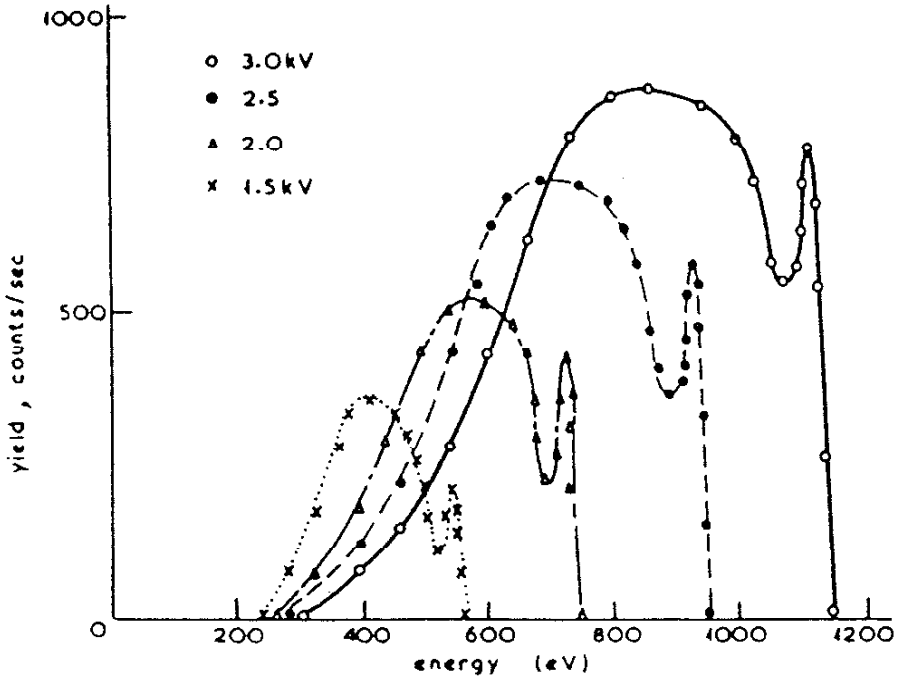

Figure 41. Energy distribution for Ar^+ ions leaving a 3 x 10^{-2} Torr (4 Pa) argon discharge for various discharge voltages. From Armour, et al. (40).

There is also lack of agreement in the energy distribution of doubly ionized species impacting the substrate. The work by Davis and Vanderslice (39) indicates that the peak is within 10 percent of the applied bias as shown in figure (42). The work by Armour, et al. (40) indicates that the peak is at less than half the discharge voltage as shown in figure (43).

Armour, et al. (40) found that the peak in the number of energetic neutrals occurs at about 20 percent of the discharge voltage as shown in figure (44). Increasing the discharge voltage increases the number, width of distribution and average energy of the energetic neutrals as shown in figure (44). The effect of increasing pressure is to increase the number of energetic particles while reducing the average and maximum values of the distribution as found by Armour, et al. (40) and shown in figure (45).

VII.A.4. EFFECTS OF ION BOMBARDMENT

A summary of the possible interactions of ions with surfaces has been given by Chapman (21) and the review presented here is taken largely from this source, keeping in mind that it is not unreasonable to apply these interactions to energetic neutrals due to the Auger neutralization process which effectively converts ions to neutral particles as they approach the surface. An illustration of some of the possible interactions is shown in figure (46). The interactions include (21):

1) Reflection of the ion with the possibility of it being neutralized in the process (21). The probability of being neutralized has been discussed by Hagstrom (38) as being dependent on ion and

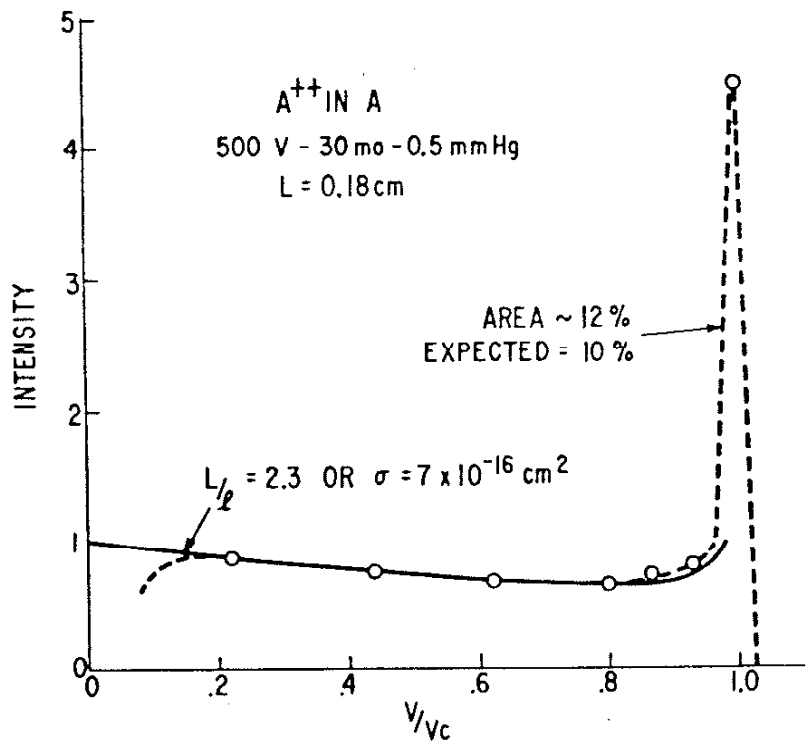

Figure 42. Energy distribution for Ar++ from an argon discharge. From Davis and Vanderslice (39).

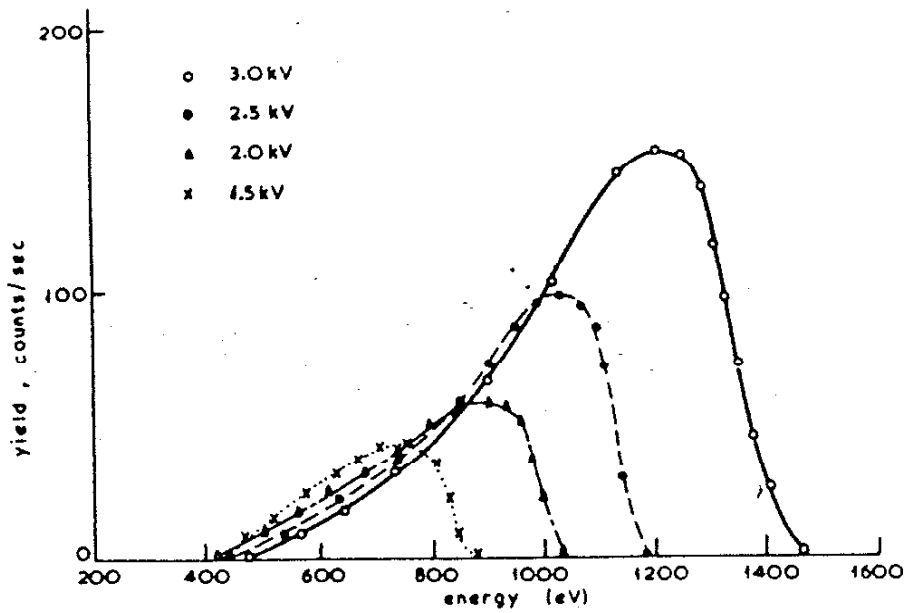

Figure 43. Energy distribution for Ar++ leaving an argon discharge for various discharge voltages. From Armour, et al. (40)

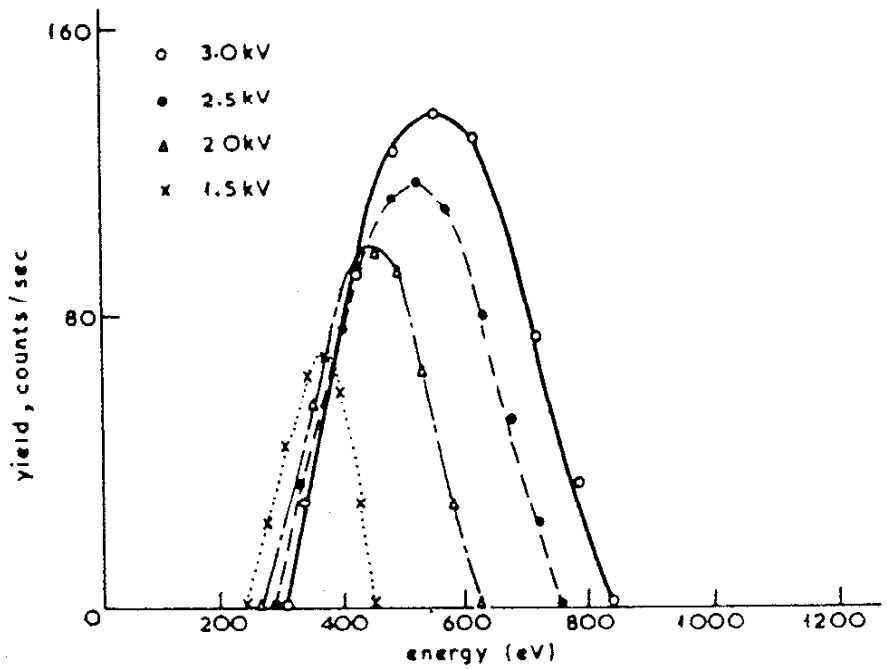

Figure 44. Energy distribution of the neutral particles leaving a 3 x 10^{-2} Torr (4 Pa) argon discharge for various discharge voltages. From Armour, et al. (40).

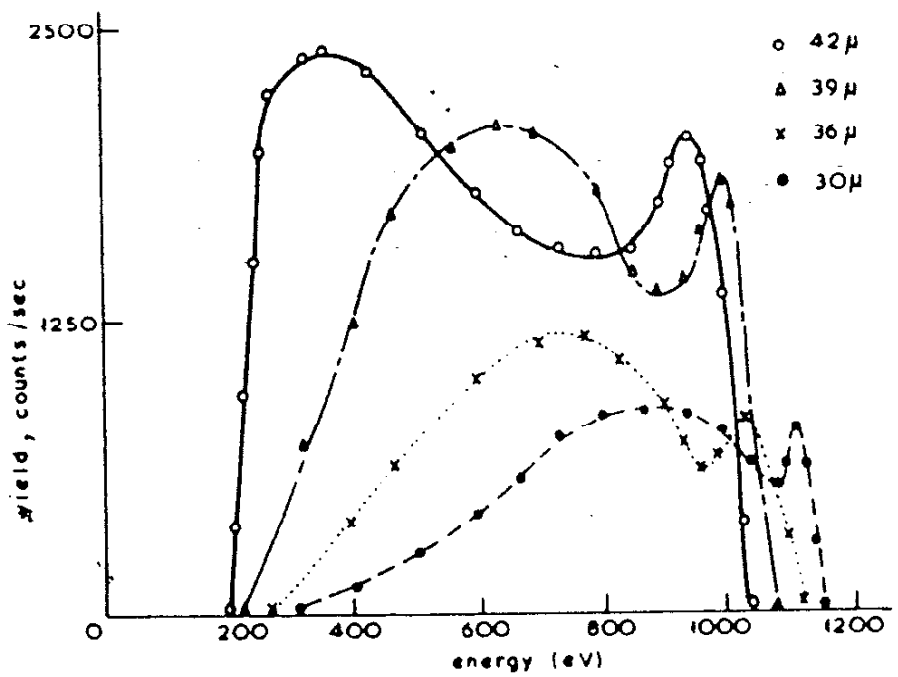

Figure 45. The effect of pressure on the energy distributions of Ar^+ ions leaving a 3 kV argon discharge. From Armour, et al. (40).

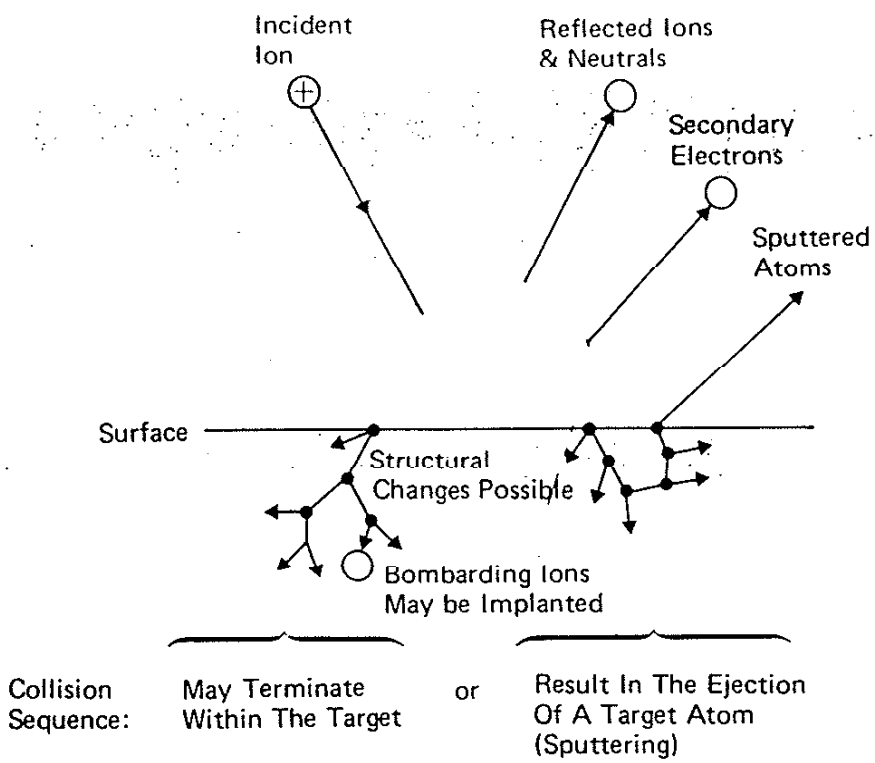

Figure 46. Interactions of ions with surfaces. From Chapman (21).

surface species and the energy of the incident ion. The reflection of ions from a surface is the basis for Ion Scattering Spectroscopy (ISS), which gives information on ion - surface interactions and allows characterization of near surface layers (21).

2) Ejection of secondary electrons from the target surface may be stimulated by ion impact. The yield of secondary electrons is dependent on the species of incident ion, the composition of the target surface, the energy of the incident ion, and the crystallographic orientation of the target surface as shown in figures (47) and (48) (21). Secondary electrons accelerated away from the cathode are important to sustain ionization in the discharge.

3) The incident ion may be implanted in the target as in ion implantation. The implantation depth increases with incident ion energy. Use of a computer program developed and discussed by Ziegler, et al. (41) for ion/substrate combinations and ion energies relevant to this work gave implantation depths on the order of a hundred angstroms (ten nanometers). Ion implantation has found application in integrated circuit technology for generating specific doping profiles in Si wafers; it has also found application in selectively surface hardening steels (21).

4) The incident ion may cause structural rearrangements such as vacancies, interstitials, changes in stoichiometry, and changes in electrical charge levels and distributions (21). The near-surface regions in which these rearrangements and changes in stoichiometry have taken place are referred to as the altered surface layers. Work by Mattox (20) and Teer and Salem (8) indicates that ion

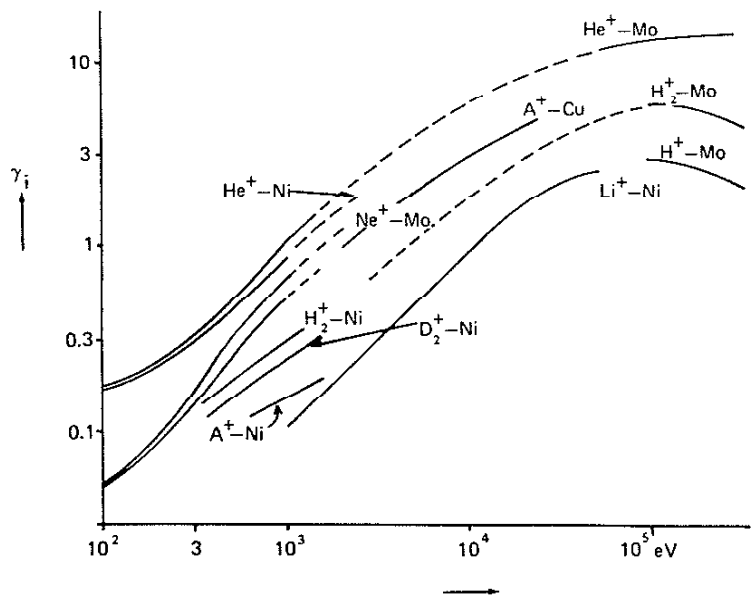

Figure 47. Secondary electron emission coefficient for ions of various energies falling on the surface of various substances. From Chapman (21).

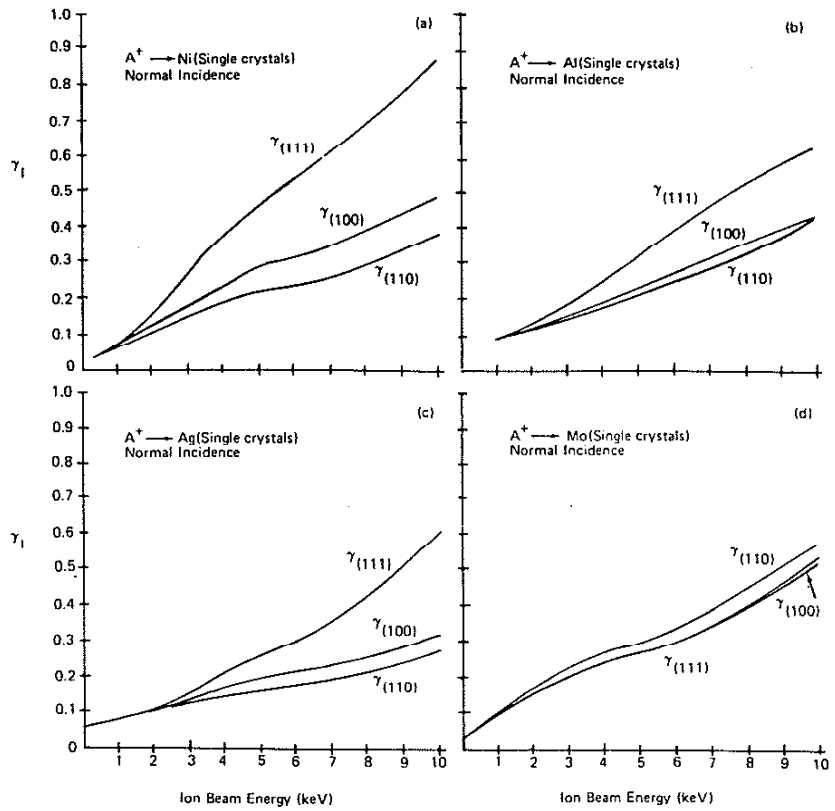

Figure 48. Secondary electron emission coefficient as a function of ion beam energy, substrate material, and substrate crystallographic orientation. From Chapman (21).

bombardment induced structural rearrangements during coating deposition allows enhanced diffusion between the coating and the substrate when ion bombardment accompanies coating deposition.

5) The incident ion may cause sputtering of one or more target atoms. Sputtering occurs when the incident ion sets up a series of collisions between atoms in the target leading to ejection of one or more atoms. The sputtering yield in atoms per incident ion varies with incident ion species (figure (49)), residual gas pressure (figure (50)), incident ion energy (figures (49) and (51)), target composition (figure (52)), and target crystallography (figure (53)) (21). Sputtering is an important mechanism for the removal of substrate surface contaminants such as oxides and organics prior to coating deposition by ion plating (21).

Chapman (21) describes the sputtering process as a series of binary collisions in the target resulting in the ejection of one or more target atoms. Since sputtering con be considered the process of transferring energy from the incident ion (or energetic neutral) to the sputtered atoms and sputtered atoms can come only from the near surface layers, the sputtering yield S should be proportional to the energy deposited in a thin layer near the surface which is determined by the nuclear stopping power S(E) (21). The nuclear stopping power for bombardment energies up to about 1 keV has an equation of the form:

$$S(E) = m_i m_t E * \text{constant}/(m_i + m_t) \qquad (11)$$

where m_i is the mass of the incident ion, m_t is the mass of the

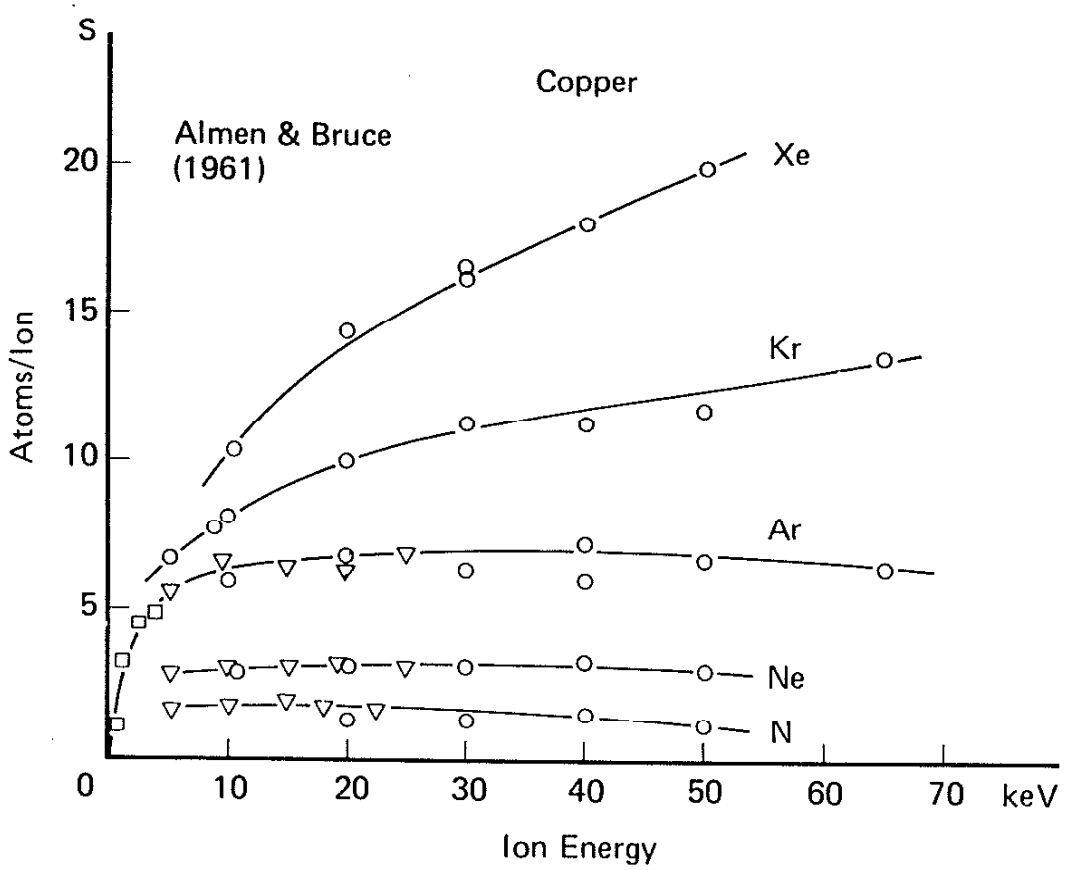

Figure 49. Sputter yield of copper atoms as a function of ion species and ion energy. From Chapman (21).

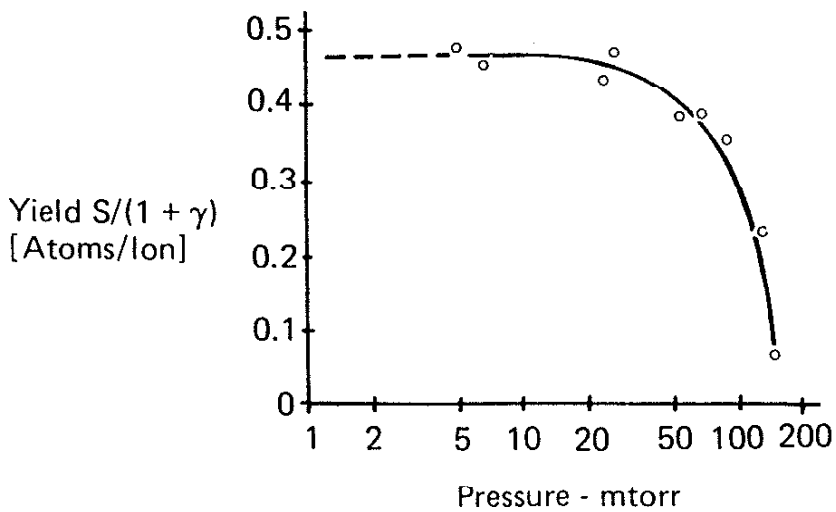

Figure 50. Variation of sputtering yield of nickel with argon gas pressure for 150 eV ion energy. From Chapman (21).

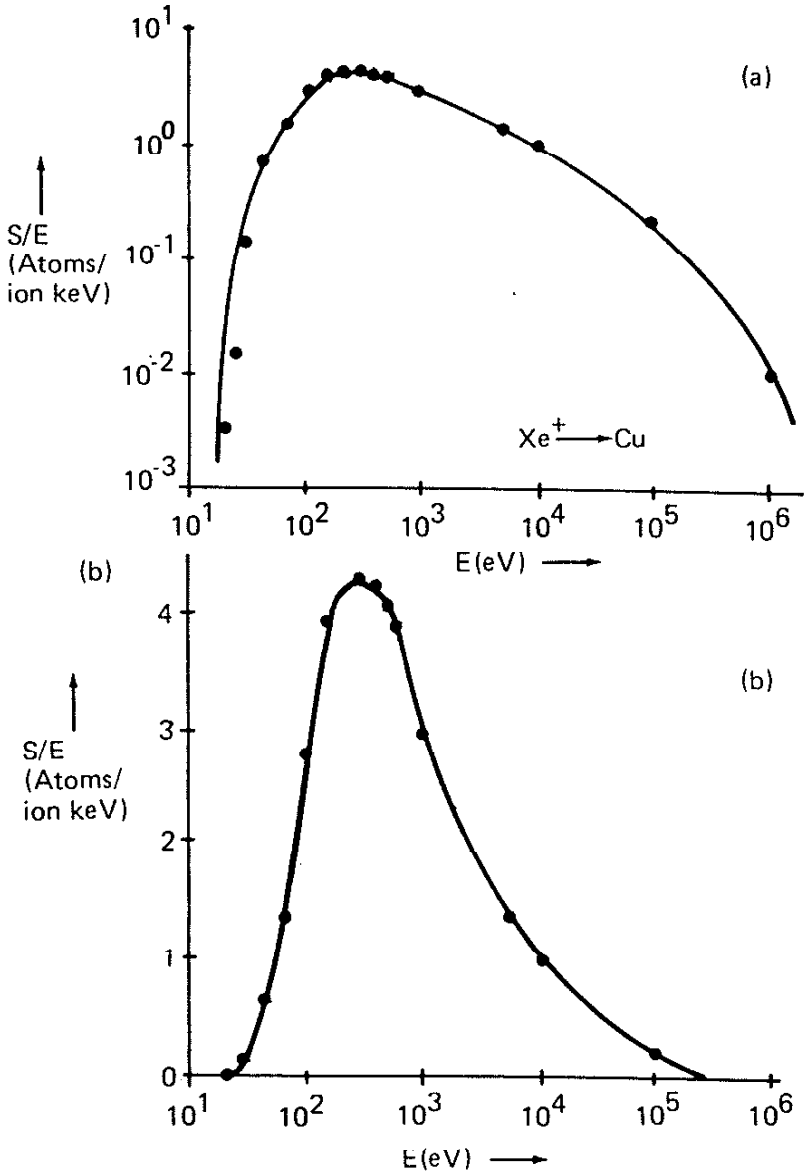

Figure 51. Variation of the sputtering yield per unit energy input of xenon on copper vs. ion energy. From Chapman (21)

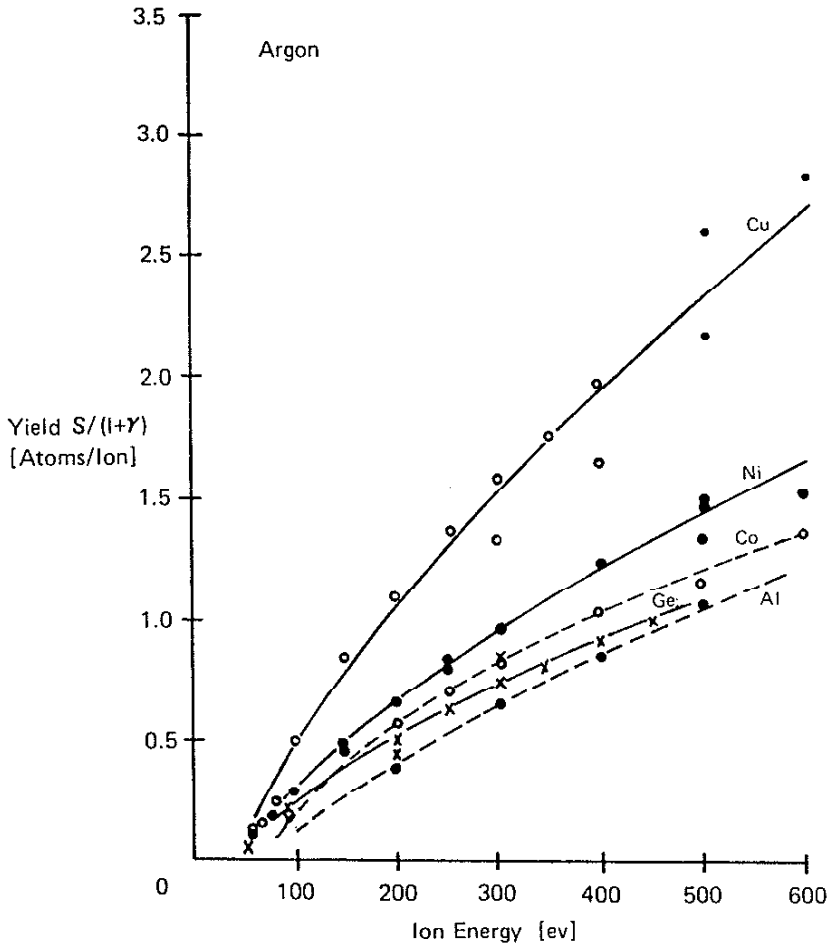

Figure 52. Variation of sputter yield as a function of target composition and ion energy. From Chapman (21).

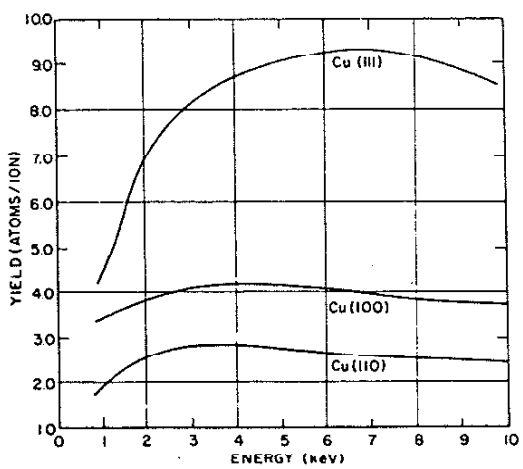

Sputtering yield of the three low-index planes of Cu bombarded by normal-incidence A^+ ions.

Figure 53. Variation of sputter yield as a function of target crystallographic orientation and ion energy. From Chapman (21).

target atom and E is the energy of the incident ion (21). The nuclear stopping power is used to predict the form of the sputtering yield S as:

$$S = 3\alpha 4 m_i m_t E/(4\pi^2(m_i + m_t)^2 U_0) \quad (12)$$

where U_0 is the surface binding energy of the target material, and α is an increasing monotonic function of m_t/m_i with values of 0.17 for $m_t/m_i = 0.1$ and 1.4 for $m_t/m_i = 10$ (21). At higher energies the equation must be modified to account for changes in assumptions about atomic interactions. Above 1 keV, the sputtering yield is given by Chapman (21) as:

$$S = 3.56\alpha z_i z_t m_i S_n(E)/((z_i^{2/3}+z_t^{2/3})(m_i+m_t)U_0 \quad (13)$$

where $S_n(E)$ is a reduced stopping power and is a function of a reduced energy based on the actual energy, masses, and atomic numbers z_i and z_t of the atoms involved in the interaction. Equation (13) gives reasonable results when compared with experimental results as shown in figure (49) for noble gases bombarding copper (21).

Thornton (18) has described the general dependence of sputtering yield on the angle of ion incidence with the surface as shown in figure (54). Ions incident to the target surface at an angle θ, passing through a region of depth d where primary sputtering momentum exchanges occur, will have their path length through that region increased by a factor of $\sec\theta$ before leaving the region (18).

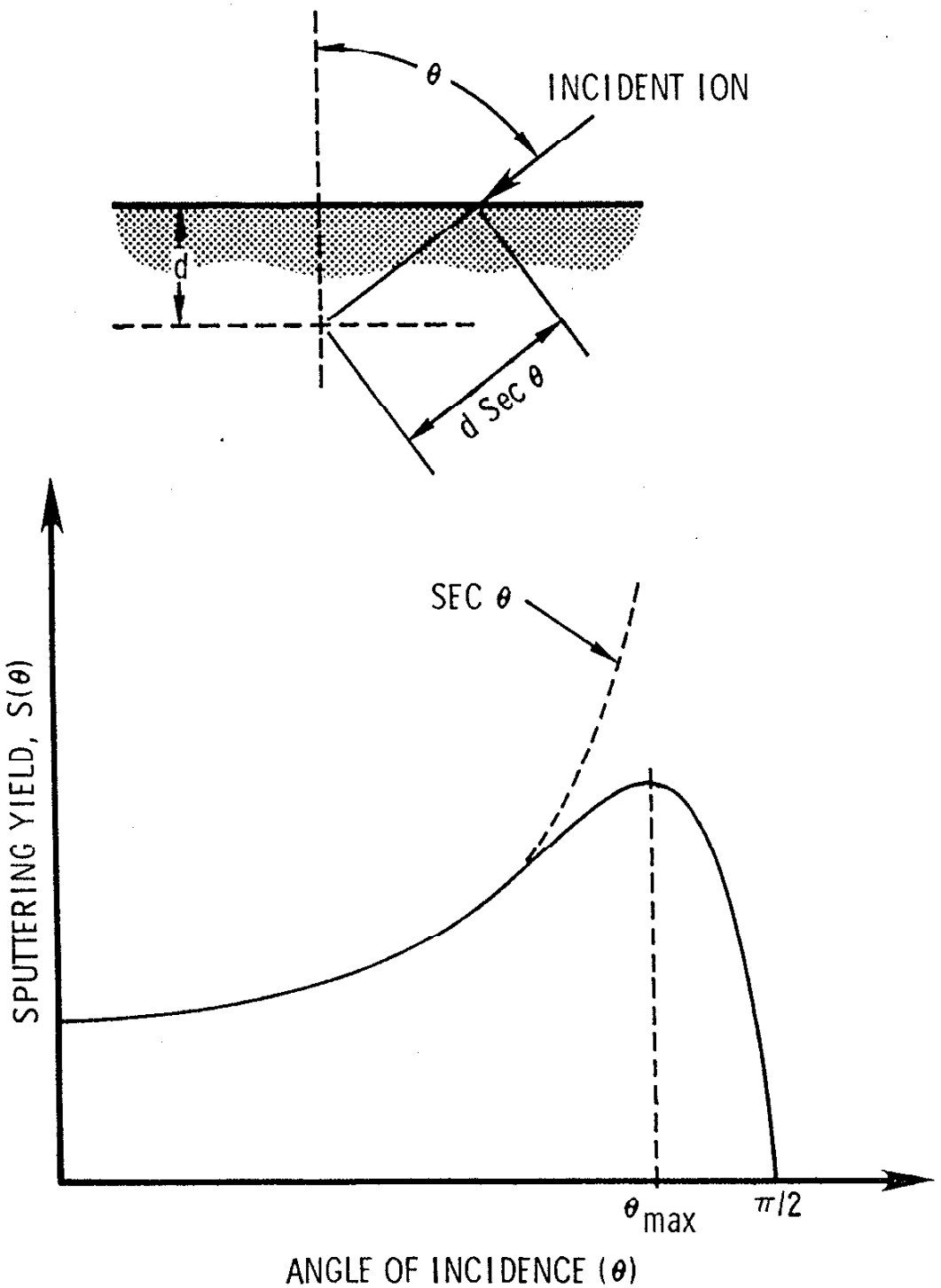

Figure 54. Schematic diagram showing variation of sputtering yield with ion angle of incidence at constant ion energy. From Thornton (18).

At large angles of incidence, the yield decreases because ion reflection from the surface becomes dominant. In glow discharge processes such as ion plating, the ions generally approach the surface in a direction normal to the surface; this promotes smoothing of single element surfaces and cone formation due to differences in sputtering yield on contaminated and multicomponent surfaces (18).

The primary purpose of ion bombardment of the substrate surface prior to coating deposition by ion plating is to remove surface contaminants by sputter cleaning to provide for better adhesion of the coating to the substrate. Typical discharge parameters for effective sputter cleaning given by Mattox (20, 42) involve several millitorr (7.5 millitorr = 1 Pa) of inert gas pressure, 3 or more kV of discharge voltage, and about 2 tenths of a milliamp per square centimeter or more current density at the cathode.

VII.A.5. EVAPORATION OF COATING MATERIAL

Evaporation of Al source material for ion plating deposition as relevant to this thesis is by electron beam evaporation. The following discussion of electron beam evaporation comes largely from Glang (34). In electron beam evaporation, a stream of electrons is accelerated through electric fields of typically 5 to 15 kV and allowed to impinge on a focal point on the evaporant surface where the kinetic particle energy is converted into heat and temperatures exceeding 3000 Celsius (3273 K) may be obtained (34). An advantage of this method is that energy can be concentrated in a given region of the evaporated surface to cause evaporation while

other regions of the evaporant are maintained at lower temperatures thus reducing the interaction between the evaporant and the supporting crucible (34). A hot cathode in the form of a filament is universally employed as the electron source in electron source in electron beam evaporators (34). Tungsten wire is the preferred filament material due to its strength and shape retention at high temperatures required for efficient electron emission (34). Filament life is limited by reactions with evaporant and residual gas vapors and by sputtering due to bombardment by high energy positive ions created by interaction of the electron beam with evaporant and residual gas atoms (34). Ionization of residual gas atoms and evaporant atoms also causes loss of beam energy and focus (34). In general it is desirable to operate the filament at pressures below 10^{-4} Torr (1.33×10^{-1} Pa) (34). In ion plating systems where the operating pressures are on the order of 10^{-3} Torr (1.33 Pa) and above, it is advantageous to use magnetic fields to bring the electron beam through a differential pumping aperture in a baffle plate to allow the elevated pressures in the deposition region required for the ion plating process while maintaining sufficiently low pressures in the filament region to ensure long filament life (34). Since no amount of protection will give filaments an infinite life, it is necessary that electron gun be constructed so that the filament can be easily replaced (34).

A thermodynamic understanding of the equilibrium vapor pressure above a heated evaporant can be derived from the Clapeyron equation (9):

$$(\delta P/\delta T)_{eq} = (H_v - H_c)/T(V_v - V_c) \quad (14)$$

where P is the pressure, T is the temperature, $(H_v - H_c)$ is the change in enthalpy in going from the condensed to the gaseous phase (molar latent heat of evaporation or sublimation), and $(V_v - V_c)$ is the difference in molar volume between the gaseous and condensed phases. Reasonably detailed derivations of pressure dependence on temperature can be found in Gaskell (9) and Glang (34). The material presented below comes largely from Gaskell (9).

When a condensed phase is in equilibrium with a vapor phase, the difference in volume between the phases is given by (9):

$$\Delta V = V_{vapor} - V_{condensed} \quad (15)$$

Since the volume of the vapor is much greater than the volume of the condensed phase, we can approximate the change in volume simply as the volume of the vapor (9):

$$\Delta V \cong V_{vapor} \quad (16)$$

Substituting this into equation (14) we get

$$(\delta P/\delta T)_{eq} = (H_v - H_c)/(TV_{(v)}) \quad (17)$$

If we assume that the vapor behaves as an ideal gas in equilibrium with the condensed phase, then we can apply the ideal gas equation (PV=RT) to get:

$$(\delta P/\delta T)_{eq} = P(H_v-H_c)/RT^2 \quad (18)$$

which can be rearranged to give:

$$\delta P/P = (H_v-H_c)\delta T/(RT^2) \quad (19)$$

or

$$\delta \ln P = (H_v-H_c)\delta T/RT^2 \quad (20)$$

which is known as the Clausius - Clapeyron equation. If the change in enthalpy is independent of temperature (heat capacity at constant pressure of the vapor equals heat capacity at constant pressure of the condensed phase) then integration of equation (20) gives:

$$\ln P = -(H_v-H_c)/RT + \text{constant} \quad (21)$$

From equation (21) we see that the equilibrium vapor pressure above a condensed phase increases exponentially with temperature. In the case of vaporization where the difference in C_p for the phase change is not zero, but is independent of temperature then using equation (22):

$$(H_v-H_c)_{T2} = (H_v-H_c)_{T1} + I(T_1,T_2)(C_{pv}-C_{pc})\delta T \quad (22)$$

in the form of equation (23)

$$(H_v-H_c)_T = (H_v-H_c)_{T=298} + (C_{pv}-C_{pc})(T-298)$$

$$= ((H_v-H_c)_{298} - 298(C_{pv}-C_{pc}))+ (C_{pv}-C_{pc})T \qquad (23)$$

for the change in enthalpy in equation (20) gives upon integration ($I(T_1,T_2)$ is the integral from T_1 to T_2)

$$\ln P=(298-\Delta C_p-\Delta H_{298})/RT+\Delta C_p \ln(T)/R+\text{constant} \qquad (24)$$

which is generally expressed in the form (9)

$$\ln P = A/T + B\ln T + C \qquad (25)$$

specifically considering the vapor pressure of liquid aluminum, Glang (34) gives equation (25) as:

$$\log P(\text{Torr}) = -16450/T + 12.36 - 1.023\log T \qquad (26)$$

where the temperature is in degrees Kelvin.

In the above discussion it was assumed that the vapor was in equilibrium with the condensed phase; in actuality, only the region very near the condensed phase surface approaches equilibrium during evaporation. Generally, there is a net flux of vapor away from the source to the chamber walls and the substrate. In order to know the rate of deposition at a given location for a given evaporation rate, it is necessary to know the directional distribution of coating atoms being emitted from the vapor source. The Cosine Law of Emission can be derived by considering a gaseous evaporant with a Maxwellian

speed distribution within an isothermal enclosure with an infinitesimally small opening δA_e bounded by vanishingly thin walls (34). This discussion of the derivation of the Cosine Law comes largely from Glang (34). The derivation assumes:

1) The enclosure is isothermal and has vanishingly thin walls.

2) There is an infinitesimally small opening of area δA_e.

3) The enclosure contains N molecules with a Maxwellian speed distribution.

4) Molecules impinging on the walls will be reflected without a net change in the total speed distribution.

5) Molecules moving toward the opening will leave the enclosure in the same direction and at the same speed that they possessed immediately prior to escape.

6) The total population of gas molecules in the enclosure is constant due to the presence of a condensed phase.

7) The distribution of molecules in the evaporant stream can be determined from the molecular speed distribution within the enclosure.

The distribution of molecules in the evaporant stream is described by an expression giving the number of evaporant molecules within a small solid angle δw for every direction of emission where δw is defined by its angle Φ relative to the normal to δA_e (34). The total number of molecules of speed c in the enclosure is given by equation (27):

$$\delta N_c = N\Phi(c^2)\delta c \qquad (27)$$

To exit the opening within time δt in a direction φ, a molecule must be within $c\delta t$ of the opening δA_e as indicated in figure (55) (34). The volume fraction of molecules within striking distance of the opening is $c\delta t\cos\varphi\ \delta A_e/V$; the angular fraction of these that is actually moving toward δA_e is $\delta w/4\pi$ (34). Multiplying δN_c by the volume fraction and the angular fraction give the number of molecules having a speed c exiting in the direction φ as:

$$\delta^4 N_{e,c}(\varphi) = (N/V)c\Phi(c^2)\delta c\delta A_e\delta t\cos\varphi\ (\delta w/4\pi) \qquad (28)$$

Integration over all possible speeds c gives the total number of molecules in angle increment δw where:

$$I(0,\infty)c\Phi(c^2)\delta c = C \qquad (29)$$

and

$$\delta^3 N_e(\varphi) = (N/4V)C\delta A_e\delta t\cos\varphi(\delta w/\pi) \qquad (30)$$

The amount of mass carried by the molecules is given by

$$\delta^3\delta M_e(\varphi) = m\delta^3 N_c(\varphi) \qquad (31)$$

and

$$\delta^3 M_e(\varphi) = \Gamma\delta A_e\delta t\cos\varphi(\delta w/\pi) \qquad (32)$$

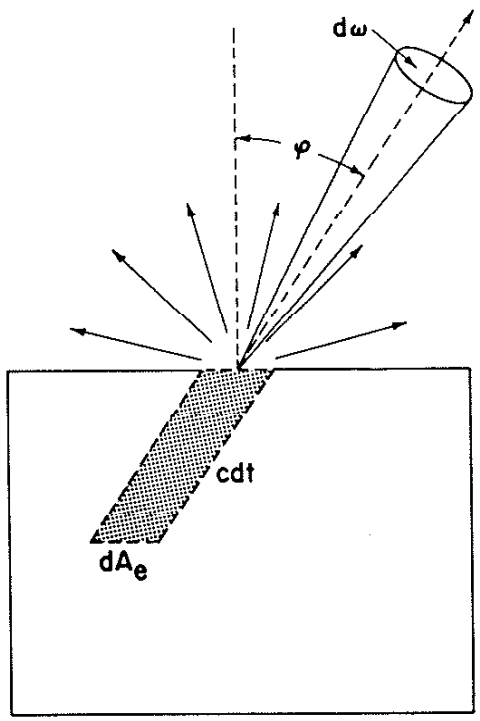

Figure 55. Effusion from an isothermal enclosure through a small orifice. From Glang (34).

where $\Gamma = (mN/4V)C$ (34). In terms of the total mass of evaporated material M_e, equation (32) can be expressed as

$$\delta M_e(\varphi) = M_e \cos\varphi(\delta w/\pi) \qquad (33)$$

Equations (32) and (33) are both expressions of the cosine law of emission which indicates that emission of material from a small evaporating area is not uniform in all directions; it favors directions approximately normal to the emitting surface where $\cos\varphi$ has maximum values (34).

The amount of material that condenses on a given surface depends on the relative position of the surface relative to the vapor source (34). The material contained in an evaporant beam of solid angle δw covers an area which increases with distance from the source r and with the angle of incidence θ relative to the surface as shown in figure (56) (34). δw corresponds to an element of the receiving surface area:

$$\delta A_r = r^2 \delta w/\cos\theta \qquad (34)$$

From this the mass deposited per unit area at a given location becomes:

$$\delta M_r(\varphi,\theta)/\delta A_r = (M_e \cos\varphi \cos\theta)/(\pi r^2) \qquad (35)$$

The cosine law is valid when the mean free path is at least ten times the diameter of the effusion opening (34). In the case of

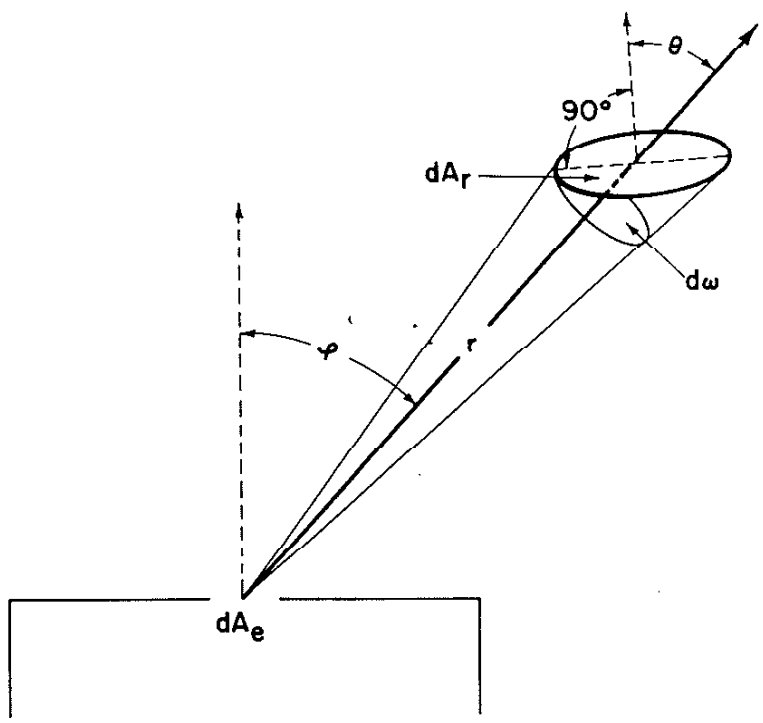

Figure 56. Surface element recieving deposit from small-area source. From Glang (34)

electron beam evaporation, this corresponds to low evaporation rates where there is no collisional interactions between the evaporant atoms once they have left the source (34). Lack of collisional interactions between coating atoms and other coating atoms or coating atoms and residual gas atoms leads to line of sight deposition at the substrate which results in a columnar coating structure and coating imperfections at surface features due to active self shadowing mechanisms under conditions where adatom surface mobility is low (25, 26, 34, 43). Dirks and Leamy (25) did computer simulations of atom by atom deposition onto substrates at various angles of incidence with and without atomic relaxation after atoms attached themselves to the substrate. Their findings were: 1) all cases produced a columnar "microstructure" similar to that observed in real evaporated coatings and 2) the angle of deviation ϕ of the column direction with respect to the surface normal was less than the angle of incidence θ of the source material with respect to the surface normal according to the rule $2\tan\phi = \tan\theta$ for $0° < \theta < 60°$ (25). Blech (26) did computer simulations of layer by layer growth of a coating at a substrate surface step to demonstrate the formation of cracks at steps in evaporated coatings due to shadowing effects. Blech (26) assumed a cosine distribution of source material and that every atom stuck where it struck the substrate (sticking coefficient = 1).

Deviations from the cosine distribution during electron beam evaporation can be promoted by the following: 1) Increasing the evaporation rate; this allows an increased probability of faster atoms overtaking and colliding with slower atoms on the way to the

substrate and increases the intensity of the discharge which which occurs where the e^- beam interacts with the vapor atoms by providing more vapor atoms in that region (34). 2) Increasing pressure decreases mean free path and promotes gas scattering of evaporant atoms (34). 3) The use of a glow discharge which promotes collisional scattering of evaporant atoms (21). During Ion plating, all of these factors are present to cause deviation from the cosine distribution and increase coating uniformity. During evaporation, substrate motion relative to the vapor source is often employed to ensure coating uniformity (18).

VII.A.6. CONDENSATION OF EVAPORANT

The following discussion of coating condensation is taken largely from Thornton (18) and Lewis and Anderson (44).

When coating atoms arrive at the surface of a substrate or growing coating they can 1) bounce off the surface, 2) adsorb on the surface and remain for a finite amount of time before being desorbed, or 3) adsorb on the surface and stick permanently (18). The probability of the first process occurring is low for low energy atoms at near normal incidence. The probability of reflection increases at large angles of incidence as was inferred from the sputtering yield graph in figure (54). Adatoms (loosely bonded atoms) move by diffusion across the surface undergoing energy exchanges with substrate atoms until they are either desorbed by evaporation or sputtering or become trapped at low energy sites to become part of the lattice (18).

Two numbers are used to describe the behavior of atoms on surfaces; these are the accommodation coefficient and the sticking coefficient (18). The accommodation coefficient gives a measure of the efficiency of the energy exchange process between the incident atom and the substrate atoms and is defined as:

$$\alpha = (T_i - T_d)/(T_i - T_s) \tag{36}$$

where T_i is the effective temperature relevant to the kinetic energy of the incident atom, T_s is the substrate temperature, and T_d is the temperature of atoms desorbing from the substrate (18). For evaporation, the accommodation process is fast enough that there is little probability of reevaporation and α can be take as unity (18). The sticking coefficient is defined as the fraction of incident atoms which adhere and remain on the substrate (18). The sticking coefficient is typically less than unity and decreases with increasing substrate temperature and decreasing adsorption energy; at high substrate temperatures the sticking coefficient can be near zero while the accommodation coefficient is near unity (18).

The average amount of time an atom spends on the surface before desorption is the mean residence time τ_r which is related to the adsorption energy E_a and the substrate temperature T by an equation of the form

$$\tau_r = \tau_o \exp(E_a/kT) \tag{37}$$

where τ_o is on the order of 10^{-13} s (18, 44). In the case of simultaneous ion bombardment during deposition, τ_r may be reduced by a factor allowing for the probability the the adatom will be sputtered off the surface before it is strongly bound to the lattice.

The adatom jumping frequency (site to site on the surface is given by

$$\nu = (1/\tau_o)\exp(-E_d/kT) \tag{38}$$

where E_d is the activation energy for surface diffusion (18, 44). The product of the jumping frequency and the residence time gives the number of surface sites visited by the adatom as (18, 44)

$$n_s = \tau_r \nu \tag{39}$$

The random walk diffusion distance that the adatom travels during this time is

$$x = a_o(n_s)^{1/2} \tag{40}$$

where a_o is the average distance between adsorption sites (18). The further the atom travels on the surface, the greater the chances of it finding a suitable site for attachment to the substrate lattice. The presence of ion bombardment during condensation may shorten the residence time by increasing the probability that the atom will be sputtered from the surface; however, the bombardment may also

created suitable sites for the attachment of the adatom to the substrate or growing coating lattice (20).

Three dimensional growth of coating crystals depends on balancing surface and volume free energies to overcome the nucleation barrier to growth (18, 44). Generation of surface energy associated with the interface between the coating and the substrate and the coating and the vacuum acts as a barrier to nucleation; the interfacial surface energy increases as r^2 where r is the radius of the nuclei. Reduction of volume free energy associated with the growth of a new crystal is a driving force for the growth for the growth to a new coating crystal; volume free energy varies as r^3. Initially, surface free energy makes it energetically more favorable to reduce the free energy by reducing the surface area of the nucleus (remove atoms (18, 44). Once nuclei of the critical size form ($\delta E/\delta r = 0$), the volume term becomes dominant and the growth of the crystal is favored (18, 44). Once growth has begun, the presence of surface free energy may still manifest itself in the form of faceted crystals since the surface free energy may vary with crystallographic direction. A generic energy expression for this situation assuming no crystallographic dependence is given by equation (41)

$$E(r) = \alpha_{cs}F_{cs}r^2+\alpha_{cv}F_{cv}r^2-\alpha_{sv}F_{sv}r^2-\alpha_{v}F_{v}r^3 \qquad (41)$$

where E(r) is the free energy of the crystal as a function of radius r, α_{cs} is the interfacial energy per unit area between the coating and the substrate, F_{cs} is a geometrical factor to account for the shape

of the interface between the coating and the substrate, α_{cv} is the interfacial energy per unit area between the coating and the vacuum, F_{cv} is a geometrical factor to account for the shape of the interface, α_{sv} is the interfacial energy per unit area between the substrate and the vacuum, F_{sv} is a geometrical factor to account for the shape of the substrate vacuum interface covered by the nucleus, α_v is the free energy per unit volume of coating nucleus, and F_v is a geometrical factor to account for the shape of the nucleus. The critical nucleus size r^* can be found by setting $\delta E/\delta r=0$ and solving for r. This gives:

$$r^* = 2(\alpha_{cs}F_{cs}+\alpha_{cv}F_{cv}-\alpha_{sv}F_{sv})/(3\alpha_v F_v) \qquad (42)$$

The value of r^* may be modified by ion bombardment which effects the energies of nucleation sites as shown in figure (57) (18, 20, 21).

According to Thornton (18), most engineering substrates have a heterogeneous distribution of sites of preferred nucleation. On these substrates, the collision rate of adatoms with these nucleation sites is higher than the collision rate of adatoms with themselves; therefore, these sites of preferred nucleation dominate in the nucleation process (18). At high temperatures and/or low coating fluxes, nucleation may only occur at these preferred sites (18). Controlling the density and distribution of preferred nucleation sites is an important consideration in controlling coating nucleation, growth, and properties (18, 20).

Coating growth will be affected by surface diffusion, bulk diffusion, and shadowing over different ranges of T/T_m where T_m is

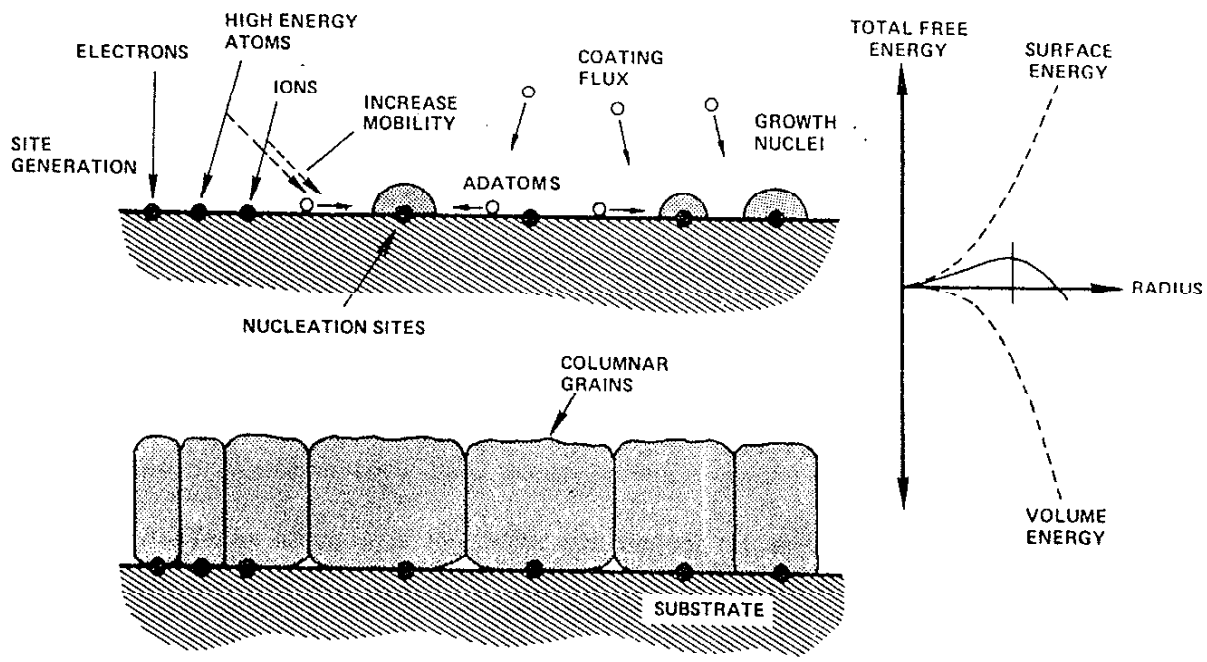

Figure 57. Schematic illustration of film nucleation and growth. From Thornton (18).

the coating melting point in Kelvins and T is the deposition temperature in Kelvins (18). The various temperature ranges are the basis for structure zone models. Movchan and Demchishin (45) proposed one of the first temperature - microstructure zone models from a study of evaporated Ti, Ni, W, ZrO_2, and Al_2O_3coatings in the late sixtys. The M & D diagram consists basically of 3 microstructural regions and a temperature axis as shown in figure (31). Significant modifications to the model have been made by Thornton (18) and Lardon, et al. (46). Thornton (18) added a transition structure between zones 1 and 2 , and a pressure axis as shown in figure (3). Lardon and co workers (46) studied the effect of applied substrate bias on the M & D model and noted that with increasing applied substrate bias, elevated temperature structures were shifted to lower temperatures.

Since Thornton's model contains the largest range of deposition parameters, it is relevant to discuss evolution of the various microstructural zones in terms of his model. The following discussion comes largely from Thornton (18).

The zone 1 structure occurs at low T/T_m where adatom diffusion is insufficient to overcome the effects of shadowing (18). The zone 1 structure consists of tapered crystals with domed tops pointing in the direction of the arriving coating flux and separated by voided boundaries (18). The zone 1 structure is promoted by elevated working gas pressure and the tapered crystals increase in diameter with increasing T/T_m (18). Oblique deposition (promoted by gas scattering) promotes the formation of open boundaries since high points on the surface receive more coating flux then low points

(valleys) (18). Coating surface roughness may arise from initial nuclei shape, preferential nucleation at substrate inhomogeneities, from substrate roughness, and from preferential growth (18). The tapered zone 1 crystals are typically much larger than the crystallographic grain size and the internal structure of the crystals is poorly defined and has a high dislocation density (18).

The zone T structure is an intermediate structure between zone 1 and zone 2 consisting of a dense array of poorly defined fibrous grains in a columnar zone 1 structure with small crystal sizes (18). The zone T structure forms on smooth, homogeneous substrates under normal coating flux incidence at T/T_m values that allow adatom diffusion to overcome roughness in the substrate and the initial nucleation (18).

The zone 2 structure occurs in a range of T/T_m where the growth process is dominated by adatom surface diffusion and consists of columnar grains separated by distinct, dense intercrystalline boundaries (18). Grain sizes increase with T/T_m and may extend through the coating thickness at high T/T_m (18). Surfaces tend to be faceted and dislocations tend to be located primarily in the intercolumnar boundary regions (18).

The zone 3 structure occurs in a range of T/T_m where bulk diffusion is the dominating influence on final structure (18). Zone 3 structures grow as columnar grains and may recrystallize into equiaxed grains if points of high lattice strain energy are generated throughout the coating during deposition (18). Strain-induced boundary motion and grain growth may cause large columnar grains

to grow from columnar as-deposited grains (18). Zone 3 structures tend to have bulk-like material behavior (18).

VII.B. CHRONOLOGICAL REVIEW

The following is a chronological review of some of the articles, reviews, and books relevant to ion plating of aluminum coatings as covered in this thesis. This review is presented in two parts: the first being a review of the work published prior to initiation of the work resulting in this thesis; and, the second being a review of the work published concurrently to the work resulting in this thesis. This material is presented chronologically by year of publication and alphabetically by first author within a given year.

VII.B.1. REVIEW OF PRIOR WORK

1963 Davis and Vanderslice (39) used an electrostatic energy analyzer to determine the ion energies and energy distributions for a series of gasses (notably, argon) at the cathode of a glow discharge. Significant among their results were: 1) The largest number of singly ionized argon ions have energies less than 50% of the cathode voltage as shown in figure (40). 2) The energy distribution of doubly ionized argon is fairly flat and has a peak at the cathode energy as shown in figure (42). 3) If the pressure is kept constant, increasing the voltage (or current) increases the dark-space distance and the proportion of high energy ions increases.

1963 Mattox and McDonald (20) deposited Cd on Fe in the presence of a glow discharge to gain increased adhesion due to surface cleaning and modification by ion bombardment. Significant among their results were: 1) Below 1500V substrate bias, no adherent coatings were formed; this being due to low particle density and low sticking coefficient of Cd on Fe. 2) Adherence was

poor in the range of 1500 to 3000V substrate bias. 3) The most adherent coatings were produced at 2 x 10^{-3} Torr (0.27 Pa) argon pressure, 4000 V accelerating potential and 0.2 mA/cm^2 cathode current. Mattox and McDonald recognized the role of ion bombardment for sputter cleaning and the creation of a surface and near surface defect structure. They considered that good adhesion is due to a transition layer between the film and substrate materials. This transition layer could be formed by diffusion for mutually soluble materials under equilibrium conditions, or by high energy particles for non mutually soluble materials contrary to what is required by equilibrium conditions. Mattox is generally credited with being the first to describe the ion plating process.

1965 Hartman (24) deposited Al films onto a piezo electric quartz crystal microbalance via evaporation from a tungsten filament to determine a relation between density and coating thickness. Significant among his results were: 1) Density decreases with decreasing coating thickness as shown in figure (58). 2) The most likely explanation for reduced density is film porosity. 3) Surface roughness is a possible explanation; however, less than bulk film density persists to thicknesses in excess of those used in experiments where surface roughness may be a source of difficulty. 4) Contaminants such as oxides due to interactions with residual atmosphere in the vacuum system and W from the filaments are a possible explanation; however both these contaminants have a higher density than bulk aluminum and therefore, cannot cause the decrease in density observed.

1967 Ferraglio and D'Antonio (4) made multilayer aluminum

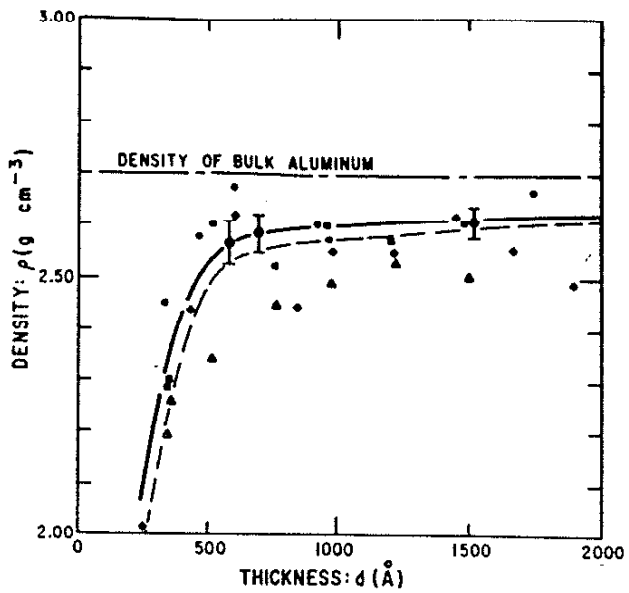

Figure 58. Aluminum film density as a function of thickness. From Hartman (24).

films by evaporation from W-wire filaments at 4 x 10^{-6} Torr (5.33 x 10^{-4} Pa) with deposition rates of about 50 angstroms per second (5 nm per second). Significant among their results were: 1) Multilayers form when the evaporation is interrupted. 2) During annealing of the multilayer films, there was no interaction between the layers at temperatures up to 200 degrees Celsius (473 K). 3) There was more scatter in resistivity measurements for multilayer coatings than for films deposited without interruption; this is true even after annealing. 4) It was proposed that multilayer coatings should have increased strength since the fracture strength of vapor deposited films increases with decreasing film thickness.

1969 Collins and co-workers (17) evaporated Al films 400 - 500 angstroms (40 - 50 nm) thick onto glass slides at 5 x 10^{-5} Torr (6.67 x 10^{-3} Pa) from a W filament and then bombarded them with argon ions in the range 80 - 120 keV to determine the effect of ion bombardment on adhesion. Significant among their results were: 1) An increase in adhesion with time for unirradiated films was observed. 2) Ion bombardment increased adhesion; this is possibly due to the formation of a glass - metal transition layer.

1969 Milillo and co-workers (47) studied the fracture strength and yield strength of evaporated Al films in the thickness range of 1015 to 3450 angstroms (101.5 to 345.0 nm). Significant among their results were: 1) The fracture strength is thickness dependent according to an equation of the form of equation (43).

$$\sigma = k + \beta t^{-1/2} \qquad (43)$$

2) The yield strength data fit either a straight line of a Petch hyperbola. 3) The mechanical behavior of the films is characterized by a measurable plastic region of strain and low elastic modulus. 4) No relation between crystallite size and strength, thickness, elastic modulus, or magnitude of plastic strain was observed. 5) A mechanism involving dislocation pileups at the film surfaces is the most reasonable explanation for the thickness dependent component of strength in vapor deposited thin films.

1969 Movchan and Demchishin (45) investigated the influence of substrate temperature on the condensation, structure, and properties of thick (up to 2mm) polycrystalline deposits of Ni, Ti, W, Al_2O_3, and ZrO_2 deposited by electron beam evaporation. Significant among their conclusions were: 1) There are three characteristic structural zones with boundary temperatures T_1 and T_2 0.3 and 0.45 - $0.5T_m$ respectively (for metals) and 0.22 - 0.26 and 0.45 - $0.5T_m$ (for oxides). 2) Mechanical properties such as microhardness, strength and ductility of the condensates are determined by the structural features of the zones. 3) The activation energy of the processes which control structure in the second zone corresponds closely to that of surface diffusion.

1970 Barna and co-workers (28) studied the effect of various evaporation arrangements on coating morphology and determined that the morphology of vacuum deposited thin films are highly influenced by the evaporation geometry through the self- gettering property of the evaporants. The evaporants studied include Al, Au, Ge, In, SiO, and Ti.

1970 Blech (26) developed a geometrical construction and computer simulation to show how cracks in coatings arise at surface steps due to shadowing effects during deposition.

1970 Dobson and Hopkins (48) deposited various metals via evaporation onto glass at pressures between 10^{-5} and 10^{-10} Torr (1.33×10^{-3} and 1.33×10^{-8} Pa) and temperatures between 300 and 700 K to study preferred orientation in the films. Significant among their results were: 1) There is a strong {111} fiber orientation for low melting point fcc metals deposited at 300 K. 2) There is an enhancement of this orientation at higher temperatures. 3) Residual pressure did not appear to affect the orientation over the pressure range studied.

1970 Maissel and Glang (49) compiled a handbook on thin film technology with contributions from 24 authors. Topics covered include: 1) preparation of thin films, 2) the nature of thin films, 3) properties of thin films, and 4) applications of thin films.

1971 Graper (50) made evaporated Al coatings from an electron beam source using various crucible liners and deposition rates. Significant among his findings were: 1) Hearth liners increase the evaporation rate per unit power for Al. 2) Hearth liners reduce the hearth volume by approximately 50% and require more operator care to avoid damage by the electron beam. 3) Hearth liners contribute significant contamination. 4) Film structures were found to be a function of deposition rate and substrate temperature.

1971 Mattox and Kominak (51) sputter deposited Ta onto biased Ta and graphite substrates. Significant among their results were: 1) coating density increased almost linearly with increasing

negative substrate bias in the range +200 to -500 volts. 2) relative stress within the film increased over the same range of biases. 3) The coatings made at -500 V bias had a shiny metallic appearance as compared with a dull matte appearance for those formed at 0 bias.

1972 Nelson (52) gives a physical background to the metallurgy of ion implantation. Relevant topics covered include: 1) precipitation during ion implantation including solubility and radiation enhanced diffusion; 2) equilibrium conditions; and, 3) applications of ion implantation and ion bombardment.

1972 Stroud and co-workers (53) bombarded 200 angstrom Al films with 30 keV oxygen ions and found that resistivity increased with increasing ion dose.

1973 Erikson (54) determined the thickness distribution for evaporated coatings from a high rate electron beam evaporation source (deposition rate approximately 25 microns per minute (1 micron = $1\mu = 10^{-6}$ m). Significant among his results were: 1) There is significant substrate heating by ion bombardment. 2) There was no observed change in the thickness distribution as compared with the evaporated coating when the substrate was biased. 3) The coatings deposited in high vacuum showed a departure from the classical cosine distribution. 4) An increase in pressure caused an increase in deviation from the cosine distribution as shown in figure (59).

1973 Mattox (42) reviews the ion plating process including some of its applications and limitations. Significant points made in the paper include: 1) Adhesion benefits from ion plating include: a) ability to sputter clean the substrate surface and maintain its

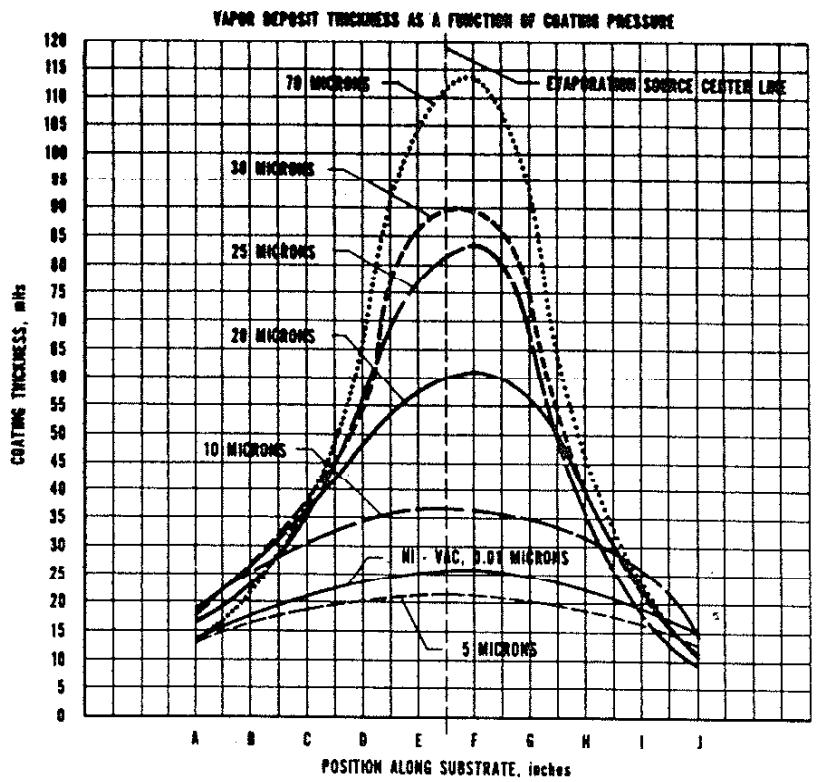

Figure 59. Coating thickness distribution as a function of chamber pressure during deposition. From Erikson (54).

cleanliness until the film begins to form; b) provide a high energy flux to the substrate giving a high surface temperature without necessitating bulk heating, thus enhancing diffusion and chemical reaction; and c) alter the surface and interfacial structure by introducing high defect concentrations, physically mixing the film and substrate material, and influencing the nucleation and growth of the depositing film. 2) Ion plating is effective in obtaining good adhesion in systems where conventional deposition processes give poor results. 3) Applications of ion plating include: a) adhesion, b) protection, and c) electrical contact. 4) A cathode current density of a few tenths of a milliamp per square centimeter is adequate for sputtering cleaning. 5) Problem areas arise from geometrical effects due to field distortion and heating effects; some of these are illustrated in figure (60).

1973 Mattox (16) reviews the factors affecting adhesion and shows that the structure of the interfacial region is probably the controlling factor in film adhesion. Significant points made in the paper include: 1) Adhesion is a macroscopic property of a two-component system and involves both the chemical bonding in the interfacial region and the fracture mechanism. 2) Aluminum atoms react strongly with an oxide surface and thus the surface mobility is low and the nucleation density high; as the Al deposition proceeds, the nuclei grow laterally and form a continuous film at low film thickness, giving a high interfacial contact area. This type of nucleation and growth can be termed "wetting growth". 3) Nucleation density, and thus adhesion, can be affected by surface impurity atoms. 4) the generally accepted criterion for adhesion

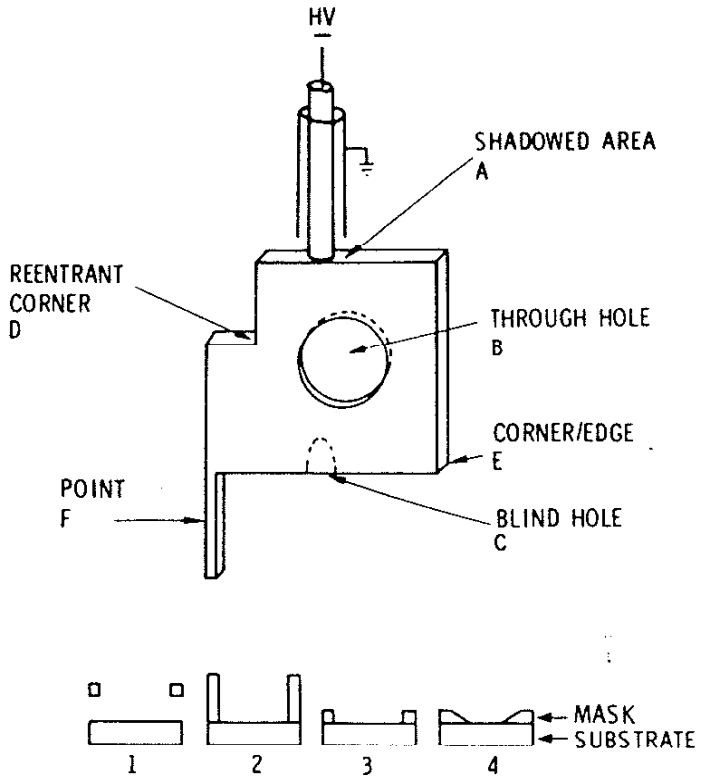

Figure 60. Some of the ion plating problem areas which are due to geometrical effects. From Mattox (42).

between a metal film and an oxide substrate is that the metal must be oxygen active so as to react chemically with the oxide surface, forming an interfacial diffusion zone. 6) The interfacial region can change with time due to migration allowing the formation of a more extensive reaction zone. 7) Ion bombardment during and after film formation has been used to enhance adhesion by altering the nucleation mode and by promoting interfacial reaction after deposition. 8) The structure and properties of the interfacial region are important in interfacial fracture. 9) Stresses due to differing properties of the film, interfacial material and substrate should be distributed over an appreciable thickness (graded) so that there are no sharp discontinuities in stress. 10) Adhesion is degraded at interfaces with high porosity, high stresses, and sharp discontinuities in stresses and material properties. 11) Interfacial shear stresses are more important to failure than are pure tensile stresses. 12) Ion bombardment during ion plating causes sputtering of the growing film, eroding the peaks, filling the valleys, and giving a less columnar structure in thick deposits. 13) Fracture of an interface on a rough surface is more difficult than on a smooth surface since a crack propagating along the interface must change directions or pass through stronger material and there is some degree of mechanical interlocking. 14) Deposition of "nodules" arising from exploding gas pockets in the melt can be reduced by vacuum pre-melting the charge prior to deposition. 15) Long term stability of the film is dependent on its morphology. Chemical processing and corrosion of the film may cause loss of adhesion; this is enhanced by film porosity and residual stresses. 16)

Problems can occur due to incorporation of gasses during deposition which can precipitate to form bubbles. 17) The most widely used single metal metallization system is evaporated aluminum.

1974 Bland and co-workers (55) deposited metallic and ceramic coatings via ion plating. Significant among their results were: 1) Ion bombardment may be used to modify the morphology of deposited coatings; there is apparently a minimum ion/depositing atom ration needed to be effective in disrupting of the columnar morphology. 2) Coating density increases with the use of ion bombardment during deposition. 3) Ion bombardment may alter the composition of alloy and compound systems. 4) Intrinsic stress and gas content of the coating dependent on ion bombardment. 5) At high biases (-500 V) there is a decrease in argon content; this is possibly due to heating.

1974 Bunshah (56) reviews data on structure/property relationships in thick films produced by high-rate evaporation deposition technology. Significant points in the paper include: 1) The higher the temperature of the substrate surface and the higher the kinetic energy of the depositing atom, the closer the resultant structure will be to the equilibrium structure. 2) Tests on zone 2 structures showed high strength and low ductility at low deposition temperatures with strength decreasing and ductility increasing with increasing deposition temperature. 3) Strength and ductility of zone 3 structures is approximately the same as for recrystallized specimens of ingot material. 4) A columnar morphology is not as corrosion resistant as an equiaxed morphology. 5) Adhesion is best

in most materials when the deposition temperature is greater than $0.3T_m$.

1974 Chapman (13) reviews measurements of thin film adhesion including testing testing methods and requirements of a thin film adhesion test, adhesion forces and types of adhesion, and methods of influencing adhesion. Significant points in this paper include: 1) It would be more practical to design tests of durability under service conditions rather than tests of adhesion. 2) There are four basic types of adhesion systems: a) interfacial adhesion; film and substrate meet at a well defined interface, b) interdiffusion adhesion; a gradual and continuous change from one material to the other, c) intermediate layer adhesion; film and substrate bonded via one or more layers of compounds of the materials with each other and/or environmental gases, d) mechanical adhesion; mechanical interlocking between coating and substrate. 3) Sputter cleaning prior to deposition improves adhesion. 4) Substrate heating during deposition helps adhesion. 5) Intermediate layers of oxygen active metals improve adhesion. 6) Ion bombardment during deposition promotes adhesion.

1974 Learn (27) investigated the effects of alloy additions on electromigration and hillock growth in flash evaporated aluminum films. Significant among the results were: 1) Cu additions reduced the density of growth hillocks. 2) Si additions had no significant effect on hillock growth. 3) At increased substrate temperatures during deposition, the density of hillocks decreased while the dimensions of individual hillocks increased. 4) Poor step coverage

was observed for depositions at low substrate temperatures. 5) Cu additions improve electromigration resistance.

1974 Love and Bower (33) deposited 150 microns thick Al films via electron beam evaporation onto Ni ribbon in an oil diffusion pumped vacuum system. They analyzed the coatings for contamination, determined the sources and defined techniques to eliminate them. Significant results include: 1) Deposition rates were 0.6 mils/hour (4.23 nm/sec) at 10 inches (25.4 cm) from the source at 9 kW in 10^{-6}Torr (1.33 x 10^{-4} Pa) vacuum. 2) Chemical cleaning of the Al source material gave rise to contamination both from the chemicals and from the handling. 3) Biased surfaces such as the leads to the electron gun give rise to contamination. 4) Contamination was reduced by more careful handling and shielding of biased surfaces with grounded Al foil.

1974 Steube and McCrary (57) describes the use of IVD (ion vapor deposited) aluminum coatings on various aerospace parts. Significant points include: 1) The use of a bias during deposition produces greater adhesion and improved coating uniformity. 2) The process is not confined to line of sight applications due to gas scattering of depositing atoms. 3) Fixturing may be difficult, especially in cases where substrate motion is required. 4) substrate heating may be a problem in materials not adequately protected by a heat sink.

1975 Dhere and co-workers (29) deposited high purity Al films via evaporation and showed a {111} texture orientation at low thicknesses transforming to a {311} texture at higher thicknesses over the the range of 15 - 200 μm.

1975 Holland (58) reviews the use of glow discharges for substrate treatment and film deposition. Topics covered include: surface cleaning, ion plating, and reactive evaporation.

1975 Vulli (59) describes the use of a flux of nitrogen in the substrate region to minimize oxidation of oxygen reactive metals (Al, La, Dy) during deposition by evaporation from a W filament.

1975 Goldstein and Bertone (11) tested Al and Ag coatings vacuum deposited onto Teflon. Significant among their results were: 1) The performance of Al films was superior to that of Ag and Ag with metal overlayers during scratch testing. 2) During "flex testing", Al films were more adherent than Ag films under both stretching and crinkling conditions. 3) Results of both tests indicate that aluminized Teflon is more durable than silvered Teflon.

1975 Kemmochi and Hirano (60) investigated electromigration of grain boundaries in high purity Al. Grain boundary migration may be affected by the additions of Cu, Si, and Zr; reduction or enhancement will depend on whether the boundary migrates in or against the direction of the electric current. In general, additions of Cu, Si, and Zr to Al increase the activation energy for grain boundary migration.

1975 Schiller and co-workers (61) describes "alternating ion plating" which consists essentially of subjecting the substrate to alternating exposure to fluxes of ions and coating vapors during deposition. This process produces coatings with similar properties to those produced by conventional ion plating.

1975 Weaver (14) reviews adhesion of thin films including difficulties in measuring adhesion, measurement techniques, notably

scratch testing, and adhesion to polymer surfaces. Significant points of this paper include: 1) Adhesion measurements are limited by two fundamental difficulties: a) being able to obtain perfect contact (or even a known area of perfect contact) and b) being able to apply stress in such a way that the force (or energy) required to separate the two materials may be accurately determined. 2) Adhesion of Al on some polymers increases with time. 3) Glow discharge cleaning prior to deposition improves adhesion of Al to some polymers.

1976 Glaser and co-workers (62) describes ion evaporation which is similar to ion plating except that there is no working gas and the substrate biases are greater than 20 kV. Results of testing this method showed the following: 1) Adhesion was found to exceed that attainable by evaporation, sputtering, and ion plating. 2) The implantation depth for Al in n type Si was determined by the p-n junction method as 0.1 - 0.3 μm. 3) In tensile testing of Cu films, ion evaporated films were found to have twice or more the tensile strength of ion plated films (2×10^7 N/m^2 (20 MPa) or more and 1×10^7 N/m^2 (10 MPa) respectively).

1977 Chevallier (63) deposited coatings of Pd, Pt, and Ir onto various substrates via evaporation and ion plating. Significant among the results were: 1) Thickness profiles on geometrically complex objects indicate that ion plating produces more uniform coating thicknesses than evaporation as shown in figure (61). 2) Ion plating produced more adherent coatings than evaporation.

1977 Dhere and co-workers (30) deposited high purity, thick (7 - 65 μm) Al films via evaporation. Significant among their

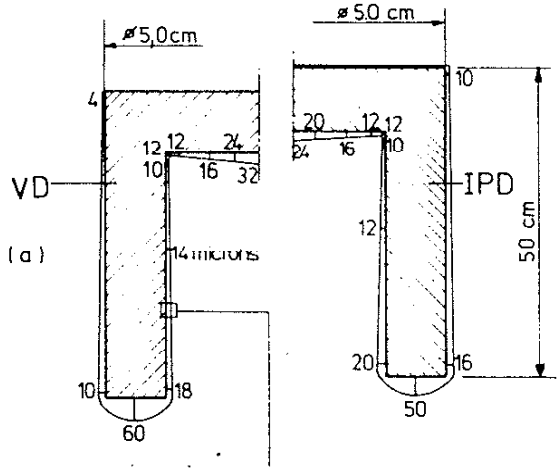

Figure 61. Thickness profile of an Ir coating on a graphite crucible for evaporation (left) and ion plating (right). From Chevallier (63).

results were: 1) small and large thicknesses had a one dimensional {311} texture orientation. 2) Medium thicknesses had a mixed one dimensional {111} and one dimensional {311} texture orientation. 3) Surface grain size increased with deposition rate up to about 100 kiloangstroms per minute (167 nm/sec) and then showed a decrease.

1977 Dirks and Leamy (25) reviews the generation of columnar microstructure due to shadowing processes and demonstrates the shadowing mechanism via atomistic computer simulations of the deposition process. Significant points of this paper include: 1) In columnar films, the columns are oriented at an angle ϕ such that $\tan\theta = (\tan\phi)/2$ where θ is the angle between the substrate surface normal and the vapor beam. 2) The columnar structure has effects on the magnetic, optical, electrical, mechanical and other physical properties of the film. 3) Surface topography, specific surface area, oxygen uptake, and adhesion to the substrate are also affected by the existence of the columnar structure. 4) Column formation is generally more prominent in films produced by oblique incidence deposition than in films produced by normal incidence deposition. 5) Geometric shadowing of the vapor beam by the growing film is responsible for the formation of the columnar microstructures in both crystalline and amorphous materials. 6) The columnar morphology is sensitive both to the nucleation and growth process and to the diffusion process; it is unstable and may be eliminated by annealing or by high temperature deposition.

1977 Dugdale (64) deposited metals and ceramics via evaporation and sputtering onto biased and unbiased substrates. Significant results include: 1) All coatings showed the presence of

columnar growth. 2) Denser coatings were attained by biasing the substrate negatively during deposition. 3) Substrate cleaning via ion bombardment prior to deposition improved adhesion.

1977 Ghate and co-workers (65) reviews the metallization of microelectronics. Significant points include: 1) Al is the most widely used metal in micro electronics for providing contacts and interconnections. 2) Contact resistance of the Al-Si interface is sensitive to surface preparation, residual gasses present during Al deposition, and contact sintering. 3) Al forms low resistive contacts with p and n type silicon. 4) Alloy penetration can be impeded by the use of Al + Si films for interconnections. 5) Substrate heating and some form of substrate rotation are desirable to improve step coverage of evaporated Al films. 6) Additions of Cu suppress hillock growth and increase electromigration resistance. 7) Microstructure control by deposition process optimization will be a key factor in fabricating reliable interconnections.

1977 Kubovy and Janda (6) studied the influence of residual gas pressure on the internal stress in evaporated Al films. Significant results of their work were: 1) The stress of evaporated films is more sensitive to film contamination by oxygen from the residual atmosphere than is their resistivity. 2) Lightly contaminated films were crystalline with a metallic Al structure. 3) Highly oxidized films were amorphous and dielectric.

1977 Marinov (66) describes the effect of ion bombardment on the initial stages of thin film growth for Ag on amorphous substrates. Significant among his results were: 1) Ion bombardment causes an enhance mobility of both adatoms and crystallites,

thereby accelerating the nucleation, growth, and coalescence of the nuclei. 2) The change in the structure of the substrate surface that takes place under ion bombardment leads to the creation of active sites that stimulate the nucleation process.

1977 Mcleod and Hartssough (67) deposited Al onto Si via sputtering. Significant among their results were: 1) Increased source to substrate distance resulted in improved coating reflectance. 2) An increase in pressure to 15 x 10^{-3} Torr (2 Pa) improved film reflectance. 3) Films deposited in a single pass were less reflecting than those of equal thickness built up in small increments by multiple passes. 4) Coatings made with no substrate motion and the substrate centered in front of the source were more reflective than those with motion during deposition. 5) The amount and type of residual gas was found to have a strong effect on reflectance with the effect of residual nitrogen being larger than that of water and hydrogen. 6) Hillock density was low in films deposited at low substrate temperatures. 7) Radiation damage to oxidized Si wafers coated using planar magnetron sputtering is less than that produced by electron beam evaporation. 8) Sputter deposition provides increased alloy compositional control over that achievable by electron beam evaporation.

1977 Ohsaki and co-workers (68) deposited Al onto carbon fibers via ion plating prior to vacuum hot pressing the fibers into a carbon fiber reinforced aluminum composite. Significant among their conclusions were: 1) Ion plating techniques are applicable to the carbon fiber reinforced aluminum production process. 2) By applying ion plating techniques and vacuum hot press molding,

comparatively good mechanical properties can be obtained when high strength carbon fibers are used as the reinforcing material.

1977 Prummer (69) describes the process of explosive cladding to deposit thin foils as films down to 0.5 μm thick.

1977 Safai and Herman (3) investigated the microstructure and some of the microstructure - process relations for plasma-sprayed aluminum coatings. Significant among their findings were: 1) Slight recovery was observed in some of the TEM samples despite the low voltages (2 - 3 kV) used for ion milling. 2) Pore content increases with spraying distance. 3) In general, the morphology of the impinged particles is effectively controlled by the particle size and location within the coating and the topography of the underlying surface. 4) Porosity can be minimized by optimizing spraying parameters; however, porosity cannot be completely eliminated. 5) The presence of pores inhibits particle-particle cohesive bonding and thus degrades the mechanical properties of the coatings. 6) In general, the presence of thin oxide layers in a sprayed aluminum coating is detrimental.

1977 Sherman (70) deposited 10 μm Al films onto Kapton via evaporation at 1×10^{-6} Torr (1.33×10^{-4} Pa) and observed a strong (111) fiber texture.

1977 Teer and Salama (71) deposited adherent graphitic carbon structures via ion plating onto metallic substrates with bulk temperatures below 400 Celsius (673 K). The structures observed were comparable to graphitic fibers made from pyrolytic carbon produced at 2000 Celsius (2273 K) and heat treated at 3000 Celsius (3273 K).

1977 Teer and Salem (8) deposited Al onto Ti via ion plating to produce a graded interface 5 μm or more deep. Significant among their findings were: 1) Dense, adhesive, noncolumnar structures were obtained over a range of substrate biases from 3 to 4 kV and gas pressures from 10 to 40 μ (1.33 to 5.33 Pa) of argon. 2) The ion plated aluminum coating on titanium bolts prevented galvanic corrosion of aluminum alloy L71 under a wide variety of testing conditions. 3) The interfacial material was found to consist of solid solution Al in Ti with $TiAl_3$. 4) The Al film hardness was 80 kg/mm^2, the interface hardness was 500 kg/mm^2, and the substrate hardness was 350 kg/mm^2. 5) The interfacial material had a lower coefficient of friction then Ti and gave a better than two orders of magnitude increase in wear resistance. 6) Use of and argon-nitrogen atmosphere during deposition gave a further decrease in coefficient of friction, a further increase in hardness, and a further increase in wear resistance.

1977 Tolk and co-workers (72) compiled a book concerning the inelastic interactions between ions and surfaces including Auger neutralization of ions as they approach a surface. This book contains contributions from 20 authors.

1978 Dahlgren and co-workers (73) review some of the metallurgical characterization techniques used on coatings. Topics include: 1) coating structures (crystal structures, lattice parameters, microstructures) 2) coating composition (alloy compositions, impurities) 3) coating properties (adherence, resistivity, mechanical properties).

1978 Fujishiro and Eylon (74) ion plated platinum onto titanium alloys to give them improved creep resistance, oxidation resistance, and high cycle fatigue strength.

1978 Hirsch and Varga (75) attained improved adhesion of Ge on glass and other substrates by bombarding the substrate surface with 1650 eV Ar ions from an ion beam source during deposition.

1978 Holloway and McGuire (76) reviews some of the various analytical techniques used to acquire surface and near surface information on coatings. Topics include: 1) physical principles of the techniques, 2) sensitivity, resolution, detection limits and quantification, 3) chemical bonding information, 4) lateral resolution, 5) depth resolution, 6) sample requirements and sample modification by the probe.

1978 Lardon and co-workers (46) deposited Al and Ti films via ion plating at various substrate biases and substrate temperatures to determine the effects of bias and temperature on coating morphology. Significant among their results were: 1) Ion plated films of Ti and Al show the same temperature dependent morphological zones as those produced in the absence of ion bombardment; however, the zone boundaries are shifted to lower temperatures as the applied bias potential is increased. 2) Dense, adherent protective coatings of aluminum can be applied to steel substrates at relatively low temperatures by ion plating.

1978 Lewis and Anderson (44) composed a book covering various aspects of the nucleation and growth of thin films. Relevant topics include: Adsorption, steady state nucleation theory and rates, and nucleation and growth experiments.

1978 Teer and Delcea (77) deposited Cu coatings onto Ni substrates via ion plating in a triode supported system. Significant among their results were: 1) Coating structures similar to zone 1 structures of Movchan and Demchishin are produced by ion plating at low bias power densities. 2) At higher bias power densities, denser structures approaching those of zone 2 are produced. 3) A further increase in bias power density produces dense structures with grain sizes of about 1 μm. 4) increasing the bias power density by use of a triode-assisted discharge produced dense structures with very fine (0.1 μm) grain size. 5) The high surface temperature is most likely the most significant effect in densification of the coating structures. 6) Ion plating can produce dense coatings at relatively low substrate temperatures.

1978 Thornton (22) reviews the basic principles of magnetron sputtering sources. This review includes: 1) basic concepts of plasma physics, 2) the glow discharge, 3) current-voltage characteristics, and 3) the performance of magnetrons as sputtering sources.

1978 Walls and co-workers (78) used AES (Auger Electron Spectroscopy) to study evaporated and ion plated Cu and Ag coatings on Ni substrates. Significant among their findings were: 1) The argon content of ion plated Cu and Ag coatings is less than 1%. 2) For mutually soluble coating/substrate couples, thermal diffusion is the most important mechanism in forming a graded interface between coating and substrate. 3) Ion plating at 3 kV causes the formation of a graded interface of about 200 nm thickness between the coating and substrate even when the coating and substrate

materials are insoluble. 4) The most probable mechanism for the formation of the graded interface is ion implantation.

1979 Franks and co-workers (79) formed various coating/ substrate combinations by evaporation while simultaneously bombarding the substrates with 5 kV argon ions from a saddle field ion source to show that ion bombardment enhances film bonding.

1979 Marinov (80) used reflection high energy electron diffraction (RHEED) to observe crystalline Si surfaces transforming to amorphous under 1 - 5 kV ion bombardment. He observed that the time required for complete amorphization depends on the ion density.

1979 McLeod and Hughes (5) studied the effects of deposition parameters on Al coating properties in production processes of high rate, automatic coating systems. Significant among their findings were: 1) Both residual gas and temperature play significant roles in the characteristics of step coverage, reflectivity, and resistivity of sputtered coatings; in general, it is best from the standpoint of coating properties to take measures to reduce the pressures of residual contaminant gasses and to take measures to minimize wafer temperature rise during deposition. 2) The use of sputter etching appears to be a useful technique for removing adsorbed gases and stray condensate from the substrates. 3) The primary contaminant during deposition of Al is water vapor.

1980 Chapman (21) published "Glow discharge processes". Topics covered include: gas theory, gas phase collision processes, DC and RF glow discharges, sputtering and its application, and plasma etching. Chapmans book gives a good fundamental

understanding of what is going on in ion plating glow discharges and glow discharges in general.

1980 Hirsch and Varga (81) investigated the use of an "annealing" effect associated with ion bombardment simultaneous to evaporative deposition. Significant among their findings were: 1) Observations point to the existence of an annealing effect caused by atomic rearrangement in bombardment induced temperature spikes. 2) The annealing mechanism begins to be effective at a critical minimum bombardment intensity which is sufficient to ensure that most all of the deposited material is subjected to rearrangement soon after condensation. 3) The "annealing" is not significantly affected by the bombardment induced uptake of argon. 4) There is no critical level of argon content that marks the onset of enhanced film adherence.

1981 Coad and co-workers (19) compared the effects of substrate heating and ion cleaning on coating adhesion. Significant among their conclusions were: 1) It is important from an adhesion standpoint to remove organic and other superficial contaminants from the substrate surface prior to coating deposition. 2) If poor adhesion results after cleaning, it is probably caused by brittle fracture at, of near the interface due to thermally induced stresses in the coating. 3) It is desirable to avoid forming brittle material in the interfacial region and to maintain ductility. 4) In cases where interdiffusion would cause the formation of a brittle intermetallic phase, it is beneficial to retain a thin oxide or some other intermediate layer as a diffusion barrier between the coating and substrate. 5) Heating in a non-tarnishing atmosphere prior to

coating deposition decomposes organic contaminants and generally leads to good adhesion limited only by conditions favoring brittle fracture. 6) Ion cleaning has a number of disadvantages (geometric shadowing and enhancement, cross contamination, sputter yield varies with composition) but is useful as a means for heating. 7) Oxygen discharge cleaning is useful for burning off carbon and carbonaceous materials.

1981 Hurley (36) reviews the process occurring in the dark space adjacent to the substrate in biased deposition systems. Relevant topics covered in this review include: 1) Various particles (neutrals, metastables, positive ions, negative ions, electrons, and photons) present and their roles in the dark space. 2) physical processes occurring in the dark space. 3) collisions at the substrate including gas incorporation, implantation, diffusion effects, and structural changes. 4) The role and behavior of the triode in discharge enhancement.

1981 Laugier (15) deposited Al onto glass via evaporation at 5 x 10^{-5} Torr (6.67 x 10^{-3} Pa). Significant among his results were: 1) Adhesion increased with time as shown in figure (62). Intrinsic compressive stress increases with increasing coating thickness as shown in figure (63). 3) Intrinsic stress shows a slight dependence on deposition rate as shown in figure (63).

1981 Sundquist and Myllyla (82) ion plated Al bronze coatings onto forming tools to improve the wear life of the tools; the use of enhancement of the discharge during deposition gave further improvement of the life to the coatings.

1982 Ahmed and Teer (83) deposited Al/Al oxide coatings onto

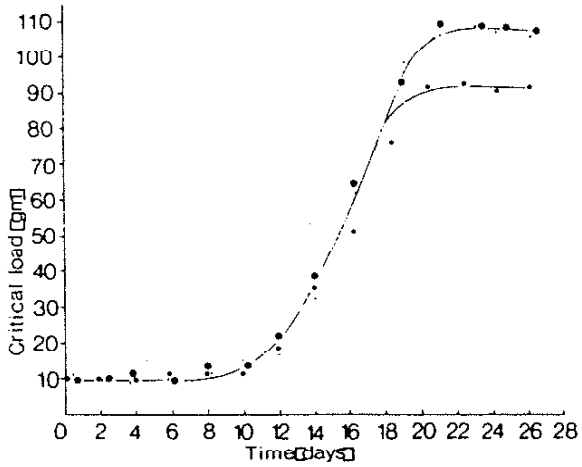

Figure 62. Adhesion of evaporated aluminum films to glass as a function of time. From Laugier (15).

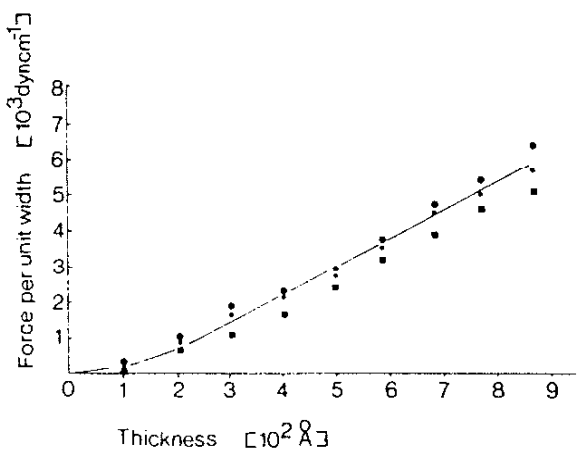

Compressive intrinsic force S_{Int} *vs.* thickness: ■, 4 Å s^{-1}; ●, 5 Å s^{-1}; •, 6 Å s^{-1}.

Figure 63. Intrinsic compressive force as a function of coating thickness and deposition rate. From Laugier (15).

steel substrates via triode enhanced ion plating of Al with pulsed oxygen gas. Significant among their results were: 1) The crystalline phase of the films is dependent on the oxygen flow and the substrate bias at fixed substrate temperature. 2) Non crystalline films were formed at high oxygen flow and low substrate bias. 3) Crystalline films were formed at low oxygen flow and high substrate bias.

1982 Arya and Singh (84) studied the conduction properties of 50 angstrom (5 nm) Al_2O_3 films. They determined that conduction at 77 K is due to tunneling and at room temperature conduction is due to the Schottky mechanism.

1982 Bujor and co-workers (85) studied the initial oxidation behavior of evaporated Al films using AES, ELS, and ESD. Significant among their results were: 1) Oxidation of evaporated Al films occurs by a two stage process. 2) There is a change in the oxidation rate at an exposure of about 50 L. 3) The first oxidation stage corresponds to the chemisorption of oxygen. 4) The second stage corresponds to the growth of an oxide layer.

1982 Bunshah (86) compiled "Deposition Technologies for Films and Coatings". Bunshah's book consists of 14 chapters contributed by 11 authors. Topics covered include: 1) applications of plasmas in deposition processes; 2) effects of surface preparation on adhesion; 3) evaporation; 4) sputter deposition; 5) ion plating technology; 6) chemical vapor deposition; 7) plasma assisted chemical vapor deposition; 8) electroplating; 9) plasma and D-gun deposition; 10) microelectronic applications; and 11) characterization of thin films (microstructural and chemical).

1982 Dobrev (87) surveys the formation of preferred fiber textures in coatings bombarded with ions. Significant points of this paper include: 1) A <110> fibrous texture is formed in vacuum-condensed fcc and hcp metals films during ion bombardment with 10 keV argon ions irrespective of the initial crystallite orientation. 2) A <110> texture is initiated and developed during the growth process in silver films condensed under simultaneous bombardment with 10 keV argon ions. 3) The anisotropy of incident ion penetration and the propagation of impacts in the crystal lattice are considered as the most probable causes of the observed texture formation.

1982 Donnelly and co-workers (88) deposited thin (0.2 μm) Al films by evaporation and then bombarded them with 5 keV helium ions. Significant among their results were: 1) Helium retention is about 3 atomic percent at ion doses above about 2×10^{17} ions/cm^2 at room temperature and falls sharply at doses below that. 2) Helium retention is slightly higher for samples implanted at a lower temperature (120 K). 3) SEM observations indicate gross deformation of the foil increasing with increasing ion dose. 4) TEM observations indicate bubble and hole formation in the foil increasing with increasing ion dose.

1982 Hurley and Williams (10) experimented with the ion plating of metals onto various polymer substrates. Significant among their results were: 1) Ion plating may only lead to substantial improvement in film quality with certain film - substrate combinations due to the substrate damage that may be produced when using sufficient power density to improve the coating properties of some metals. 2)Ion plating produced improver coating

adhesion over that produced by evaporation. This paper also reviews some of the considerations of adhesion of metal films to plastic substrates.

1982 Mattox (32) reviews the effect of substrate surface preparation on coating adhesion. Significant points of this paper include: 1) Good adhesion is promoted by; a) strong atom- atom bonding in the interfacial region, b) low local stress levels, c) an absence of easy deformation and fracture modes, and d) no long-term degradation modes. 2) Interfacial region may be classed as mechanical, monolayer to monolayer, compound, diffusion, or pseudo-diffusion and combinations of these types. 3) The factors which most strongly influence the mechanical properties of a coating are microstructure, incorporated impurities, and internal stresses all of which are dependent on the deposition variables. 4) Sputter cleaning is the most widely applicable technique for removing trace surface contamination prior to coating deposition.

1982 Raven (89) achieved increased adhesion of Se films on brass by using ion plating as opposed to evaporation.

1982 Sinha (90) reviews metallization technology for VLSI circuits. Significant points of this paper include: 1) Long, narrow stripes of Al are more prone to electromigration failure. 2) Shallow junctions are more prone to failure by Al-Si reaction and electromigration at the contacts. 3) Electromigration resistance is promoted by a strong [111] texture

1982 Winters (91) observed that ion bombardment of solid surfaces produces a layer of altered chemical composition for chemisorbed nitrogen in W and Mo bombarded by Ar and Xe ions in the

energy range 0 - 7 keV. Significant among his results were: 1) The sputter yield of nitrogen tends to increase as the atomic weight of the surrounding atoms increases. 2) The effect of substrate mass upon the sputtering yield is most important at small ion energies. 3) Because nitrogen tends to have a high sputtering yield when it is surrounded by atoms of high atomic weight, it is predicted that ion bombarded multicomponent systems will tend to be depleted of nitrogen in the surface region.

1983 Barna and co-workers (92) studied the effects of oxygen codeposition on epitaxially grown Al films. Significant among their results were: 1) The presence of oxygen promotes the formation of growth steps, pinning sites, dents, macrosteps, and hillocks. Under the same conditions, only dents develop on (100) and (110) faces. 2) Contamination layers partially of completely covering the surface of crystals can develop by accumulating oxygen species on (111) faces leading to orientational separation of crystals during growth. 3) Whiskers develop at a high level of oxygen contamination on amorphous substrates.

1983 Klemperer and Williams (93) bombarded evaporated films of Al and Ni with Xe ions and observed that their chemical reactivity was modified. Significant among their results were: 1) Metal surfaces subjected to a light Xe bombardment become amorphous and liquid-like in structure. 2) The amorphous liquid-like metal surface is chemically unreactive. 3) Heavy, concentrated ion bombardment damages the surface and physically opens it. 4) After severe radiation damage, the surface is readily chemically attacked. 5) Metals evaporated in Xe at 78K contain occluded Xe. Their

structure may be amorphous at room temperature; but, their chemical reactivity is unimpaired.

1983 Nandra and co-workers (94) studied the effects of ion bombardment before and/or during the thermal evaporation of Au onto Cu using an ion gun and ion energies up to 6 keV. Significant among their findings were: 1) Ion bombardment improved coating adherence. 2) Below 1.5 keV ion bombardment there was no noticeable effect on porosity. 3) When the beam energy is increased to 5 keV or above, a significant reduction in the porosity in the coating is obtained when the ion to coating atom ratio is 0.038 and above. This indicates that there is some threshold beam energy and ion to atom ration below which the porosity cannot be reduced by ion mixing.

VII.B.2. REVIEW OF CONCURRENT WORK

1984 Armour and co-workers (40) examined the energy distribution of particles leaving an ion plating discharge. Significant among their findings were: 1) The peak in the energy distribution of singly ionized argon is at less than half the discharge voltage and there is an increase in energy and number with increasing voltage as shown in figure (41). 2) The distribution of doubly ionized argon behaves similarly; however, the energies are shifted slightly higher and the numbers are smaller as shown in figure (43). 3) There is a peak in the energy distribution of neutral particles at about 20% of the applied bias as shown in figure (44). 4) Neutral particles are responsible for the bulk of the energy deposited at the cathode during ion plating. 5) Increasing pressure

causes an increase in the number of singly ionized argon; however, there is a slight shift to lower energies as shown in figure (45).

1984 Bodo and Sundgren (95) studied the effects of argon ion bombardment pretreatment on the adhesion of evaporated Ti on polyethylene. Significant among their results were: 1) Adhesion increased with increasing ion dose up to a critical dose and then declined. 2) at maximum adhesion values, failure was in the PE bulk indicating the the strength of the Ti/PE interface was higher then the cohesive strength of the PE itself. 3) The strong adhesion is related to a carbide like Ti-C formation at the interface. 4) Ion bombardment removes surface impurities from the sample prep process; optimal dose depends on the surface condition of the samples. 5) The decreased adhesion at high ion doses is believed to arise from increased water vapor contamination due to an ion induce increase in the PE surface reactivity.

1984 Garg and co-workers (96) investigated effects of small additions of In, Sn, Bi, and Sb to Al on the Al-Si interdiffusion. Significant among their results were: 1) Additions of Sn (0.014 at %) and In (0.013 at %) significantly reduce the diffusivity of Si in Al by factors of 1.3 and 2 respectively. 2) Bi (0.008 at %) additions slightly reduced the diffusivity of Si in Al. 3) The overall effect of these additions on the interdiffusion in the temperature range 400-560 Celsius (673-833 K) is small.

1984 Matthews and Gethin (97) developed a thermodynamic model to predict the substrate temperature resulting from heating effects in ion assisted processes. Significant among their results were: 1) Substrate temperature increases with increasing cathode

discharge power density as shown in figure (64). 2) Simultaneous deposition during ion bombardment, as in ion plating, causes a further increase in substrate temperature which is most significant at lower cathode discharge power densities as shown in figure (65). 3) An increase in thermal contact resistance between the substrate and a water cooled fixture of heat sink will increase the substrate temperature. 4) Leakage current to the cooling water may be significant in determining the true current density at the cathode. 5) Radiative cooling of the substrate may be enhanced by allowing the substrate to "see" the cool chamber walls.

1984 Thornton (18) reviews physical vapor deposition. Topics covered include: the vacuum environment, evaporation (rates, sources, thickness distributions), Molecular beam epitaxy, sputtering, triodes, magnetrons, thin film growth and properties, microstructures, and metallization of semiconductor devices.

1985 Garosshen and co-workers (1) review Al metallization technology for semiconductor devices. Significant points of this paper include: 1) Al is the preferred metal for interconnects on Si base devices due to its low resistivity (2.7 $\mu\Omega$cm) and good overall processibility. 2) Typical industrial metallization techniques include evaporation, sputtering, and chemical vapor deposition. 3) Problems associated with aluminum metallization include step coverage, interdiffusion, electromigration, stress relaxation, and corrosion. 4) Step coverage can be improved by: a) raising the substrate temperature to promote surface diffusion; b) enlarging the source area to minimize the "line of sight problem"; c) varying the source/wafer geometry to provide the same benefits as enlarging

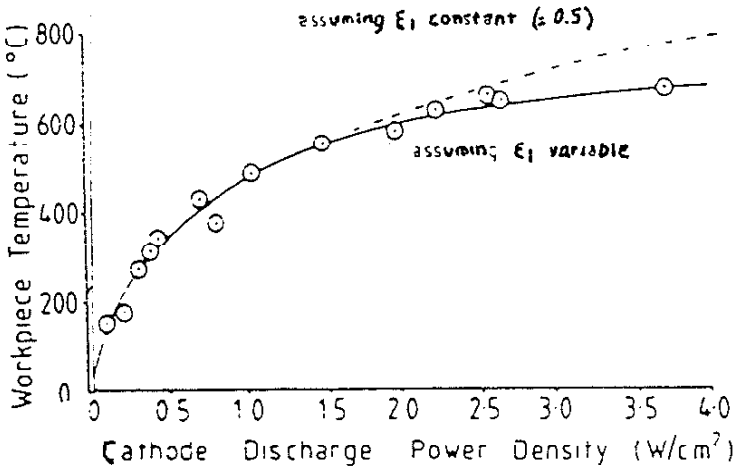

Figure 64. Substrate temperature increase with increasing cathode discharge power density for discharge heating only. From Matthews and Gethin (97).

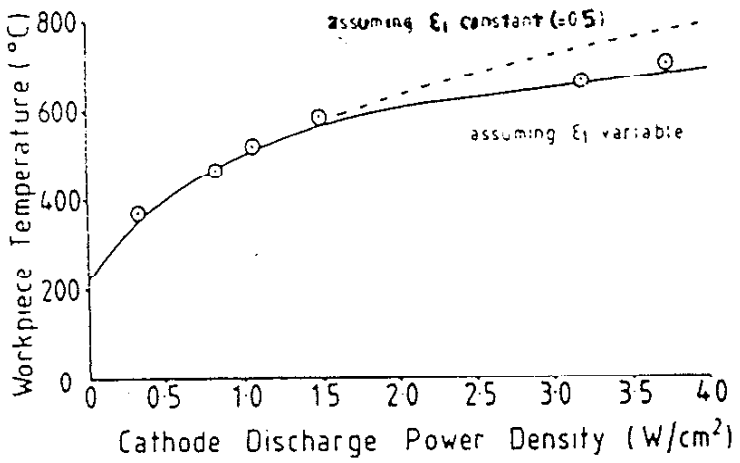

Figure 65. Substrate temperature increase with increasing cathode discharge power density for discharge heating in the presence of and evaporation source (ion plating conditions). From Matthews and Gethin (97).

the source area; and d) increasing the source- substrate distance to enhance the probability of atomic collisions and increase the degrees of freedom for deposition paths. 5) Interdiffusion can be reduced by alloying the Al with small amounts of Si to satisfy the solubility requirement at the processing temperature or by using a barrier layer of an inert material between the Al and Si. 6) Electromigration may be reduced by small additions of Cu and Mg to form precipitates at grain boundaries to inhibit Al self diffusion in an electric field. 6) Stress relaxation arises due to differences in thermal expansion coefficients and may manifest itself in the formation of hillocks in Al films on Si. 7) Localized galvanic corrosion is enhanced by alloy additions such as Cu and the presence of halogen ions. Measures to reduce this problem include rinsing with deionized water and packaging to seal the chip from the environment.

1985 Hershkovitz, Blech, and Komem (98) studied the stress relaxation phenomenon in thin aluminum films deposited onto silicon strips by the cantilever beam technique using x-ray diffraction. Significant among their conclusions were: 1) Stress induced to thin aluminum films deposited on substrates, whether tensile or compressive, relaxes at constant temperature. 2) The relaxation characteristic curves (residual stress vs. time) indicates that several modes or mechanisms are active giving rise to fast, intermediate, and slow relaxations. 3) The intermediate relaxation terminates with a remnant stress that decreases very slowly with time. 4) The time constant for the intermediate relaxation mechanism has an activation energy of 0.43 eV for compression and

0.23 eV for tension. 5) For aluminum films deposited by electron beam evaporation the absolute value of the remnant compressive stress increased with temperature, indicating relaxation by grain boundary diffusional creep. For films deposited by magnetron sputtering the absolute value of the compressive remnant stress decreased with temperature, indicating relaxation by shear or sliding. 6) The results are not universal but depend strongly on the structure of the aluminum film.

1985 Leet (99) reviews the fundamentals of ion plating and discusses his characterization of evaporated and ion plated Ti coatings. Significant among his conclusions were: 1) Biased deposition gives rise to texturing of the coating. 2) Ion plating tends to produce a chemically graded interface. Coatings for the thesis of Leet were produced in the same system as the coatings for this thesis.

1985 Miyoshi and co-workers (100) used a metallic glass to determine the temperature rise in a substrate during ion plating by observing the degree of crystallization in the glass after processing. They determined that there was a 500 degree Celsius (773 K) substrate temperature increase when ion plating was conducted for 15 seconds with a substrate bias of 3.5 kV and a substrate current density of 0.5 mA/cm^2 in argon at 0.27 Pa (20 mTorr). The extent of the crystallized region was 10 to 15 microns below the substrate surface.

1985 Paccagnella and co-workers (101) observed that Si diffuses faster in Al thin film than in wrought Al with dislocation

diffusion being the most probable mechanism for enhanced diffusion in the thin films.

1985 Park and co-workers (23) deposited Al onto oxide steps on Si wafers to observe the effects of 150 V substrate bias on the step coverage. Significant among their conclusions were: 1) Step coverage was improved significantly by using a bias. 2) The bias caused and increase in the deposition temperature. 3) Use of a bias at a low substrate temperature did not improve step coverage. 4) All films showed strong preferred orientation.

1985 Petrova and Stoeva (102) observed an increase in the density of mobile ions when using electron beam evaporation of aluminum rather than W filament evaporation onto MOS devices. This effect is attributed to the effect of radiation damage and substrate heating during the electron beam deposition of Al.

1985 Sequeda (103) reviews the process of integrated circuit fabrication. Topics covered include: wafer manufacture, circuit design, lithography, metallization, etching, and packaging. Significant points include: 1) Additions of 2-4 atomic % Cu to Al reduces electromigration of interconnects. 2) Additions of 1-2 atomic % Si to Al reduces interdiffusion at the junctions.

1985 Sheng and co-workers (104) developed a simple method for the rapid measurement of the thickness of ultrathin metal films in the range from a few angstroms to about 100 angstroms (10 nm). The method is applicable to most metals with atomic numbers greater than or equal to 13 (aluminum). The method is based on the observation that backscattered intensity of an electron beam from the film increases linearly with increasing film thickness at low

thicknesses. This, of course, requires that the substrate have a sufficiently low atomic number not to interfere with the measurement; they got good results depositing films on glassy carbon substrates. The method works best for high atomic number materials since the backscatter coefficient increases as the square of the atomic number of the film material.

1985 Yamada and co-workers (105) investigated the orientational relationships between Al and Si for epitaxial Al on Si deposited using an ionized cluster beam (ICB). Significant among their conclusions were: 1) The crystal orientation of the Al films on Si (111) is Al (111) parallel Si (111) and Al [-110] parallel Si [-110]. The two orthogonal Al (110) parallel Si (100) orientations Al [001] parallel Si [011] and Al [-110] parallel Si [011] were found mixed together in a film deposited onto the Si (100) substrate. 2) In-situ AES and RED observations showed that use of higher accelerating voltages in ionized clusters results in almost layer-by-layer growth and a flat film surface. 3) The interface between the epitaxial Al film and the Si (111) substrate was stable and well defined without alloy penetration after annealing for 30 minutes at 450 Celsius (723 K).

1985 Ziegler, Biersack and Littmark (41) compiled a book describing calculations and computer programs to determine the stopping and range of ions in solids.

1986 Ahmed (106) investigated the effects of pulsed oxygen during ion plating of aluminum on the resulting coating structure and properties. Characterization techniques included SEM, TEM, X-ray diffraction, microhardness, and Rutherford backscattering.

Significant among the conclusions were: 1) Thermionically assisted triode ion plating can be utilized with a pulsed oxygen process to reactively deposit dense, hard and highly adherent aluminum/ aluminum oxide coatings. 2) The crystalline phase of the films is dependent on the oxygen flow and pulse rates and on the substrate bias. Noncrystalline films were formed at high oxygen flow rates and low substrate bias. More crystalline films were formed at low oxygen flow rates and high substrate bias. 3) The results may be explained on the basis of the formation of new heterogeneous nucleation sites owing to the deposition of oxygen impurities which hinder ordinary columnar growth of the aluminum coating.

1986 Badachhape, Margrave, and Brotzen (107) describe the removal of aluminum and aluminum alloy films from the surface of silicon substrates by volatizing the substrate in a reaction with fluorine gas.

1986 Bangert and co-workers (108) conducted ultramicrohardness measurements in an SEM on aluminum films evaporated under various conditions. Coating thicknesses were on the order of 1.5 microns. Significant among their findings were: 1) The true hardness of the film can only be found at low indentation depths where the substrate has a relatively minor contribution to the deformation process. 2) Film hardness increases with increasing oxygen partial pressure during evaporation.

1986 Boxman and co-workers (109) investigated the fast deposition of metallurgical coatings and production of surface alloys using a pulsed high current vacuum arc. Coating/substrate combinations investigated included; aluminum on steel, molybdenum

on copper, and TiN on steel. Significant results of the aluminum work included: 1) In the tests with currents exceeding 0.85 kA the central portion of the substrate had a shiny appearance, indication that the surface temperature had exceeded the melting temperature of the coating material during the arcing cycle. 2) The extent of the shiny region increased with increasing peak current. 3) At sufficiently high currents, the underlying substrate as well as the coating is melted. 4) Deposition rates in excess of 64 microns per second were attained.

1986 Gee, Hodgkinson, and Wilson (110) investigated the effects of deposition parameters on the reflection anisotropy in evaporated aluminum mirror coatings deposited onto blocks of fused silica. Significant among their conclusions were: 1) Reflection anisotropy occurs in aluminum films deposited in the presence of small quantities of oxygen. 2) Aluminum films deposited serially at normal rates (~1 nm per second), pressures (~ 10^{-5} Torr (1.33 x 10-3 Pa)), and angles (0° - 45°) from an array of sources onto large telescope mirrors may contain polarization-sensitive regions and a nonzero mean anisotropy if the residual gases permit oxidation to occur. 3) Anisotropy depends most on the last film deposited and, for a given array of sources which must be fired serially because of restrictions on the current from the power supply, there may be a best order of deposition to minimize anisotropy. 4) The requirements for small anisotropy are just those for small absorption and scattering losses.

1986 Kaganowicz and Robinson (111) investigated the relation between flow, power, and presence of a carrier gas during plasma

deposition of silicon nitride. Significant among their conclusions were: 1) The properties of deposited films depend not only on the natures and quantity of starting materials being introduced into the deposition chamber; but, also on that portion of those materials that are decomposed or activated by the glow discharge. 2) The extent of decomposition and activation may be affected, in a different way for different materials, by the power density in the substrate vicinity, the gas flow in the system, flows and nature of additional gas flows into the system (inert and reactive), and the pumping rate of the system. 3) Composition of the coating corresponds to the amounts of starting materials that have been decomposed by the plasma and are available for reaction and not to the amounts of starting materials introduced into the system.

1986 Kay (112) investigated the non-bulk-like physical properties arising in thin films due to ion bombardment during film growth. Structural. optical, and electrical measurements indicated that resulting changes in optical and electrical non- bulk-like characteristics are primarily due to changes in the void fraction and grain size associated with ion bombardment during film growth.

1986 Koleshko, Belitsky, and Kiryushin (113) investigated the stress relaxation mechanisms in thin aluminum films. Significant among their conclusions were: 1) At temperatures above 0.2 T_{mp} and at sufficiently high tensile stresses (below the flow stress) the stress relaxation in aluminum films develops mainly by dislocation climb mechanisms, and strain rates are more than $10^{-8}s^{-1}$. 2) The analysis of the deformation mechanism maps (DMM) made it possible to introduce the yield limit for thin films and to show that for thin

aluminum films this yield limit has two components. One component is associated with stress relaxation by low temperature dislocation climb and grain boundary diffusional creep and the other corresponds to the stress relief controlled by high temperature dislocation climb. If the stress is equal to the flow stress of a thin film, then at sufficiently low temperatures one component equals another component of the yield limit.

1986 Kubiak and co-workers (114) investigated the use of polytetrafluoroethylene (PTFE) bearings in vacuum systems. The material performed well at temperatures below 200 Celsius (473 K) at rotational speeds between 10 and 1000 rpm while allowing attainable base pressures of 10^{-8} Pa.

1986 Manory (115) investigated the use of "Tempilaq" color temperature indicating markers for monitoring surface temperatures in plasma treatments. The markers gave good agreement with thermocouple measurements and little difficulty with volatization of the marking material.

1986 Munz (116) investigated the use of titanium aluminum nitride coatings as an alternative to titanium nitride films. The coatings were sputter deposited from targets of various compositions at various nitrogen flow rates. Coatings were evaluated by x-ray diffraction, SEM, microhardness testing, oxidation resistance testing, and drilling performance. Results indicate that the incorporation of Al into the nitride films improves the oxidation resistance of the coating and the cutting performances of coated drills. X-ray results indicated that the substitutional

incorporation of aluminum in the TiN lattice may form a metastable phase.

1986 Roberts and Dobson (117) investigated the microstructure of aluminum thin films on amorphous SiO_2. Significant among their results were: 1) The early stages of film growth were characterized by an island or connected-network structure and a random grain orientation. 2) The thickness at which complete coverage occurred ranged from 15 nm at 295 K to 100 nm at 625 K, and above this a <111> fibre texture became apparent. 3) The mean grain size of the aluminum increases with the deposition temperature in the range 295 - 675 K. 4) The mean grain size increases with deposition rate in the range 1-10 nm s^{-1} at low temperatures, but is independent of deposition rate at higher temperatures. 5) The presence of nitrogen or oxygen during deposition tends to reduce the grain size. 6) Post deposition annealing promotes grain growth, but the process is slow except at high temperatures (approaching 700 K). 7) Growth hillocks are present on films deposited at room temperature but can be completely suppressed by the use of high deposition temperature, high deposition rate and low oxygen partial pressure. 8) Electron-beam- and tungsten-filament-deposited films are very similar in microstructure. 9) Sputter deposited films are characterized by a small grain size and a random orientation of the grains.

1986 Skelly and Gruenke (118) investigated the use of a substrate bias on the filling of vias during the sputter deposition of aluminum. They observed a significant improvement in coverage by using dc bias sputtering as opposed to unbiased sputtering.

1986 Sundgren and Hentzell (119) reviewed the present state of art in hard coatings grown from the vapor phase. Significant points and topics in the paper include: 1) Consideration s in coating/substrate selection. 2) Relations between microstructure and hardness in hardness in hard coatings. 3) Metastable phases and metastable atom positions are often observed in thin refractory films. Examples include supersaturated solid solutions and the incorporation of C and N in interstitial positions in carbides and nitrides. 4) Coating textures. 5) Review of nitrides, carbides, oxides, borides, intermetallics, and diamondlike carbon films.

1986 Testoni and Stair (120) investigated the role of surface defects in aluminum surface oxidation by subjecting an aluminum surface to various surface treatments and observing the effects on the dominant defect structures and the initial oxide observed. Characterization included low energy electron diffraction (LEED) and Auger electron spectroscopy (AES) oxidation kinetics measurements. Significant among their results were: 1) The detailed Al(111) surface structure depends upon the surface preparation. 2) Steps, mosaics, and facets can form depending upon the sputtering time and the duration and temperature of annealing. 3) The oxidation threshold of the surface depends upon the type and concentration of surface defects, with steps being the most important.

1986 Vogel and Bergmann (121) reviewed and investigated the problems encountered with the introduction of ion plating to large-scale coating of tools. Significant points of this paper include: 1) Tool performance is greatly improved by using coatings. 2) Difficulties are often encountered with surfaces to be coated due to

poor surface structures created by grinding and finishing operations and contamination during cleaning processes. 3) Material inspection before coating is important from a quality control standpoint; however, this may cause problems with reduced adhesion and corrosion due to fingerprints on degreased materials. 4) Ion plating of tools with titanium nitride using evaporator sources has become a very reliable procedure.

1987 Ball and Todd (122) investigated the use of sputter deposited multilayer films of Al, Ti, Cr, Nb, and Zr annealed to form intermetallics and give improved electromigration resistance to the film. Characterization techniques included; surface profilometry, x-ray diffraction, and differential scanning calorimetry. Significant among their results were: 1) Alternate layers of Al and Ti was the only combination to form an as deposited aluminide. 2) The first intermetallic to form in most cases is the most aluminum-rich intermetallic. 3) From the group of transition metals tested, zirconium and titanium stand out as the metals most likely to be effective in minimizing electromigration in multilayer conductors of Al-Cu alloy on a transition metal.

1987 Bessaudou, Machet, and Weissmantel (123) investigated the theoretical and experimental aspects of the thickness distribution of thin films deposited by evaporation under an inert support gas at various pressures as a first step toward describing material transport in ion plating. A good match was made between measured thickness values and calculated thickness values for evaporated silver at pressures above a few Pascals and low evaporation rates; whoever, since their model is based on diffusion,

it breaks down at lower pressures so as not to be valid in the pressure range most frequently used in ion plating.

1987 Bessaudou, Machet, and Weissmantel (124) investigated the theoretical and experimental aspects of thickness distribution of thin films deposited by evaporation in the pressure regime appropriate to ion plating. The model presented in this work as a follow up to the diffusion model presented in their previous paper (123) uses a modified cosine distribution with Monte Carlo scattering to account for the mean free path of a particle in the system being on the order of the dimension of the system. The use of a virtual source located just above the real source in the model gave good agreement between calculated thickness values and experimentally measured thickness values for evaporated silver.

1987 Brown (125) investigated the influence of polyethylene terephthalate (PET) on the texture of evaporated aluminum films and found that the coatings exhibit a texture such that {111} planes are parallel to the PET surface with no evidence of in-plane anisotropy. The perfection of the {111} texture was reduced on more crystalline polyester surfaces. The coatings were evaluated by TEM after dissolving away the substrates.

1987 Egert and Scott (126) investigated ion plating parameters, coating structure, and corrosion protection for aluminum coatings on uranium. Characterization techniques included SEM and corrosion testing. Significant among their results were: 1) A transition from a loosely joined columnar structure to a dense noncolumnar structure was observed with increasing applied substrate bias and decreasing deposition rate. This implies that the

ratio of ratio of the energetic particle bombardment rate to the coating atom arrival rate has a significant influence on the coating structure. 2) Dense, noncolumnar coatings deposited at high substrate bias (-2 kV) and low deposition rates (0.035 μm/min) were found to provide the most effective corrosion protection.

1987 Horikoshi (127) reviews evacuation and gas desorption mechanisms and presents a new set of equations for the analysis of the evacuation process.

1987 Ma and co-workers (128) investigated structural transformations induced by nitrogen implantation into aluminum, cobalt, copper and gadolinium films. Ion energies were on the order of 100 keV. Characterization techniques included TEM and X-ray diffraction. Aluminum nitride was observed for an implantation dose of $2x10^{17}$ N^+ cm^{-2} + $5x10^{17}$ N^+ + N_2^+ cm^{-2} and not for implantation doses of $5x10^{17}$ N^+ cm^{-2} and less although a slight expansion of the planar spacings of the aluminum was observed at the lower doses.

1987 Mathewson and co-workers (129) investigated the synchrotron radiation induced gas desorption in aluminum vacuum chamber after chemical and argon glow discharge cleaning. The argon discharge provided a superior reduction in the gas desorption to the chemical cleaning; however, chemical cleaning was chosen as the method of choice due to the low removal rate of argon from the system by the titanium sublimation pumps.

1987 Pandey, Gangopadhyay, and Suryanarayana (130) investigated the formation of metastable phases in evaporated Al-Zr films using TEM. As deposited film were supersaturated solid

solutions and annealing led to the formation of an equilibrium structure through the formation of a sequence of metastable phases.

1987 Pargellis (131) investigated the thickness distribution of sputter deposited copper inside substrate holes. A good agreement between calculated and observed thicknesses was achieved by integrating the contributions to thickness from the points on the source visible to the location and assuming a cosine distribution from the individual source area elements.

1987 Schiller and co-workers (132) reviewed high-rate vapor deposition and large systems for coating processes. Significant topics of this paper include: 1) High-rate electron beam sources, systems, and applications. 2) High-rate sputtering sources and systems. 3) Reactive sputtering in large-scale systems.

1987 Scott (133) reviewed the ion plating literature and investigated evaporated and ion plated copper films on cordierite glass ceramic substrates. Characterization techniques included AES, SIMS, TEM, EDX, SEM, and adhesion testing. Significant results of this work include: 1) A shift in coating morphology from a open boundary columnar structure in the evaporated case to a fully dense equiaxed/columnar structure at 5 kV substrate bias. 2) An amorphous interfacial layer 250 angstroms (25 nm) thick was formed in the ceramic for deposition at 5 kV. 3) There was a definite improvement in coating adhesion with increasing applied substrate bias. 4) The coating adhesion was degraded significantly by post deposition heat treatments. 5) The coatings were deposited in the same system as was used for this thesis.

1987 Shah (134) reviewed the ion plating literature and investigated evaporated and ion plated nickel films on cordierite glass ceramic substrates. Characterization techniques included AES, SIMS, TEM, EDX, SEM, and adhesion testing. Significant results of this work include: 1) Coating adhesion increased with increasing substrate bias on non- sputter cleaned substrates; however, optimal adhesion was obtained by evaporating onto a sputter cleaned substrate. 2) Use of a 3 kV substrate bias during deposition caused a shift toward a zone 2 structure from the zone 1 structure observed in the evaporated case. 3) The coatings were deposited in the same system as was used for this thesis.

1987 Slusser and MacDowell (135) investigated sources of surface contamination affecting the electrical characteristics of semiconductors. Sources of contamination included: 1) Aluminum, chromium, iron, and nickel from sputtering of lenses or platens in ion implanters. 2) Aluminum in the hydrogen peroxide used in some oxidizing precleaning solutions. 3) Boron in hydrochloric acid solutions concentrates at the wafer surface during precleaning. 4) Chromium from dry etch processing.

VII.C. TEM SAMPLE PREPARATION

Flat samples:

1. Section coating/substrate couple into narrow strips such that 2 or more pieces coating to coating will fit in a 3mm outside diameter stainless steel tube. It may be necessary to reduce the substrate thickness by machining or grinding before doing this; optimally, a substrate of appropriate thickness (less than 1 mm) will be used for coating. It is also helpful to round the corners of the substrate that are away from the coating so as to allow a wider strip to fit in the tube and to fill as much of the empty space as possible; optimally, the coatings could be made on half rounds of a size such that 2 of them fit face to face in a 3mm OD tube.

2. Prepare the stainless steel tube by etching with glyceregia or another suitable etchant if you are not using stainless steel tubing. Wash the tubing with a clean organic solvent to provide a good bonding surface for epoxy.

3. Wash the coated substrates with a suitable organic solvent to provide a good bonding surface for epoxy.

4. Bond the coated substrates together coating to coating with epoxy.

5. Insert the bonded substrates into the tube and fill the excess space with epoxy. For some systems, it works better if the substrates are allowed to harden after the initial bonding and then the epoxy is sanded off to allow the sandwich to fit into the tube with fresh epoxy.

6. Slice ~ 0.6 mm thick disks of the composite with a low speed diamond saw.

7. Sand and polish the sample from both sides to flatten it and remove damage material to a thickness of about 150 microns. Using a dimpler with a flattening tool at this stage is very helpful.

8. Thin the center of the sample to about 50 microns using a dimpling tool.

9. Mount the disc on a liquid nitrogen cold stage in an ion mill and mill until a perforation occurs at the interface. For some samples it is helpful to mount beam blockers on the stage so that the milling only occurs within 45 degrees of a perpendicular to the interface. It is also helpful to mill the sample from only one side for a while once the first perforation occurs. Unfortunately, the things that tend to promote a higher success rate on samples also promote longer milling times.

10. Nonconductive coatings should be carbon coated. The carbon coating also helps to prevent problems with the epoxy surfaces charging.

"Jelly Roll" Samples

1. Coatings should be prepared on as thin of foils of the substrate material as is practically possible. The foils should be thick enough to resist excessive wrinkling and provide adequate handling strength. The foils should be thin enough so that the effective strain at the coating surface is small when the foil is tightly coiled; optimally want radius of curvature divided by composite (coated foil) thickness to be a large number.

2. Prepare the 3 mm OD stainless steel tube by etching and washing with an organic solvent to provide a good bonding surface for epoxy. The tube length should be about 2 cm.

3. Clean the coated foils with an organic solvent to provide a good bonding surface for epoxy. The foils should be in strips about as wide as the length of the tube they will be put into. The length should be suitable to allow filling of the tube when tightly coiled while leaving enough material to hold onto.

4. Feed a pair of small, clean thermocouple wires or other small, clean wires through the stainless steel tube and mount the wires on a fixture to prevent them from twisting at the ends while being parallel and close together along their length and while passing through the tube. About 10 to 15 cm between the anchor points is a good distance.

5. Slide the tube toward one set of the anchor points or the other. Insert the foil between the wires at the midpoint between the anchors.

6. Fold the foil coating to coating at the midpoint and bring the ends of the strip together; the foil will only be around one of the wires at this point.

7. Using an appropriate tool, apply epoxy to all surface of the foil near the wires.

8. Wrap the foil around the while holding tension until a roll is built up that will just fit inside the tube. Be sure to have epoxy on all the surfaces as this acts a lubricant during the coiling of the foil. Do not be surprised if the wires twist a lot and it is necessary to make more turns with the foil than there is in the composite roll. Be sure to use sufficient tension while coiling; too much tension will break the foil and too little will yield a poor sample.

9. Hold tension on the sample while rolling the tube over the coil. The tube should be rolled in such a manner as to continue coiling the roll. If the edge of the tube is not able to cut the foil as the roll is inserted, it may be necessary to have an assistant cut the foil just ahead of the tube edge as the roll is inserted. Be sure to have excess epoxy on the foil and in the tube for this step since when the coil relaxes slightly in the tube, voids may be created if there is not sufficient epoxy available to fill them as they try to form. Use of epoxy that has begun to set is not recommended; if possible, the sample should be coiled and inserted before the epoxy begins to set. Working in a cold room will delay setting of the epoxy sufficiently to allow adequate time for working.

10. Cut slices and thin the samples as described above for the flat samples. It is not necessary to use beam blocks and one sided ion milling for the coiled samples.

VII.D. RAW ADHESION DATA

This appendix is a tabulation of raw adhesion data.

Table D1 (same as Table 2.)
Table of Substrate Surface Conditions

Substrate	Condition	
1 Al	Tarnished	- as-cold-rolled (CR), EtOH rinse
2 Al	Chem etch	- as-CR, KOH wash, dil. acid rinse, EtOH rinse
3 Al	Oxidized	- as CR, KOH wash, dil. acid rinse, EtOH rinse, air anneal at 600 C, EtOH rinse
4 Cu	Tarnished	- as recieved, EtOH rinse
5 Cu	Chem etch	- as recieved, 40% HNO_3_ wash, EtOH rinse
6 Cu	Chem polish	- as recieved, 40% HNO_3_ wash, chem polish, EtOH rinse
7 Ti	Tarnished	- as recieved, EtOH rinse
8 Ti	Chem polish	- as recieved, chem polish, EtOH rinse

Table D2. Table of deposition conditions.

Deposition Conditions

Label	kV	mA	Enhancement	Sputter preclean
A	0.0	0.0	None	None
B	2.5	10	None	None
C	5.0	20	None	None
D	2.5	20	90V, 1.2A	None
E	5.0	40	90V, 1.2A	None
F	5.0	11	None	5kV, 11mA, 5min.
G	0.0	0.0	None	5kV, 11mA, 5min.

1 ksi = 6.90 MPa

Substrate/Deposition condition: 1 Al/A

Raw values

ksi	MPa
0.00	0.00
0.08	0.55
0.00	0.00
0.08	0.55
0.02	0.14

Substrate/Deposition condition: 2 Al/A

Raw values

ksi	MPa
0.91	6.28
2.24	15.46
0.93	6.42
0.62	4.28
2.45	16.91

Substrate/Deposition condition: 3 Al/A

Raw values

ksi	MPa
0.03	0.21
0.06	0.41
0.20	1.38
0.04	0.28
0.45	3.11

Substrate/Deposition condition: 4 Cu/A

Raw values

ksi	MPa
0.00	0.00
0.00	0.00
0.01	0.07
0.00	0.00
0.01	0.07

Substrate/Deposition condition: 5 Cu/A
Raw values

ksi	MPa
0.00	0.00
0.01	0.07
0.00	0.00
0.09	0.62
0.00	0.00

Substrate/Deposition condition: 6 Cu/A
Raw values

ksi	MPa
0.00	0.00
0.37	2.55
0.14	0.97
0.00	0.00
0.01	0.07

Substrate/Deposition condition: 7 Ti/A
Raw values

ksi	MPa
0.00	0.00
0.00	0.00
0.00	0.00
0.00	0.00
0.00	0.00

Substrate/Deposition condition: 8 Ti/A
Raw values

ksi	MPa
0.00	0.00
1.39	9.59
0.00	0.00
0.00	0.00
0.00	0.00

Substrate/Deposition condition: 1 Al/B
Raw values

ksi	MPa
0.52	3.59
0.72	4.97
0.57	3.93
0.20	1.38
0.78	5.38

Substrate/Deposition condition: 2 Al/B
Raw values

ksi	MPa
0.89	6.14
3.27	22.56
0.10	0.69
2.58	17.80
1.11	7.66

Substrate/Deposition condition: 3 Al/B
Raw values

ksi	MPa
3.10	21.39
2.50	17.25
2.04	14.08
1.18	8.14
1.64	11.32

Substrate/Deposition condition: 4 Cu/B
Raw values

ksi	MPa
0.01	0.07
0.00	0.00
1.66	11.45
0.39	2.69
0.82	5.66

Substrate/Deposition condition: 5 Cu/B
Raw values

ksi	MPa
8.78	60.58
4.98	34.36
9.62	66.38
9.48	65.41
4.85	33.47

Substrate/Deposition condition: 6 Cu/B
Raw values

ksi	MPa
2.20	15.18
3.72	25.67
9.45	65.21
6.96	48.02
9.32	64.31

Substrate/Deposition condition: 7 Ti/B
Raw values

ksi	MPa
1.22	8.42
2.12	14.63
0.17	1.17
2.39	16.49
0.60	4.14

Substrate/Deposition condition: 8 Ti/B
Raw values

ksi	MPa	
4.87	33.60	
6.96	48.02	
5.99	41.33	
4.52	31.19	
10.37	71.55	No fail
9.74	67.21	retest of above

Substrate/Deposition condition: 1 Al/C
Raw values

ksi	MPa
3.48	24.01
5.11	35.26
5.92	40.85
3.99	27.53
6.73	46.44

Substrate/Deposition condition: 2 Al/C
Raw values

ksi	MPa
3.97	27.39
3.28	22.63
8.18	56.44
7.32	50.51
5.11	35.26

Substrate/Deposition condition: 3 Al/C
Raw values

ksi	MPa
1.38	9.52
3.21	22.15
1.55	10.70
2.43	16.77
3.27	22.56

Substrate/Deposition condition: 4 Cu/C
Raw values

ksi	MPa
0.31	2.14
0.27	1.86
0.26	1.79
0.43	2.97
0.74	5.11

Substrate/Deposition condition: 5 Cu/C
Raw values

ksi	MPa
8.66	59.75
3.18	21.94
8.10	55.89
9.89	68.24
3.16	21.80

Substrate/Deposition condition: 6 Cu/C
Raw values

ksi	MPa
8.14	56.17
6.60	45.54
2.49	17.18
5.68	39.19
9.47	65.34

Substrate/Deposition condition: 7 Ti/C
Raw values

ksi	MPa
3.04	20.98
2.94	20.29
3.75	25.88
1.43	9.87
3.87	26.70

Substrate/Deposition condition: 8 Ti/C
Raw values

ksi	MPa
7.46	51.47
6.85	47.27
7.13	49.20
7.62	52.58
9.53	65.76

Substrate/Deposition condition: 1 Al/D
Raw values

ksi	MPa
0.07	0.48
1.41	9.73
1.18	8.14
0.67	4.62
0.80	5.52

Substrate/Deposition condition: 2 Al/D
Raw values

ksi	MPa
8.71	60.10
9.95	68.66
7.24	49.96
8.34	57.55
10.40	71.76

Substrate/Deposition condition: 3 Al/D
Raw values

ksi	MPa
3.07	21.18
4.20	28.98
5.00	34.50
0.08	0.55
3.08	21.25

Substrate/Deposition condition: 4 Cu/D
Raw values

ksi	MPa
0.28	1.93
0.67	4.62
0.16	1.10
0.16	1.10
0.10	0.69

Substrate/Deposition condition: 5 Cu/D
Raw values

ksi	MPa
10.08	69.55
3.98	27.46
8.40	57.96
3.29	22.70
5.90	40.71

Substrate/Deposition condition: 6 Cu/D
Raw values

ksi	MPa
0.69	4.76
1.19	8.21
0.59	4.07
0.87	6.00
0.90	6.21

Substrate/Deposition condition: 7 Ti/D
Raw values

ksi	MPa
2.14	14.77
1.15	7.94
0.15	1.04
3.02	20.84
2.56	17.66

Substrate/Deposition condition: 8 Ti/D
Raw values

ksi	MPa	
6.27	43.26	
1.26	8.69	
1.05	7.25	
3.69	25.46	
10.50	72.45	No failure
10.52	72.59	Retested above, no failure

Substrate/Deposition condition: 1 Al/E
Raw values

ksi	MPa
1.04	7.18
1.49	10.28
1.01	6.97
0.99	6.83
1.60	11.04

Substrate/Deposition condition: 2 Al/E
Raw values

ksi	MPa
9.81	67.69
8.76	60.44
0.79	5.45
9.49	65.48
0.68	4.69

Substrate/Deposition condition: 3 Al/E
Raw values

ksi	MPa
2.67	18.42
0.35	2.42
2.10	14.49
3.72	25.67
4.34	29.95

Substrate/Deposition condition: 4 Cu/E
Raw values

ksi	MPa
0.21	1.45
0.13	0.90
1.51	10.42
0.06	0.41
0.29	2.00

Substrate/Deposition condition: 5 Cu/E
Raw values

ksi	MPa	
1.82	12.56	
4.74	32.71	
0.48	3.31	
10.42	71.90	No failure
10.17	70.17	Retest of above, no failure
4.36	30.08	Retest of above

Substrate/Deposition condition: 6 Cu/E
Raw values

ksi	MPa	
4.30	29.67	
7.46	51.47	
1.27	8.76	
0.05	0.35	
10.35	71.42	No failure
10.44	72.04	Retest of above, no failure

Substrate/Deposition condition: 7 Ti/E
Raw values

ksi	MPa
1.65	11.39
5.07	34.98
5.68	39.19
3.06	21.11
3.13	21.60

Substrate/Deposition condition: 8 Ti/E
Raw values

ksi	MPa	
0.08	0.55	
1.78	12.28	
3.58	24.70	
7.70	53.13	
10.48	72.31	No failure
10.49	72.38	Retest of above, no failure

Substrate/Deposition condition: 2 Al/F
Raw values

ksi	MPa
0.28	1.93
3.18	21.94
0.99	6.83
2.06	14.21
2.47	17.04

Substrate/Deposition condition: 8 Ti/F
Raw values

ksi	MPa
1.58	10.90
10.37	71.55
8.62	59.48
4.92	33.95
10.38	71.62

Substrate/Deposition condition: 2 Al/G
Raw values

ksi	MPa
4.90	33.81
5.10	35.19
3.96	27.32
5.09	35.12
3.89	26.84

Substrate/Deposition condition: 8 Ti/G
Raw values

ksi	MPa
10.38	71.62
10.38	71.62
10.38	71.62
10.34	71.35
10.39	71.69

VIII. REFERENCES

1. T. J. Garosshen, et al., "Aluminum Metallization Technology for Semiconductor Devices", J. of Metals, May, (1985)

2. M. G. Fontana and N. D. Green, Corrosion Engineering, 2nd ed., Mcgraw Hill, (1978)

3. S. Safai and H. Herman, "Microstructural Investigation of Plasma-Sprayed Aluminum Coatings", Thin Solid Films, 45, 295, (1977)

4. P. L. Ferraglio and C. D. D'Antonio, Structure of Vapor Deposited Aluminum Films", Thin Solid Films, 1, 499, (1967/68)

5. P. S. McLeod and J. L. Hughes, "Effects of Sputter Etching and Process Techniques on the Properties of Sputtered Aluminum Films", J. Vac. Sci. Tech., 16 (2), Mar/Apr, (1979)

6. A. Kubovy and M. Janda, "The Influence of Residual Gas Pressure on the Stress in Aluminum Films", Thin Solid Films, 42, 169, (1977)

7. R. Brick, A. Pense, and R. Gordon, Structure and Properties of Engineering Materials, 4th ed., Mcgraw- Hill, (1977)

8. D. G. Teer and F. B. Salem, "The Formation of Low Friction Wear-Resistant Surfaces on Titainium by Ion Plating", Thin Solid Films, 45, 583, (1977)

9. D. R. Gaskell, Introduction to Metallurgical Thermodynamics, Mcgraw-Hill, (1981)

10. R. E. Hurley and E. N. Williams, "Ion Plating of Metal Films on Plastic Substrates", Thin Solid Films, 92, 99, (1982)

11. L. F. Goldstein and T. J. Bertone, "Evaluation of Metal- Film Adhesion to Flexible Substrates", J. Vac. Sci. Tech., 12 (6), Nov/Dec, (1975)

12. D. S. Campbell, Chapter 12 in Handbook of Thin Film Technology, ed by L. Maissel and R. Glang, McGraw-Hill, (1983)

13. B. N. Chapman, "Thin-Film Adhesion", J. Vac. Sci. Tech., 11 (1), Jan/Feb, (1974)

14. C. Weaver, "Adhesion of Thin Films", J. Vac. Sci. Tech., 12 (1), Jan/Feb, (1975)

15. M. Laugier, "Adhesion and Internal Stress in Thin Films of Aluminum", Thin Solid Films, 79, 15, (1981)

16. D. M. Mattox, "Thin Film Metallization of Oxides in Microelectronics", Thin Solid Films, 18, 173, (1973)

17. L. E. Collins, et al., "Effect of Ion Bombardment on the Adhesion of Aluminum Films on Glass", Thin Solid Films, 4, 41, (1969)

18. J. A. Thornton, "Physical Vapor Deposition" in Semiconductor Materials, and Process Technologies, ed. by G. E. Mcguire, Noyes, (1984)

19. J. P. Coad, et al., "The Effects of Substrate Heating and Ion Cleaning on Thick Film Adhesion", Vacuum, 31 (8/9), 365, (1981)

20. D. M. Mattox and J. E. McDonald, "Interface Formation During Thin Film Deposition", J. Appl. Phys., 34, 2493, (1963)

21. B. Chapman, Glow Discharge Processes, John Wiley and Sons, (1980)

22. J. A Thornton, "Magnetron Sputtering: Basic Physics and Application to Cylindrical Magnetrons", J. Vac. Sci. Tech., 15 (2), Mar/Apr, (1978)

23. Y. H. Park, et al., "Influences of D. C. Bias on Aluminum Films Prepared with High Rate Magnetron Sputtering Cathode", Thin Solid Films, 129, 309, (1985)

24. T. E. Hartman, "Density of Thin Evaporated Aluminum Films", J. Vac. Sci. Tech., 2 (5), Sept/Oct, (1965)

25. A. G. Dirks and H. J. Leamy, "Columnar Microstructure in Vapor-Deposited Thin Films", Thin Solid Films, 47, 219, (1977)

26. I. A. Blech, "Evaporated Film Profiles over Steps In Substrates", Thin Solid Films, 6, 113, (1970)

27. A. J. Learn, "Aluminum Alloy Film Deposition and Characterization", Thin Solid Films, 20, 261, (1974)

28. A. Barna, et al., "The Effect of Evaporation Arrangement on the Morphology and Structure of Vacuum-Deposited Thin Films", Thin Solid Films, 5, 201, (1970)

29. N. G. Dhere, et al., "Purity and Morphology of Aluminum Films", Thin Solid Films, 30, 267, (1975)

30. N. G. Dhere, et al., "The Morphology of Thick Evaporated Aluminum Films and Their Purity as Determined by Proton- Induced X-Ray Analysis", Thin Solid Films, 44, 29, (1977)

31. L. Maissel, Chapter 4 in Handbook of Thin Film Technology, ed. by L. Maissel and R. Glang, McGraw-Hill, (1983)

32. D. M. Mattox, "Adhesion and Surface Preparation", Chapter 3 in Deposition Technologies for Films and Coatings, ed by R. F. Bunshah, Noyes, (1982)

33. R. B. Love and W. K. Bower, "Thick Deposits of Ultrahigh-Purity Aluminum", J. Vac. Sci. Tech., 11 (6), Nov/Dec, (1974)

34. R. Glang, Chapter 1 in Handbook of Thin Film Technology, ed by L. Maissel and R. Glang, McGraw-Hill, (1983)

35. R. Glang, et al., Chapter 2 in Handbook of Thin Film Technology, ed by L. Maissel and R. Glang, McGraw-Hill, (1983)

36. R. E. Hurley, "Physical Processes in the Substrate Dark Space in Biased Deposition Systems", Thin Solid Films, 86, 241, (1981)

37. B. D. Cullity, Elements of X-ray Diffraction, 2nd ed., Addison-Wesley, (1978)

38. H. D. Hagstrom, "Low Energy De-excitation and Neutralization Processes Near Surfaces", in Inelastic Ion-Surface Collisions, ed by N. H. Tolk, et al., Academic Press, NY, (1977)

39. W. D. Davis and T. A. Vanderslice, "Ion Energies at the Cathode of a Glow Discharge", Phys. Rev., 131 (1), (1963)

40. D. G. Armour, et al., "Characteristics of the Ion and Neutral Fluxes Incident on the Substrate in an Ion Plating Discharge", Vacuum, 34, 295, (1984)

41. J. F. Ziegler, ed., The Stopping and Ranges of Ions in Matter, v1, Pergamon, NY, (1985)

42. D. M. Mattox, "Fundamentals of Ion Plating", J. Vac. Sci. Tech., 10 (1), (1973)

43. R. F. Bunshah, Chapter 4 in Deposition Technologies for Films and Coatings, ed. by R. F. Bunshah, Noyes, (1982)

44. B. Lewis and J. C. Anderson, Nucleation and Growth of Thin Films, Academic Press, NY, (1978)

45. B. Movchan and A. Demchishin, "Study of the Structure and Properties of Thick Vacuum Condensates of Nickel, Titanium, Tungsten, Aluminum Oxide and Zirconium Dioxide", Phys. Met. Metallogr., 28, 83, (1969)

46. M. Lardon, et al., "Morphology of Ion-Plated Titanium and Aluminum Films Deposited at Various Substrate Temperatures", Thin Solid Films, 54, 317, (1978)

47. F. Milillo, et al., "Strength Versus Thickness in Vapor Deposited Aluminum Films", Thin Solid Films, 3, 51, (1969)

48. P. Dobson and B. Hopkins, "Preferred Orientation in Metal Films Deposited on Glass", Thin Solid Films, 5, 97, (1970)

49. L. Maissel and R. Glang, eds., Handbook of Thin Film Technology, McGraw-Hill, USA, (1970)

50. E. Graper, "Deposition of Aluminum from an Electron Beam Source", J. Vac. Sci. Tech., 9 (1), 33

51. D. Mattox and G. Kominiak, "Structure Modification by Ion Bombardment During Deposition", J. Vac. Sci. Tech., 9 (1), 528

52. R. Nelson, "Metallurgical Applications of Ion Implantation and Ion Bombardment", Vacuum, 23(3)

53. P. Stroud, H. Lindsany, and J. Perkins, "Some Preliminary Studies of the Structure of Ion Bombarded Thin Films", Vacuum, 23 (4)

54. E. Erikson, "Thickness Distribution of a Metal-Alloy from a High-Rate Electron Beam Source", J. Vac. Sci Tech., 11 (1), 366, (1974)

55. R. Bland, et al., "Effect of Ion Bombardment During Deposition on Thick Metal and Ceramic Deposits", DJ. Vac. Sci. Tech., 11 (4), 671, (1974)

56. R. Bunshah, "Structure and Property Relationships in Evaporated Thick Films and Bulk Coatings", J. Vac. Sci. Tech., 11 (4), 633, (1974)

57. K. Steube and L. McCrary, "Ion-Vapor-Deposited Aluminum Coatings for Irregularly Shaped Aircraft and Spacecraft Parts", J. Vac. Sci. Tech., 11 (1), 362, (1974)

58. L. Holland, "Substrate Treatment and Film Deposition in Ionized and Activated Gas", Thin Solid Films, 27, 185, (1975)

59. M. Vulli, "Preparation of Thin Metallic Films of Aluminum, Lanthanum and Dysprosium with Minimum Oxidation", Vacuum, 26 (3), 105

60. K. Kemmochi and K. Hirano, "Electromigration of Grain Boundaries in Aluminum", Thin Solid Films, 25, 353, (1975)

61. S. Schiller, et al., "Alternating Ion Plating - A Method of High Rate Ion Vapor Deposition", J. Vac. Sci. Tech., 12 (4), 858, (1975)

62. P. Glaser, et al., "Ion Evaporation", Thin Solid Films, 32, 69, (1976)

63. J. Chevallier, "Platinum Metals Coatings by Vacuum Deposition Processes", Thin Solid Films, 40, 223, (1977)

64. R. Dugdale, "D. C. Glow Discharge Techniques for Surface Treatment and Coating", Thin Solid Films, 45, 541, (1977)

65. P. Ghate, et al., "Metallization in Microelectronics", Thin Solid Films, 45, 69, (1977)

66. M. Marinov, "Effect of Ion Bombardment on the Initial Stages of Thin Film Growth", Thin Solid Films, 46, 267, (1977)

67. P. Mcleod and L. Hartsough, "High-Rate Sputtering of Aluminum for Metallization of Integrated Circuits", J. Vac. Sci. Tech., 14 (1), 263, (1977)

68. T. Ohsaki, et al., "The Properties of Carbon Fiber Reinforced Aluminum Composites Formed by the Ion-Plating Process and Vacuum Hot Pressing", Thin Solid Films, 45, 563, (1977)

69. R. Prummer, "Explosive Cladding of Thin Films", Thin Solid Films, 45, 205, (1977)

70. D. Sherman, "Deposition of Uniform Aluminum Films on Kapton Laminates by Electron Beam Evaporation", Thin Solid Films, 45, 573, (1977)

71. D. Teer and M. Salama, "The Ion Plating of Carbon", Thin Solid Films, 45, 553, (1977)

72. N. Tolk, et al., Inelastic Ion-Surface Collisions, Academic Press, NY, (1977)

73. S. Dahlgren, et al., "The Metallurgical Characterization of Coatings", Thin Solid Films, 53, 41, (1978)

74. S. Fujishiro and D. Eylon, "Improved High Temperature Mechanical Properties of Titanium Alloys by Platinum Ion Plating", Thin Solid Films, 54, 309, (1978)

75. E. Hirsch and I. Varga, "The effect of Ion Irradiation on the Adherence of Germanium Films", Thin Solid Films, 52, 445, (1978)

76. P. Holloway and G. McGuire, "Chemical Characterization of Coatings by Analytical Techniques Sensitive to the Surface and Near-Surface", Thin Solid Films, 53, 3, (1978)

77. D. Teer and B. Delcea, "Grain Structure of Ion-Plated Coatings", Thin Solid Films, 54, 295, (1978)

78. J. M. Walls, et al., "A Comparison of Vacuum-Evaporated and Ion-Plated Thin Films Using Electron Spectroscopy", Thin Solid Films, 54, 303, (1978)

79. J. Franks, et al., "Ion Enhanced Film Bonding", Thin Solid Films, 60, 231, (1979)

80. M. Marinov, "Influence of Ion Bombardment on the Surface Structure of Silicon Single Crystals", Thin Solid Films, 61, 363, (1979)

81. E. Hirsch and I. Varga, "Thin Film Annealing by Ion Bombardment", Thin Solid Films, 69, 99, (1980)

82. H. Sundquist and J. Myllyla, "Wear of Ion-Plated Aluminum Bronze Coatings Under Arduous Metal-Forming Conditions", Thin Solid Films, 84, 289, (1981)

83. N. Ahmed and D. Teer, "The Properties of Ion-Plated Aluminum/Aluminum-Oxide Coatings Deposited in a Pulsed Oxygen Gas", in Plasmas and Cathode Sputtering, 4th International Colloquium, (Proc. Conf.), France, (1982)

84. S. Arya and H. Singh, "Conduction Properties of Thin Al_2O_3 Films", Thin Solid Films, 91, 363, (1982)

85. M. Bujor, et al., "A Study of the Initial Oxidation of Evaporated Thin Films of Aluminum by AES, ELS, and ESD", J. Vac. Sci. Tech., 20 (3), March, (1982)

86. R. Bunshah, ed., Deposition Technologies for Films and Coatings, Noyes, Park Ridge, (1982)

87. D. Dobrev, "Ion-Beam-Induced Texture Formation in Vacuum-Condensed Thin Metal Films", Thin Solid Films, 92, 41, (1982)

88. S. Donnelly, et al., "Helium Ion Bombardment of Thin Aluminum Films", Thin Solid Films, 94, 289, (1982)

89. M. S. Raven, "The Adhesion and Interface Chemistry of Ion-Plated Selenium", Thin Solid Films, 87, 337, (1982)

90. A. Sinha, "Metallization Technology for Very-Large-Scale Integration Circuits", Thin Solid Films, 90, 271, (1982)

91. H. Winters, "Mass Effect in the Physical Sputtering of Multicomponent Materials", J. Vac. Sci. Tech., 20 (3), 493, (1982)

92. P. Barna, et al., "Effects of Co-Depositing Oxygen on the Growth Morphology of (111) and (100) Al Single Crystal Faces in Thin Films", Vacuum, 33 (1), 25, (1983)

93. D. Klempere and D. Williams, "Changes in the Chemical Reactivity of Metals Exposed to an Inert Gas Glow Discharge", Vacuum, 33 (5), 301, (1983)

94. S. Nandra, et al., "Modification of Gold Coatings by Ion Bombardment During Deposition", Thin Solid Films, 107, 335, (1983)

95. P. Bodo, and J. Sundgren, "Adhesion of Evaporated Titanium to Polyethylene: Effects of Ion Bombardment Pretreatment", J. Vac. Sci. Tech., A, 2 (4), (1984)

96. N. Garg, et al., "Diffusion of Silicon in Aluminum-Rich Alloy Thin Films", Thin Solid Films, 112, 317, (1984)

97. A. Matthews and D. Gethin, "Heating Effects in Ionization-Assisted Processes", Thin Solid Films, 117, 261, (1984)

98. M. Hershkovitz, I. A. Blech, and Y. Komem, "Stress Relaxation in Thin Aluminum Films", Thin Solid Films, 130, 87, (1985)

99. D. Leet, Microstructure and Interface Studies of Evaporated and Ion Plated Titainium Coatings, M. S. Thesis, UIUC, (1985)

100. K. Miyoshi, et al., "Metallic Glass as a Temperature Sensor During Ion Plating", Thin Solid Films, 127, 115, (1985)

101. A. Paccagnella, et al., "Silicon Diffusion in Aluminum", Thin Solid Films, 128, 217, (1985)

102. R. Petrova and R. Stoeva, "Activation of Mobile Ions in SiO_2 Films Caused by Substrate Heating During Electron Beam Evaporation of Aluminum", Thin Solid Films, 124, L9, (1985)

103. F. Sequeda, "Integrated Circuit Fabrication - A Process Overview", Journal of Metals, May, (1985)

104. Y. Sheng, et al., "A Simple Method for the Rapid Measurement of the Thickness of Ultrathin Metal Films", Thin Solid Films, 131, 131, (1985)

105. I. Yamada, et al., "Aluminum Epitaxy on Si(111) and Si(100) Using an Ionized Cluster Beam", Thin Solid Films, 124, 179, (1985)

106. N. Ahmed, "Ion-Plated Aluminum/Aluminum Oxide Coatings Using a Pulsed Oxygen Process", Thin Solid Films, 144, 103, (1986)

107. R. Badachhape, J. Margrave, and F. Brotzen, "Separation of Thin Aluminum Films from Silicon Substrates", Thin Solid Films, 139, L77, (1986)

108. H. Bangert, et al., "Ultramicrohardness Measurements on Aluminum Films Evaporated Under Various Conditions", Thin Solid Films, 137, 193, (1986)

109. R. Boxman, et al., "Fast Deposition fo Metallurgical Coatings and Production fo Surface Alloys Using a Pulsed High Current Vacuum Arc", Thin Solid Films, 139, 41, (1986)

110. J. Gee, I Hodgkinson, and P, Wilson, "Reflection Anisotropy in Evaporated Aluminum: Consequences for Telescope Mirror Coatings", J. Vac. Sci. Tech. A, 4 (4), July/Aug, (1986)

111. G. Kaganowicz and J. Robinson, "Relation Between Flow, Power, and Presence of Carrier Gas During Plasma Deposition of Thin Films", J. Vac. Sci. Tech. A, 4 (4), July/Aug, (1986)

112. E. Kay, "Summary Abstract: Non-Bulk-Like Physical Properties of Thin Films Due to Ion Bombardment During Film Growth", J. Vac. Sci. Tech. A, 4 (3), May/Jun, (1986)

113. V. Koleshko, V. Belitsky, and I. Kiryushin, "Stress Relaxation in Thin Aluminum Films", Thin Solid Films, 142, 199, (1986)

114. R. Kubiak, et al., "The Use of Polytetrafluoroethylene Bearings in Ultrahigh Vacuum", J. Vac. Sci. Tech. A, 4 (4), July/Aug, (1986)

115. R. Manory, "A Simple Method for Monitoring Surface Temperatures in Plasma Treatments", J. Vac. Sci. Tech. A, 4 (5), Sep/Oct, (1986)

116. W. Munz, "Titanium Aluminum Nitride Films: A New Alternative to TiN Coatings", J. Vac. Sci. Tech. A, 4 (5), Sep/Oct, (1986)

117. S. Roberts and P, Dobson, "The Microstructure of Aluminum Thin Films on Amorphous SiO_2", Thin Solid Films, 135, 137, (1986)

118. D. Skelly and L. Greunke, "Significant Improvement in Step Coverage Using Bias Sputtered Aluminum", J. Vac. Sci. Tech. A, 4 (3), May/Jun, (1986)

119. J. E. Sundgren and H. T. G. Hentzell, "A Review of the Present State of Art in Hard Coatings Grown from the Vapor Phase", J. Vac. Sci. Technol. A, 4 (5), Sep/Oct (1986)

120. A. Testoni and P. Stair, "Summary Abstract: The Role of Surface Defects in Aluminum Surface Oxidation", J. Vac. Sci. Tech. A, 4 (3), May/Jun, (1986)

121. J. Vogel and E Bergmann, "Problems Encountered with the Introduction of Ion Plating to Large-Scale Coating of Tools", J. Vac. Sci. Tech. A, 4 (6), Nov/Dec, (1986)

122. R. Ball and A. Todd, "The Formation of Titanium, Chromium, Niobium and Zirconium Aluminides in Thin Films for Interconnections", Thin Solid Films, 149, 269, (1987)

123. A. Bessaudou, J. Machet, and C. Weissmantel, "Transport of Evaporated Material Through Support Gas in Conjunction with Ion Plating: I", Thin Solid Films, 149, 225, (1987)

124. A. Bessaudou, J. Machet, and C. Weissmantel, "Transport of Evaporated Material Through Support Gas in Conjunction with Ion Plating: II", Thin Solid Films, 149, 237, (1987)

125. D. Brown, "Aluminized Polyester Films: Influence of Substrate on Metal Texture", Thin Solid Films, 149, 105, (1987)

126. C. Egert and D. Scott, "A Study of Ion Plating Parameters, Coating Structure, and Corrosion Protection for Aluminum Coatings on Uranium", J. Vac. Sci. Tech. A, 5 (4), Jul/Aug, (1987)

127. G. Horikoshi, "Physical Understanding of Gas Desorption Mechanisms", J. Vac. Sci. Tech. A, 5 (4), Jul/Aug, (1987)

128. E. Ma, et al., "Structural Transformation Induced by Nitrogen Implantation in Thin Metal Films", Thin Solid Films, 147, 49, (1987)

129. A. Mathewson, et al., "Comparison of the Synchrotron Radiation Induced Gas Desorption in Aluminum Vacuum Chambers after Chemical and Argon Glow Discharge Cleaning", J. Vac. Sci. Tech. A, 5 (4), Jul/Aug, (1987)

130. S. Pandey, D. Gangopadhyay, and C. Suryanaryana, "Metastable Phases in Vapour-Deposited Al-Zr Thin Films", Thin Solid Films, 146, 273, (1987)

131. A. Pargellis, "Distribution of Copper Deposited inside Holes by Sputtering", J. Vac. Sci. Tech. A, 5 (6), Nov/Dec, (1987)

132. S. Schiller, et al., "High-Rate Vapor Deposition and Large Systems for Coating Processes", J. Vac. Sci. Tech. A, 5 (4), Jul/Aug, (1987)

133. P. Scott, Analysis of Ion Plated Cu/Cordierite Film and Interface Structure and Chemistry, M. S. Thesis, UIUC, (1987)

134. M. Shah, Structure/Chemistry/Properties of Ion Plated Nickel Films on Glass-Ceramic Substrates, M. S. Thesis, UIUC, (1986)

135. G. Slusser and L. MacDowel, "Sources of Surface Contamination Affecting Electrical Characteristics of Semiconductors", J. Vac. Sci. Tech. A, 5 (4), Jul/Aug, (1987)